The
Philosophical Magazine

FIRST PUBLISHED IN 1798

A Journal of Theoretical Experimental and Applied Physics

Vol. 6 October 1961 No. 70
Eighth Series

UNIVERSITY OF HAWAII
LIBRARY
FEB 5 '62

25s. 0d., plus postage
Annual Subscription £13 10s. 0d., payable in advance

ALERE FLAMMAM

Printed and Published by
TAYLOR & FRANCIS LTD
RED LION COURT, FLEET STREET, LONDON, E.C.4

THE PHILOSOPHICAL MAGAZINE

Editor

Professor N. F. Mott, M.A., D.Sc., F.R.S

Editorial Board

Sir Lawrence Bragg, O.B.E., M.C., M.A., D.Sc., F.R.S.
Sir George Thomson, M.A., D.Sc., F.R.S.
W. H. Taylor, M.A., D.Sc.

Authors wishing to submit papers for publication in the Journal should send manuscripts directly to the Publishers.

Manuscripts should be typed in *double* spacing on one side of quarto (8 × 10 in.) paper, and authors are urged to aim at absolute clarity of meaning and an attractive presentation of their texts.

References should be listed at the end in alphabetical order of authors and should be cited in the text in terms of author's name and date. Diagrams should normally be in Indian ink on white card, with lettering in soft pencil, the captions being typed on a separate sheet.

A leaflet giving detailed instructions to authors on the preparation of papers is available on request from the Publishers.

Authors are entitled to receive 25 offprints of a paper in the Journal free of charge, and additional offprints can be obtained from the Publishers.

The *Philosophical Magazine* and its companion journal, *Advances in Physics*, will accept papers for publication in experimental and theoretical physics. The *Philosophical Magazine* publishes contributions describing new results, letters to the editor and book reviews. *Advances in Physics* publishes articles surveying the present state of knowledge in any branch of the science in which recent progress has been made. The editors welcome contributions from overseas as well as from the United Kingdom, and papers may be published in English, French and German.

A Note on Thermoelectric Power and Inelastic Scattering

By A. M. GUÉNAULT† and D. K. C. MACDONALD
Division of Pure Physics, National Research Council, Ottawa, Canada

[Received March 18, 1961]

ABSTRACT

Recently Kasuya, Bailyn and de Vroomen have independently proposed that spin-dependent scattering of electrons by magnetic impurity ions would provide a mechanism to account for the 'giant' thermoelectric powers observed in certain dilute alloys at very low temperatures. A simplified model discussed here indicates directly that the essential requirement is that of two largely independent groups of conduction electrons whose mobilities are significantly different, but in which the groups are coupled by (spin-dependent) inelastic scattering. It also follows in general agreement with experiment that resistive anomalies are to be looked for when such 'mutual electron-drag' is present.

A starting point for the solution of electron transport problems is the so-called 'Boltzmann equation' for the electron distribution function, f; and the Boltzmann equation may be written formally:

$$\left(\frac{df}{dt}\right)_{\substack{\text{fields}\\ \text{or drift}}} + \left(\frac{df}{dt}\right)_{\text{coll.}} = 0. \qquad . \quad . \quad . \quad . \quad . \quad (1)$$

If the electron scattering is purely elastic, such as by lattice vibrations at 'high' temperatures ($kT \gtrsim h\nu$) or by impurity ions whose scattering may be represented by a simple electrostatic potential, then it is argued on a quasi-free electron model that the collision term (which is generally an integral over all possible scattering processes ($\mathbf{k}$, $\mathbf{k}'$)) may be written:

$$\left(\frac{df_{\mathbf{k}}}{dt}\right)_{\text{coll.}} = -\frac{f_{\mathbf{k}}(E)-f_0(E)}{\tau}, \qquad . \quad . \quad . \quad . \quad . \quad (2)$$

where $f_0(E)$ denotes the distribution function in equilibrium and E denotes the energy of an electron having wave vector $\mathbf{k}$. The 'relaxation time' τ is a direct function of the scattering matrix elements appropriate to the collisions, but does *not* involve the Pauli exclusion principle (cf. Mott and Jones 1936, p. 260, Peierls 1955, p. 116). This means that any energy-dependence of τ would arise directly from an energy-dependence of the matrix element for an electron making the transition ($\mathbf{k}$, $\mathbf{k}'$) in the absence of any other electrons; we shall assume in what follows that the matrix elements themselves are constant or at most relatively slowly varying functions of the total electron energy, E.

---

† National Research Council Postdoctorate Fellow.

Quite generally, the absolute thermoelectric power, S, may be written:

$$S = \frac{1}{eT} \int (E-\zeta)\sigma(E) \frac{\partial f_0}{\partial E} dE \bigg/ \int \sigma(E) \frac{\partial f_0}{\partial E} dE \quad . \quad . \quad . \quad . \quad (3\,a)$$

where, to quote Ziman (1959), $\sigma(E)$ is "the electrical conductivity which the metal would have, at absolute zero, if the Fermi level, ζ, came at the energy E". If eqn. (2) is valid, it may be shown (cf. Mott and Jones, loc. cit. p. 310, Wilson 1953, p. 205) that as a first approximation the thermoelectric power due to electron diffusion may be written:

$$S = \frac{\pi^2 k^2 T}{3e} \frac{\partial \ln \sigma(E)}{\partial E} \quad . \quad . \quad . \quad . \quad . \quad . \quad . \quad . \quad . \quad . \quad . \quad (3\,b)$$

$$= \frac{\pi^2 k^2 T}{3e} \left(\frac{\partial \ln n(E)}{\partial E} + \frac{\partial \ln v^2(E)}{\partial E} + \frac{\partial \ln \tau(E)}{\partial E} \right) \quad . \quad . \quad . \quad (3\,c)$$

where the derivatives are to be evaluated at the Fermi level, ζ.

When the scattering is inelastic the situation becomes more complex, and generally speaking the collision integral *cannot* be reduced rigorously to the form of eqn. (2). Consider however a simple inelastic collision problem in which electrons make purely inelastic collisions with 'atoms' each of which has a ground state and an excited state (both non-degenerate) separated by an energy, ϵ; let us assume for the moment that the scattering matrix elements are strictly constant. In that case we write:

$$\left(\frac{df_{\mathbf{k}}}{dt}\right)_{\text{coll.}} = -\frac{f_{\mathbf{k}}(E)}{\tilde{\tau}} \frac{\exp(-\epsilon/kT)}{1+\exp(-\epsilon/kT)} (1 - \langle f_{\mathbf{k}'}(E+\epsilon) \rangle)$$
$$+ \frac{\langle f_{\mathbf{k}'}(E+\epsilon) \rangle}{\tilde{\tau}} \frac{1}{1+\exp(-\epsilon/kT)} (1 - f_{\mathbf{k}}(E)), \quad . \quad . \quad (4)$$

for transitions out of the electron state $\mathbf{k}$ to one of *higher* electron energy, and the reverse transition into the state $\mathbf{k}$. A similar expression (replacing $+\epsilon$ by $-\epsilon$) must be added for the transitions between the state $\mathbf{k}$ and ones of *lower* electron energy. An elementary calculation now shows that if as a first approximation we replace $\langle f_{\mathbf{k}'}(E+\epsilon) \rangle$ by $f_0(E+\epsilon)$, then:

$$\left(\frac{df_{\mathbf{k}}}{dt}\right)_{\text{coll.}} = -\frac{f_{\mathbf{k}}(E) - f_0(E)}{\tau'} \quad . \quad . \quad . \quad . \quad . \quad . \quad (5\,a)$$

where

$$\frac{1}{\tau'} = \frac{1}{\tilde{\tau}} \left(\frac{\exp(\eta)+1}{[1+\exp(-\beta)][\exp(\eta+\beta)+1]} + \frac{\exp(\eta)+1}{[1+\exp(\beta)][\exp(\eta-\beta)+1]} \right) \quad (5\,b)$$

$$\eta \equiv \frac{E-\zeta}{kT}; \quad \beta \equiv \frac{\epsilon}{kT}.$$

The first term in $1/\tau'$ derives from eqn. (4); the second term naturally derives from the second group of electron transitions.

$\tilde{\tau}$, like τ in eqn. (2) will be at most a *slowly varying* function of electron energy. We note that in this case the collision integral has been reduced to the precise form of eqn. (2) (and we remark particularly that f_0 and $f_{\mathbf{k}}$ are to be evaluated for the *same* electron energy, E) but now the Pauli exclusion principle has figured directly in producing an overall relaxation time, τ', which now varies quite rapidly within the thermal 'tail' of the Fermi distribution. In fact if we rewrite eqn. (5 *b*) as:

$$\frac{1}{\tau'} = \frac{1}{\tilde{\tau}}\lambda;$$

then λ varies in the neighbourhood of ζ when $\beta \sim 1$ such that:

$$\frac{1}{\lambda}\left|\frac{\partial\lambda}{\partial E}\right| \lesssim \frac{1}{kT} \quad . \quad . \quad . \quad . \quad . \quad . \quad . \quad . \quad . \quad . \quad (6)$$

(cf. sketch of λ in the figure). Since the collision integral in this case has been reduced to precisely the form of eqn. (2), we can immediately write eqn. (3 *b*) or (3 *c*) for the diffusion thermoelectric power, but of course we must now write:

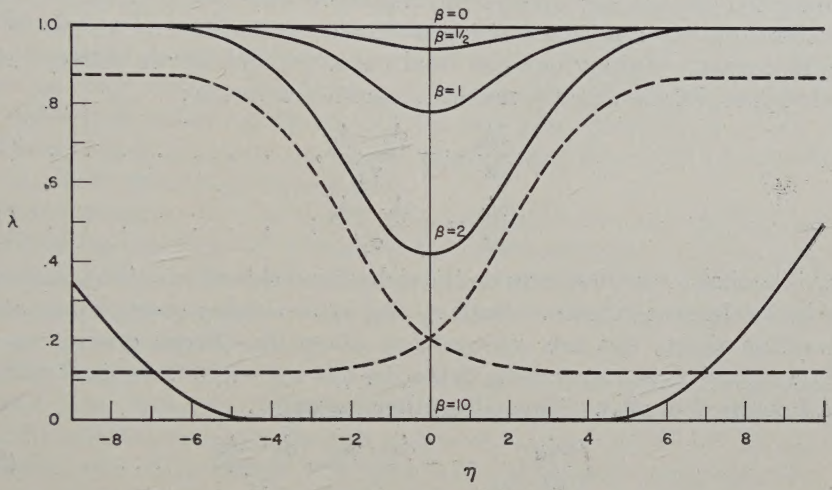

Variation of λ with η for various values of β (full lines). The two dashed curves show separately the behaviour for $\beta=2$ of the two terms in eqn. (5), which determine $1/\tau_3'$ and $1/\tau_4'$.

$$\left(\frac{\partial \ln \tau'(E)}{\partial E}\right)$$

as the last term in eqn. (3 *c*).

The fact that $\tau'(E)$ varies now very rapidly with the electron energy (cf. eqn. (6)) might lead us to suppose that a very large thermoelectric power would result whenever inelastic scattering occurs, but if we examine eqn. (5 b) more carefully we see that λ, although highly energy-dependent, is *symmetrical* in η, and it appears (cf. de Vroomen and Potters 1961) that this is a rather general consequence when only inelastic scattering is involved. The contribution from this factor to the last term in eqn. (3 *c*) when evaluated at $E=\zeta$ ($\eta=0$) will be zero, and therefore we cannot expect to encounter an anomalous thermoelectric power from inelastic scattering alone; this has also been pointed out by de Vroomen and Potters (loc. cit.) by considering the Peltier heat appropriate to the thermoelectric question.

Recent work by Kasuya (1959), Bailyn (1961) and de Vroomen† (1959; see also de Vroomen *et. al.* 1960, de Vroomen and Potters 1961) on the anomalous transport properties of dilute alloys containing magnetic ions as solute has prompted us to consider a simple formal model where two groups of electrons contribute to electron transport. Let these two groups have distribution functions ϕ and ψ. We suppose that each group has a relaxation time τ_1 and τ_2 independent of the other and for convenience let us assume these relaxation times are elastic, although this does not appear mandatory. We suppose in addition that the two groups are *inelastically*-coupled to one another; an electron transition from ϕ to ψ involves a gain of electron energy ϵ, and a transition in the reverse direction a corresponding loss in energy. Taking our cue from eqns. (4) and (5) we suggest as a crude approximation for the mutual inelastic scattering:

$$\frac{d\phi_{\mathbf{k}}}{dt} = -\frac{\phi_{\mathbf{k}} - \psi_{\mathbf{k}}}{\tau_3'}, \qquad (7\,a)$$

$$\frac{d\psi_{\mathbf{k}}}{dt} = -\frac{\psi_{\mathbf{k}} - \phi_{\mathbf{k}}}{\tau_4'}; \qquad (7\,b)$$

$1/\tau_3'$ is similar to the *first* term on the right-hand side of eqn. (5 *b*), and $1/\tau_4'$ similar to the second term. Both τ_3' and τ_4' are highly energy-dependent relaxation times, but are *asymmetrical* about the Fermi energy $(\eta = 0)$ (cf. the figure); however we note that $\tau_3'(+\eta) = \tau_4'(-\eta)$ (cf. also de Vroomen and Potters, loc. cit.). Thus altogether we write:

$$\left(\frac{d\phi_{\mathbf{k}}}{dt}\right)_{\text{coll.}} = -\frac{\phi_{\mathbf{k}} - \phi_0}{\tau_1} - \frac{\phi_{\mathbf{k}} - \psi_{\mathbf{k}}}{\tau_3'} \qquad (8\,a)$$

and

$$\left(\frac{d\psi_{\mathbf{k}}}{dt}\right)_{\text{coll.}} = -\frac{\psi_{\mathbf{k}} - \psi_0}{\tau_2} - \frac{\psi_{\mathbf{k}} - \phi_{\mathbf{k}}}{\tau_4'}. \qquad (8\,b)$$

Equations (8 *a* and *b*) can then be readily solved when an electric field (say E_x) is applied to the common system and we find that:

$$f_{\mathbf{k}} \equiv \phi_{\mathbf{k}} + \psi_{\mathbf{k}} = f_0 - \frac{eE_x\tau'}{m}\frac{\partial f_0}{\partial v_x} \qquad (9)$$

where

$$\tau' = \frac{\tau}{2}\left(1 - \frac{\delta(\tau_1\tau_4' - \tau_2\tau_3')}{\tau(\tau_1\tau_4' + \tau_2\tau_3' + \tau_3'\tau_4')}\right) \qquad (10)$$

where $\tau \equiv \tau_1 + \tau_2$,

and $\delta \equiv \tau_1 - \tau_2$.

Since the overall system is characterized by a single relaxation time τ' as given by eqn. (10) we can once more apply eqn. (3 *c*) directly and expect to discover anomalously large thermoelectric powers when τ' is both highly energy-dependent in the Fermi tail and asymmetrical about $\eta=0$. We note that if $\delta=0$, implying that the independent relaxation times of the two groups are equal, the inelastic coupling characterized by τ_3' and τ_4' will not contribute in any way to τ' and no thermoelectric power anomaly will be expected. Also if the inelastic scattering is absent (τ_3', $\tau_4' \to \infty$) or overwhelmingly strong (τ_3', $\tau_4' \to 0$) the model predicts again no highly energy-dependent term in τ'. Thus eqn. (10) shows directly *within the limitations of our model* that an anomalous thermoelectric power is only to be looked for in such a system if there is appreciable, but not overriding, inelastic coupling, and if the independent relaxation times of the two groups of electrons differ significantly from one another.

---

† We are grateful to Drs. Bailyn and de Vroomen for sending us copies of their manuscripts before publication.

If τ_3' and τ_4' *do* contribute significantly then this will only be in the temperature region where inelastic collisions are frequent, i.e. when $\beta \sim 1$, (when $\beta \ll 1$, the collisions become essentially elastic and τ_3' and τ_4' will cease to be highly energy-dependent, while when $\beta \gg 1$ the inelastic collisions become very rare). But then, putting the last derivative in eqn. (3 *c*) of order (but rather less than) $1/kT$ (cf. eqn. (6)), we see immediately that a thermoelectric power somewhere approaching the order of magnitude (k/e) (about 86 μv/deg.) might arise.

It is interesting to note that this is the same order of magnitude as one expects for the limit of 'phonon-drag' thermoelectric power on a simple argument, and it is not difficult to see that there is at least a formal analogy between the two processes; the present situation could perhaps be referred to as 'mutual electron-drag'.

The same conditions for the existence of an anomalous thermoelectric power (viz. presence of both elastic and inelastic collisions and unequal elastic collision times for the two groups of carriers) have been reached by Kasuya (loc. cit.), Bailyn (loc. cit.) and de Vroomen (loc. cit.) for the system where we have conduction electrons being scattered in a metal by relatively dilute concentrations of magnetic impurity ions (transition elements). These ions are assumed to have their magnetic degeneracy split by some common 'pseudo-Weiss field'. In that case the two groups of electrons are those with plus and minus spins; the independent (and elastic) transitions are those in which an electron is elastically scattered by an ion *without* a 'spin-flip', while the mutual inelastic coupling arises when an electron is scattered *with* a spin-flip, and correspondingly the magnetic ion involved makes a transition from one energy level to another. We are certainly inclined to believe that the Kasuya–Bailyn–de Vroomen model (which arises as a logical extension of an earlier model by Schmitt (1956); cf. also Brailsford and Overhauser (1960)) is probably the right one for interpreting the highly anomalous thermoelectric powers observed experimentally at very low temperatures (cf. e.g. MacDonald *et al.* 1958, 1960, Gold *et al.* 1960). However, our elementary discussion of the problem leads us to ask also whether other situations could not arise in which two groups of conduction electrons, mutually coupled by some appropriate inelastic scattering (but not *necessarily* involving spin-flips), might lead to a similar result. More specifically we wonder whether the *parent* transition metals themselves, involving s-band and d-band conduction electrons coupled presumably by some inelastic transitions, might not give rise to a similar kind of situation.

Note added in proof.—Kasuya (loc. cit.) has suggested that a ‘ spin-flipping ’ inelastic electron scattering mechanism within a single band may lead to an anomalously large thermoelectric power in pure transition metals.

Finally we can see quite readily that this strong energy dependence of the overall relaxation time can also give anomalies in the electrical conductivity. Mott and Jones (loc. cit., p. 266) give for the actual conductivity, σ_x:

$$\sigma_x = \sigma_x(\zeta) + \frac{\pi^2}{6}(kT)^2 \frac{\partial^2 \sigma_x(\zeta)}{\partial \zeta^2} \quad \ldots \ldots \qquad (11)$$

where $\sigma_x(\zeta)$ is the conductivity we would expect if the Fermi ‘tail’ were quite sharp at energy ζ.

On our present model this can be written

$$\frac{\sigma_x}{\sigma_x(\zeta)} = 1 + \frac{\pi^2}{6\tau'}\left(\frac{\partial^2 \tau'(\eta)}{\partial \eta^2}\right)_{\eta=0} \quad \ldots \ldots \qquad (12)$$

Normally the second term in eqn. (12) is of order $(kT/\zeta)^2$ and can therefore be neglected, but in the present situation it appears possible to get significant values of $(1/\tau')(\partial^2\tau'(\eta)/\partial\eta^2)$ for $\beta \sim 1$. Furthermore this will give a *temperature dependent* term in σ_x, as the value of the derivative will depend on temperature through β (cf. the figure).

Consequently eqn. (12) predicts directly on this model that a resistive anomaly should also be looked for arising directly from the highly energy-dependent relaxation time.

Note added in proof.—However, more detailed estimates indicate that it is very difficult to account reasonably for the *magnitude* of the resistive anomalies typically observed.

REFERENCES

BAILYN, M., 1961, *Phys. Rev.* (submitted for publication).

BRAILSFORD, A. D., and OVERHAUSER, A. W., 1960, *J. Phys. Chem. Solids*, **15,** 140.

DE VROOMEN, A. R., 1959, Thesis, Leiden.

DE VROOMEN, A. R., and POTTERS, M. L., 1961, *Physica*, **27,** 657.

DE VROOMEN, A. R., VAN BAARLE, C., and CUELENAERE, A. J., 1960, *Physica*, **26,** 19.

GOLD, A. V., MACDONALD, D. K. C., PEARSON, W. B., and TEMPLETON, I. M., 1960, *Phil. Mag.*, **5,** 765.

KASUYA, T., 1959, *Progr. theor. Phys., Japan*, **22,** 227.

MACDONALD, D. K. C., PEARSON, W. B., and TEMPLETON, I. M., 1958, *Phil. Mag.*, **3,** 657; 1960, *Ibid.*, **5,** 867.

MOTT, N. F., and JONES, H., 1936, *Theory of Properties of Metals and Alloys* (Oxford: Clarendon Press).

PEIERLS, R. E., 1955, *Quantum Theory of Solids* (Oxford: Clarendon Press).

SCHMITT, R. W., 1956, *Phys. Rev.*, **103,** 83.

WILSON, A. H., 1953, *Theory of Metals*, 2nd ed. (Cambridge: University Press).

ZIMAN, J. M., 1959, *Proc. roy. Soc.* A, **252,** 63.

Rotational Bands in the 1p-Shell

By A. B. CLEGG
Clarendon Laboratory, Oxford

[Received March 9, 1961]

ABSTRACT

It is noted that certain states of 1p-shell nuclei are strongly excited in the inelastic scattering of medium energy protons from these nuclei while other states are weakly excited. It is suggested that these observations can be understood if these nuclei are distorted, with rotational bands. The connection with other nuclear models of the 1p-shell is discussed.

---

§ 1. INTRODUCTION

IN this note we propose that the collective model can be applied to the 1p-shell in the same way as it has been applied to the 2s–1d shell (for a summary see Gove 1960). This suggestion is based on the observation that in the inelastic scattering of protons of 150–185 MeV certain states of 1p-shell nuclei are excited strongly and others very weakly (Tyrén and Maris 1958, Clegg *et al.* 1961), noting that it has been shown by Clegg *et al.* that such inelastic scattering provides an almost quantitative means of picking out strong electric quadrupole radiative transitions to the ground state. Thus, in odd-mass nuclei in the 1p-shell, we identify low-lying states which are strongly excited by inelastic scattering as states of the same rotational band as the ground state while other, weakly excited, states are taken to be members of other rotational bands. In this way a good fit is obtained to the low-lying levels of these nuclei, the only intrinsic states being those expected from the filling of Nilsson's energy levels in deformed nuclei (Nilsson 1955), taking prolate distortion in the first half of the 1p-shell and oblate distortion in the second half. Moments of inertia, intrinsic spacings and decoupling parameters involved in $K=\frac{1}{2}$ bands are determined by empirical fitting; however, it is always found that the decoupling parameter found empirically agrees very well with the value calculated for the corresponding Nilsson wave-functions. In ^{9}Be and ^{11}B there are two bands, which one would expect to mix due to the rotation-particle coupling (Kerman 1956), but the apparent selection rule on inelastic scattering suggests that this mixing is not large.

The relationships between the model proposed here and other models, particularly the intermediate coupling scheme, which is so successful in correlating so many properties of 1p-shell nuclei, are discussed in later sections.

§ 2. EXPECTED INTRINSIC STATES

The Nilsson energy level scheme for the 1p-shell consists of three levels labelled level 2: $p_{3/2}$, $K=\frac{3}{2}$; level 3: $p_{3/2}$, $K=\frac{1}{2}$; level 4: $p_{1/2}$, $K=\frac{1}{2}$. The energies of each of these levels is a function of η, the ratio of the spheroidal distortion to the spin–orbit coupling. η is positive for prolate distortion and negative for oblate distortion.

Four particles, neutron or proton with $\Omega=\pm K$, can be placed on each level. Thus for mass 7, with η positive, three particles go in level 3, forming a low-lying $K=\frac{1}{2}$ intrinsic state with a large gap before the next intrinsic state is reached. For mass 9 level 3 will be filled with four particles and the fifth will be on level 2 or 4; thus there will be two close intrinsic states with $K=\frac{1}{2}$, $\frac{3}{2}$ and then a big gap before any more show up. For mass 13, with η negative, three holes are placed on level 4 forming a low-lying $K=\frac{1}{2}$ intrinsic state with a large gap before the next intrinsic state. For mass 11 level 4 is filled with four holes and the fifth hole is on level 2 or 3 forming two low-lying intrinsic states of $K=\frac{1}{2}$, $\frac{3}{2}$ with a large gap to the next intrinsic state. One notes that the intrinsic states proposed for ^{11}B are formed in a different manner from those used in the fits made to the $(4n+3)$ nuclei in the 2s–1d shell: ^{23}Na, ^{27}Al, ^{31}P (summarized by Gove 1960). Here we have chosen intrinsic states formed by a hole on otherwise filled levels, while in the fits to the level schemes of ^{23}Na, ^{27}Al, ^{31}P a single particle has been promoted to unfilled levels. For example, if we had used this latter procedure in ^{11}B, we would have intrinsic states formed by single particles respectively on Nilsson levels 3 and 4, giving two $K=\frac{1}{2}$ bands, which do not fit the ^{11}B energy level scheme so well. One can argue that the intrinsic states we have chosen would come lower in energy due to the pairing energy; on lifting a particle from a filled or partially-filled level to an empty level one is breaking a pair so that the corresponding state should come at a higher energy. That this is so for ^{27}Al has been demonstrated by Brink and Kerman (1959). Further, experimental measurements of (p, 2p) and (p, pn) reactions on ^{24}Mg, ^{28}Si and ^{32}S suggest that the low-lying intrinsic states in the $(4n+3)$ nuclei are formed by holes in otherwise filled levels (Clegg and Foley, to be published). Thus we feel that the correct assignment of intrinsic states has been made in ^{11}B, on other grounds than that they are the ones we need to fit the experimental energy spectrum.

§ 3. MASS 11

Tyrén and Maris (1958) see strong excitation of states of ^{11}B at $4{\cdot}7\pm0{\cdot}2$ and $6{\cdot}6\pm0{\cdot}2$ MeV in the ^{11}B(p, p′) reaction. It has been shown that the lower of these two is the $J=\frac{5}{2}$ state at 4·46 MeV, and that the $J=\frac{1}{2}$ state at 2·13 MeV is weakly excited in this reaction (Clegg *et al.* 1961). The $J=\frac{3}{2}-$ state at 5·03 MeV is weakly excited (Clegg *et al.* 1961) while the $6{\cdot}6\pm0{\cdot}2$ MeV state could well be the $J=\frac{7}{2}$ state at 6·81 MeV so one suggests that the states excited are a $K=\frac{3}{2}$ rotational band based on the $J=\frac{3}{2}$

ground state and the states not excited are a $K=\frac{1}{2}$ band based on the $J=\frac{1}{2}$ state at 2·13 MeV; these intrinsic states have the merit of being those predicted by Nilsson's scheme. These two bands will mix due to the rotation–particle coupling (Kerman 1956), changing the level spacings. A fit has been made to the known level scheme and is shown in table 1 where the energies quoted for the experimental levels are the means of the energies of corresponding levels in ^{11}B and ^{11}C. The decoupling parameter for the $K=\frac{1}{2}$ band is taken to be $a=-0{\cdot}8$ which corresponds to Nilsson's level 3, $\eta=-6$. Other parameters determined empirically are $\hbar^2/2\mathscr{I}=0{\cdot}85$ MeV (we have throughout taken the same moment of inertia for both bands in the same nucleus, simply to reduce the number of parameters), $A_K=0{\cdot}60$ MeV (the matrix element of rotation–particle coupling) and the intrinsic spacing $=1{\cdot}71$ MeV. In this fit the only requirement limiting the band-mixing is that it should be weak enough so that the individual states are still largely $K=\frac{3}{2}$ or $K=\frac{1}{2}$ and then the simple features of the inelastic scattering are reproduced. An experiment is in progress to measure the ' forbidden ' transitions and so determine the band-mixing more accurately. A further contribution to the level energies is due to the rotation–vibration interaction which contributes a term to the energy of the form $-\mathrm{B}[J(J+1)+(-1)^{J+1/2}\,\delta_{J1/2}a(J+\frac{1}{2})]^2$. This term will obviously help to produce a better fit in the case of ^{11}B; however, an actual numerical fit is postponed until the band-mixing is better determined. For a pure $K=\frac{3}{2}$ band the ratio of inelastic scattering cross sections to the 6·8 and 4·46 MeV states should be 0·56, which is in reasonable agreement with the experimental results.

Table 1

State	Experimental energy (MeV)	Calculated energy (MeV)
$\frac{3}{2}-$	0	0
$\frac{1}{2}-$	2·06	2·13
$\frac{5}{2}-$	4·35	4·26
$\frac{3}{2}-$	4·90	3·06
$\frac{7}{2}-$	6·65	8·99
$\frac{5}{2}-$	—	11·43
$\frac{7}{2}-$	—	13·90

§ 4. MASS 9

In the ^{9}Be(p, p′) reaction states strongly excited are at $2{\cdot}3\pm0{\cdot}2$ MeV and ~6 MeV. The first is presumably the $J=\frac{5}{2}$ state at 2·43 MeV and the other is most probably the state at 6·76 MeV. Again one supposes that these states are a rotational band based on the $J=\frac{3}{2}$ ground state and it is immediately found that a good fit is obtained with $\hbar^2/2\mathscr{I}=0{\cdot}524$ Mev: see table 2.

However, there are other well-established states in ^{9}Be which are presumably due to the expected $K=\frac{1}{2}$ band. This band will mix with the $K=\frac{3}{2}$ band, but there is not enough information about the spins and parities of the other states of ^{9}Be to justify a detailed fit. That these states in ^{9}Be form a rotational band has previously been suggested by Blair and Henley (1958) from the strong excitation of them in the inelastic scattering of 40 Mev alpha-particles. As in the ^{11}B(p, p′) reaction the ratio of cross sections for exciting the two states in ^{9}Be(p, p′) should be 0·56 for a pure $K=\frac{3}{2}$ band, a result in reasonable agreement with experiment.

Table 2

State		$J=\frac{3}{2}$	$J=\frac{5}{2}$	$J=\frac{7}{2}$
Energies	Model	0	2·62	6·28
	Experiment	0	2·43	6·76

§ 5. Mass 7

In the ^{7}Li(p ,p′) reaction the strongly excited state is at $4{\cdot}4\pm0{\cdot}2$ Mev, which presumably corresponds to the state at 4·63 Mev, whose mirror state in ^{7}Be has $J=\frac{7}{2}-$. It is easily found that the states of ^{7}Li can be fitted with a $K=\frac{1}{2}$ band with $a=-1{\cdot}3$, calculated for level 3 with $\eta=+8$, and $\hbar^2/2\mathscr{I}=0{\cdot}54$ Mev. This gives an energy level scheme:

State	$j=\frac{3}{2}-$	$J=\frac{1}{2}-$	$J=\frac{7}{2}$	$J=\frac{5}{2}$	$J=\frac{9}{2}$
Model	0	0·49	5·08	6·21	16·24
Experiment	0	0·46	4·58	7·32	—

The experimental energies quoted are the mean of those for ^{7}Li and ^{7}Be. For such a $K=\frac{1}{2}$ band the inelastic scattering cross sections will be proportional to:

$$\mathrm{B}(\tfrac{3}{2}\rightarrow I_f)=[(\tfrac{3}{2}2\tfrac{1}{2}0\mid I_f\tfrac{1}{2})Q_0+(\tfrac{3}{2}2-\tfrac{1}{2}1\mid I_f\tfrac{1}{2})Q_1]^2$$

where Q_0, Q_1 depend on the intrinsic wave-functions. So we have

I_f	$\mathrm{B}(\frac{3}{2}\rightarrow I_f)$
$\frac{1}{2}$	$[-(\frac{1}{5})^{1/2}Q_0+(\frac{3}{10})^{1/2}Q_1]^2$
$\frac{7}{2}$	$[(\frac{18}{35})^{1/2}Q_0+(\frac{3}{10})^{1/2}Q_1]^2$
$\frac{5}{2}$	$[(\frac{3}{35})^{1/2}Q_0-(\frac{5}{14})^{1/2}Q_1]^2$

We see that if Q_0, Q_1 are of comparable magnitude the transition to the $J=\frac{7}{2}$ state at 4·63 Mev in the ^{7}Li(p, p′) reaction will be strong and the transition to the $J=\frac{5}{2}$ state at 7·47 Mev will be weak, as is observed.

This predicts that the transition to the $J=\frac{1}{2}$ state at 0·48 Mev will also be weak; measurements to check this prediction are in progress.

§ 6. MASSES 8, 12, 13

It has long been realized that ^{8}Be displays a rotational spectrum, though this has usually been described as an aspect of the alpha-particle model.

Apparently $\hbar^2/2\mathscr{I}=0{\cdot}53$ gives a good fit:

State	$J=0+$	$J=2+$	$J=4+$
Model	0	3·20	10·8
Experiment	0	2·90	11·7

Taking the $J=2+$ state of ^{12}C at 4·43 Mev to be a rotational state we find $\hbar^2/2\mathscr{I}=0{\cdot}74$ Mev while similarly the $J=\frac{3}{2}-$ state of ^{13}C at 3·68 Mev and of ^{13}N at 3·51 Mev, corresponds to $\hbar^2/2\mathscr{I}=0{\cdot}96$ Mev, taking $a=0{\cdot}25$ calculated for level 4 and $\eta=-3$.

§ 7. CONCLUSIONS

First we summarize the values of $\hbar^2/2\mathscr{I}$ found:

A	7	8	9	11	12	13
$\hbar^2/2\mathscr{I}$	0·54	0·53	0·52	0·85	0·74	0·96

These agree very well among themselves, falling into two groups: the prolate nuclei in the first half of the shell and oblate nuclei in the second half of the shell. Also the values of the decoupling parameter that are required for an empirical fit agree very well with those calculated for Nilsson wave-functions for reasonable values of η and the intrinsic levels found to be needed agree with those expected from Nilsson's energy levels so that one can imagine that this model has some physical significance. It presumably is a first approximation to the work of Kurath and Pičman (1959) who show that wave-functions constructed by the generating procedure of Peierls and Yoccoz (1957) have a very considerable overlap with wave-functions from an intermediate coupling calculation which fits the energy level spectra of 1p-shell nuclei (Kurath 1956). It has been shown by Yoccoz (1957) that this generating procedure produces an energy level spectrum approximately the same as a rotational band if the nucleus is sufficiently distorted. It is perhaps therefore significant that the more distorted nuclei ^{7}Li, ^{8}Be, ^{9}Be show closer approximations to rotational bands while in the case of the less distorted ^{11}B there is need of the rotation–vibration interaction term to obtain a more exact fit to the energy level scheme. Thus it can be suggested that the work described here shows how medium energy inelastic scattering results support the picture of Kurath and Pičman and helps to identify the physical states corresponding to their wave-functions. Further, this work suggests that, in ^{9}Be and ^{11}B, there is very little mixing between the rotational bands.

§ 8. (p,2p) REACTIONS IN THE 1p-SHELL

This picture can apparently also explain the results of (p, 2p) reactions at 150–185 MeV in the 1p-shell (Tyrén *et al.* 1958, Gooding and Pugh 1960) where it is found that only a few states are excited strongly in the residual nuclei. These results are taken to imply some simple picture of nuclear structure, where the ground state of nucleus A has very few parent states in nucleus A–1, and have been interpreted by a simple *jj*-coupling picture. This interpretation would seem to conflict with the intermediate coupling picture which has been found necessary to explain most low energy data, for example, the energy level spectra of 1p-shell nuclei (Kurath 1956), as the intermediate coupling wave-functions are apparently complicated so that the ground state of nucleus A would presumably have many parent states in nucleus A–1, contrary to the results of the (p, 2p) reactions. However, the picture presented here would describe the ground state of nucleus A as an intrinsic state made up of Nilsson wave-functions. Ejecting a proton would leave only a few intrinsic states of nucleus A–1, so that this picture presumably shows the simplicity of the intermediate coupling wave-functions necessary to understand the (p, 2p) reactions.

§ 9. COMPARISON WITH OTHER MODELS

It has already been mentioned that the rotational band in ^{8}Be has been previously ascribed to the alpha-particle model, a model in which the ^{8}Be nucleus is described as made up of two alpha-particles in a dumb-bell arrangement. It has however been shown, by Perring and Skyrme (1956), that such a model is equivalent to the shell-model picture, if the nucleon wave-functions are fully antisymmetrized. Thus if our model is an aspect of the shell-model there should be no problem in reconciling it with the alpha-particle model. (One notes that the alpha-particle model for the ^{8}Be ground state is a prolate nucleus, and the alpha-particle model for the ^{12}C ground state—three alpha-particles at the corners of an equilateral triangle—is an oblate nucleus, in agreement with our model.)

The alpha-particle model of ^{8}Be has been extended to ^{7}Li and ^{9}Be, by adding respectively one hole and one particle to ^{8}Be (Kunz 1960). In this way Kunz obtains distorted nuclei with rotational bands much the same as those described in this paper. This picture is presumably the same as adding one hole or one particle to the shell-model wave-functions of ^{8}Be so we see that our model and that of Kunz are presumably just two equivalent ways of looking at the same wave-functions.

One can see that the alpha-particle picture of ^{7}Li is equivalent to the cluster-model picture due to Phillips and Tombrello (1960), where the ^{7}Li states are taken to be made up of an alpha-particle cluster and a triton cluster, providing one adds to the cluster model the requirement of full antisymmetrization of the nucleon wave-functions. So we can take the evidence for the cluster-model as evidence for our model. A typical further example of agreement is the case where the 2·43 MeV state of ^{9}Be is shown to be made up of largely the 2+ state of ^{8}Be plus a neutron, in agreement with our assignment of both these states as the first excited states of rotational bands.

ACKNOWLEDGMENT

I wish to thank Professor D. H. Wilkinson for helpful discussions and for encouragement.

REFERENCES

BLAIR, J. S., and HENLEY, E. M., 1958, *Phys. Rev.*, **112,** 2029.
BRINK, D. M., and KERMAN, A. K., 1959, *Nucl. Phys.*, **12,** 314.
CLEGG, A. B., FOLEY, K. J., SALMON, G. L., and SEGEL, R. E., 1961, *Proc. phys. Soc., Lond.*, **78,** 681.
GOODING, T. J., and PUGH, H. G., 1960, *Nucl. Phys.*, **18,** 46.
GOVE, H. E., 1960, *Proceedings of Kingston Conference on Nuclear Structure* (University of Toronto Press), pp. 438–460.
KERMAN, A. K., 1956, *Math.-fys. Medd.*, **30,** No. 15.
KUNZ, P. D., 1960, *Annals of Physics*, **11,** 275.
KURATH, D., 1956, *Phys. Rev.*, **101,** 216.
KURATH, D., and PIČMAN, L., 1959, *Nucl. Phys.* **10,** 313.
NILSSON, S. G., 1955, *Math.-fys. Medd.*, **29,** No. 16.
PEIERLS, R. E., and YOCCOZ, J., 1957, *Proc. phys. Soc., Lond.* A, **70,** 381.
PERRING, J. K., and SKYRME, T. H. R., 1956, *Proc. phys. Soc., Lond.* A, **69,** 600.
PHILLIPS, G. C., and TOMBRELLO, T. A., 1960, *Nucl. Phys.*, **19,** 555.
TYRÉN, H., and MARIS, TH. A. J., 1958, *Nucl. Phys.*, **6,** 82.
TYRÉN, H., HILLMAN, P., and MARIS, TH. A. J., 1958, *Nucl. Phys.*, **7,** 10.
YOCCOZ, J., 1957, *Proc. phys. Soc., Lond.* A, **70,** 388.

Direct Measurements of Stacking-fault Energies from Observations of Dislocation Nodes

By A. Howie
Cavendish Laboratory

and P. R. Swann†
Department of Metallurgy, University of Cambridge

[Received February 13, 1961]

Abstract

From measurements of the radius of curvature of extended dislocation nodes observed by transmission electron microscopy, stacking-fault energies have been determined for a number of copper and silver base aluminium and zinc solid solution alloys and also for a number of nickel–cobalt alloys. Rough estimates of about 40, 25 and 150 erg cm^{-2} respectively can be made of the stacking-fault energies of copper, silver and nickel. The accuracy of the measurement and the possibility of segregation of solute atoms to stacking faults are discussed.

§ 1. Introduction

In view of the importance of the stacking-fault energy of the face-centred cubic metals in determining the equilibrium ribbon width of extended dislocations (Heidenreich and Shockley 1948) and hence in theories of work hardening (Seeger 1956, Hirsch 1959, Basinski 1959) and its further potential importance in the theory of alloy phases because of its relation to the energy difference between the hexagonal close-packed and face-centred cubic crystal structures, it is unfortunate that there are so few metals for which the value of the stacking-fault energy is accurately known. Two of the earliest estimates of stacking-fault energy remain the most reliable: that of $\gamma \approx 40$ erg cm^{-2} for copper deduced by Fullman (1951) from his determination of the twin boundary energy as ~ 20 erg cm^{-2} (on the assumption that the stacking-fault energy is twice the twin-boundary energy) and that of an internal energy $U = -20$ erg cm^{-2} (corresponding to a free energy $\gamma \approx -7$ erg cm^{-2}) estimated for cobalt by Heidenreich and Shockley from the known heat of transformation in the f.c.c.→h.c.p. transition. The values for cobalt are taken to be negative since it is convenient to regard γ as positive when the f.c.c. structure is stable. A value of $\gamma \approx 200$ erg cm^{-2} for aluminium was also estimated by Fullman.

---

† Now at Edgar C. Bain Laboratory, U.S. Steel Research Center, Monroeville, Pa., U.S.A.

Estimates of stacking-fault energy have also been made for a number of metals from observations of the mechanical properties interpreted in terms of a theory of work hardening (Thornton and Hirsch 1958, Seeger *et al.* 1959). Unfortunately, however, these results all depend on the validity of theories still held in question and the stacking-fault energy tends to appear simply as yet another adjustable parameter in the theory rather than as an independently known quantity.

The effect of stacking faults on X-ray diffraction has been used as a means of determining stacking-fault densities but since the theory applies only to faults of large area and the effect of stacking-fault ribbons is unknown, the interpretation of the results in terms of stacking-fault energy (Christian and Spreadborough 1957) has only a qualitative significance.

Fig. 1

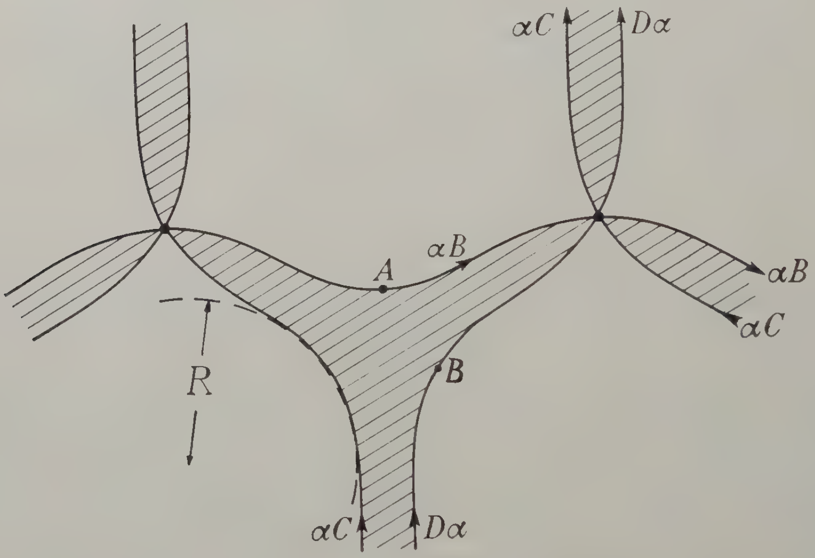

Diagram showing the arrangement of partial dislocations (for notation see Whelan 1959) to form a network of extended and contracted nodes. The shaded area is the stacking fault.

The application of transmission electron microscopy to the study of dislocations in thin foils showed that extended dislocations and stacking faults can be observed in metals of low stacking-fault energy (Whelan *et al.* 1957). Many interactions between extended dislocations have been identified and in particular one which gives rise to the formation of hexagonal networks lying on the slip planes with alternate nodes in the network being of an extended or contracted type (see fig. 1†) has been used by Whelan (1959) to obtain an estimate of the stacking-fault energy of stainless steel. Whelan considered the partial dislocation at A to be in equilibrium under a force $Gb_1^2/2R$ per unit length, due to its line tension (the line tension is taken as $Gb_1^2/2$; $\mathbf{b}_1$ is the Burgers vector of the partial dislocation and R its radius of curvature) and a force γ per unit length due to the attraction of the stacking fault. From the simple formula

---

† Figures 5 and 6 are shown as plates.

$$\gamma = Gb_1^2/2R \quad \text{. . . . . (1)}$$

the stacking-fault energy of stainless steel was estimated to be ≈ 13 erg cm^{-2}. The authors have determined stacking-fault energies in a number of alloys by this method.

§ 2. Accuracy of Stacking-fault Energies Deduced from Measurements of Dislocation Nodes

Before describing the results obtained, some discussion of the limitations of eqn. (1) should be given. The line tension T of a dislocation depends on its character, i.e. on its edge and screw components and also on its configuration. It is only approximately described by the formula $Gb_1^2/2$ and a more accurate formula (see Friedel 1953) gives

$$T \doteqdot Gb_1^2 \ln (R/b_0)/4\pi K$$

for a dislocation of radius of curvature R, where K has a value of 1 for a pure screw dislocation and $(1-\nu)$ for a pure edge dislocation (ν being Poisson's ratio). b_0 has approximately the magnitude of the Burgers vector of the dislocation. Thus an improved version of eqn. (1) is

$$\gamma = Gb_1^2 \ln (R/b_1)/4\pi KR. \quad \text{. . . . . (2)}$$

The most serious error in eqn. (2) is probably that it neglects the stresses on the partial dislocation αB at A (fig. 1) due to the other partial dislocations αC and Dα. At present there is no precise calculation of the effect of these stresses although computations are in progress (Bilby *et al.* 1960). It is possible however to make some estimates of the error involved in applying eqn. (2). The stress at A due to the two dislocations αC and Dα will certainly be considerably less than that due to a long straight partial dislocation at a distance AB (fig. 1) from A. Since in practice AB $\approx R/2$ this indicates that the force of repulsion on αB due to αC and Dα is less than $Gb_1^2/2\pi R$. The values of stacking-fault energy derived from formula (2) might therefore have to be increased by a factor of up to 1·3. An alternative estimate of the error can be obtained by replacing the two dislocations αC and Dα by dislocation loops of radius R. The stress at A from such loops has been calculated using the formulae given by Kröner (1958) with some corrections pointed out by Kroupa (private communication) and indicates that the values of stacking-fault energy obtained from (2) should be multiplied by about 1·1. This second result probably underestimates the effect but is thought to be the more accurate of the two correction factors.

The effect of external stresses on the node will also give rise to an error in eqn. (2) and can only be minimized by confining the measurements to reasonably symmetrical nodes not too close to other dislocations. (Some asymmetry will usually be present because the nodes are almost always observed in projection.)

Further errors in the determination of R could result from contrast effects since the image of a dislocation does not necessarily coincide with the dislocation (Hirsch *et al.* 1960). However, nodes are usually observed in fairly thick foils near the Bragg diffracting position for a low-order reflection and under these conditions the dislocation and its image are nearly coincident (Howie and Whelan, to be published) and the error in measuring R is not more than ~20 Å, i.e. about 10% for the smallest nodes observed.

§ 3. EXPERIMENTAL RESULTS

Stacking-fault energies have been measured for several compositions of the primary solid solutions of copper and silver base alloys containing aluminium or zinc and also for the f.c.c. nickel–cobalt alloys near the transformation composition. The nickel–cobalt alloys were donated in sheet form by the Mond Nickel Co. Ltd. The other alloys which were made in the laboratory were homogenized and rolled into sheet 250 μ thick between several annealing treatments in an argon atmosphere. All the alloys were analysed by Johnson Matthey and Co. Ltd. after the final annealing treatment. The annealed sheet was then lightly deformed and electro-thinned for examination in the electron microscope. The electro-polishing solutions and conditions used in the final thinning process are shown in table 1.

Table 1

Alloy	Electrolyte	Voltage	Temperature
Cu + Zn Cu + Al	35% HNO_3 in methyl alcohol	9–15	−20°c
Ag + Zn	6 g KCN in 100 cm³ water	6–8	20°c
Ag + Al	70% ethyl alcohol 20% perchloric acid 10% glycerol	20–40	−30°c
Ni + Co	80% ethyl alcohol 20% perchloric acid	6–8	0°c

Electron micrographs of several symmetrical isolated dislocation nodes were then obtained for each alloy using the Siemens Elmiskop I electron microscope operating at 100 kv. Examples are given in figs. 5 and 6. The projected radii of curvature R' of the partial dislocations at each node were then measured and whenever possible corrected for inclination to give the true radius of curvature R from the formula

$$R = R' \sec^2\theta\,(\cos^2\alpha + \cos^2\theta\sin^2\alpha)^{3/2}$$

where θ is the angle between the electron beam and the normal to the plane containing the node and α is the observed angle between the line of intersection of this plane with the foil surface and the normal to the partial dislocation at the point of measurement. The angles θ and α were calculated from selected area diffraction measurements. For metals in which the nodes are small ($R \lesssim 400$ Å) the dislocation arrangement is irregular and it is often impossible to be certain of the slip plane on which the nodes lie and hence to correct for the inclination. However, the correction factor is sometimes greater and sometimes less than unity and it does not seem probable that there is any large systematic error caused by ignoring it in these cases.

Fig. 2

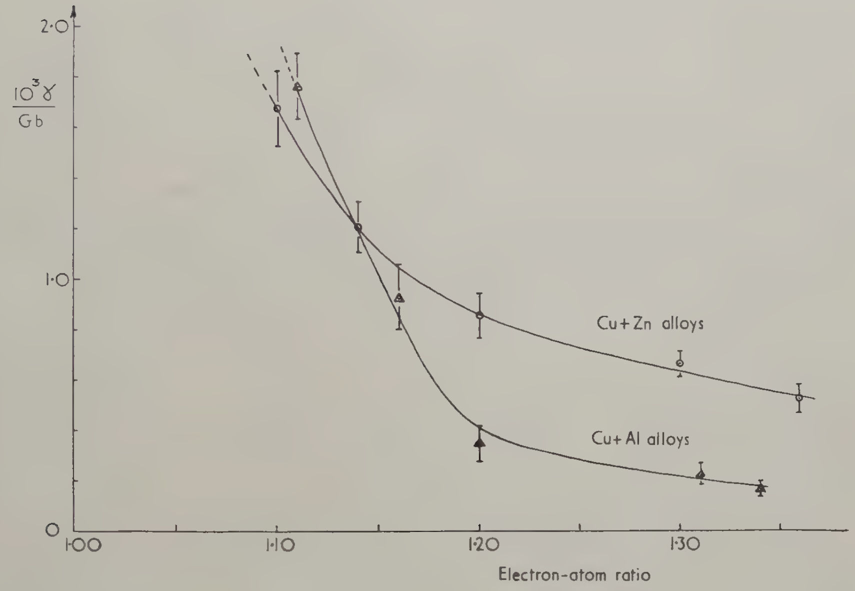

Stacking-fault energy in units of 10^{-3} *Gb* for Cu + Al and Cu + Zn alloys plotted against electron-atom ratio. For pure Cu, $10^{-3}\,Gb \approx 10{\cdot}5$ erg cm^{-2}.

The stacking-fault energy of each alloy has been calculated on the basis of at least ten different measurements. Since the values of the shear modulus G vary somewhat with alloy composition, the stacking fault energies are given in units of 10^{-3} *Gb* where **b** is the Burgers vector of a whole dislocation. Using the values of shear modulus quoted by Seeger *et al.* (1959), the quantity 10^{-3} *Gb* is found to be equal to 10·5, 7·1 and 18·6 erg cm^{-2} for pure copper, silver and nickel respectively. The results for the five alloys are given in tables 2–6 and are plotted

Fig. 3

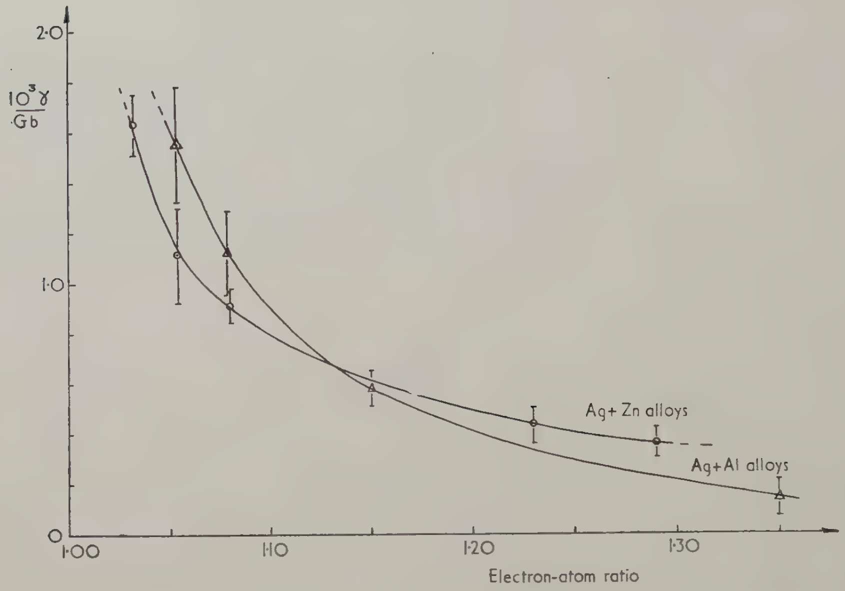

Stacking-fault energy in units of 10^{-3} Gb for Ag + Al and Ag + Zn alloys plotted against electron-atom ratio. For pure Ag, 10^{-3} $Gb \approx 7{\cdot}1$ erg cm^{-2}.

Fig. 4

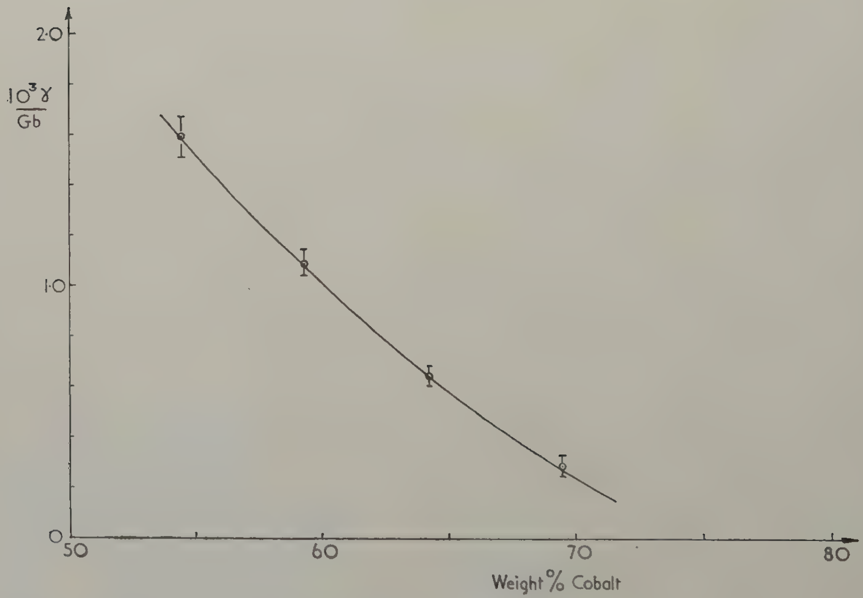

Stacking-fault energy in units of 10^{-3} Gb for Ni + Co alloys plotted against weight % Co. For pure Ni, 10^{-3} $Gb \approx 18{\cdot}6$ erg cm^{-2}.

against electron-atom ratio (or composition in the case of the nickel–cobalt alloy) in figs. 2, 3 and 4. Since no preferred orientation of the nodes in the slip plane was observed, an average value of ·5/6 for K (eqn. (2)) was employed throughout.

Table 2. Cu + Zn alloys (maximum total impurity content 0·08%)

Wt. % Zn	10·25	14·37	20·00	30·44	36·82
Electron-atom ratio	1·10	1·14	1·20	1·30	1·36
$10^3\,\gamma/Gb$	1·68 ± 0·15	1·21 ± 0·10	0·86 ± 0·09	0·67 ± 0·05	0·53 ± 0·06

Table 3. Cu + Al alloys (maximum total impurity content 0·1%)

Wt. % Al	2·25	3·53	4·55	7·27	8·05
Electron-atom ratio	1·11	1·16	1·20	1·31	1·34
$10^3\,\gamma/Gb$	1·77 ± 0·13	0·93 ± 0·13	0·35 ± 0·07	0·23 ± 0·04	0·17 ± 0·03

Table 4. Ag + Zn alloys (maximum total impurity content 0·08%)

Wt. % Zn	1·94	3·30	5·00	15·00	20·00
Electron-atom ratio	1·032	1·054	1·08	1·23	1·29
$10^3\,\gamma/Gb$	1·63 ± 0·12	1·11 ± 0·19	0·91 ± 0·07	0·53 ± 0·07	0·36 ± 0·06

Table 5. Ag + Al alloys (maximum total impurity content 0·08%)

Wt. % Al	0·69	1·00	2·00	5·00
Electron-atom ratio	1·054	1·078	1·15	1·35
$10^3\,\gamma/Gb$	1·55 ± 0·23	1·12 ± 0·17	0·58 ± 0·07	0·14 ± 0·07

Table 6. Ni + Co alloys (maximum total impurity content 0·10%)

Wt. % Co	54·50	59·40	64·29	69·48
$10^3\,\gamma/Gb$	1·59 ± 0·80	1·09 ± 0·05	0·64 ± 0·04	0·29 ± 0·03

§ 4. Discussion

4.1. *Values of Stacking-fault Energy*

There is as yet no complete calculation of the stacking-fault energy of any metal or any theory of its dependence on composition for any alloy system. It is possible however, and convenient for the subsequent discussion, to list the various contributions to the stacking-fault energy.

4.1.1. *Energy of nearest-neighbour interactions at the fault*

As a result of the different arrangement of neighbours round the atoms on the fault compared with the other atoms in the crystal there will be a change in energy of the core electrons leading to a change in the total energy of the crystal.

4.1.2. *Energy due to scattering of conduction electrons*

The fact that stacking faults strongly reflect conduction electrons has recently been convincingly demonstrated (Cotterill, to be published) by measurements of the increase in resistivity due to the presence of tetrahedra of stacking faults observed in quenched gold (Silcox and Hirsch 1959). Attree and Plaskett (1956) have calculated the stacking-fault energy due to this scattering in a monovalent metal with almost-free conduction electrons and find that part of the energy comes from the electrons which are reflected by the stacking fault and part from electrons which are localized in surface states (Tamm waves) on either side of the fault.

The results of figs. 2 and 3 show that the addition of zinc or aluminium to either copper or silver lowers the stacking-fault energy and that for low solute-content alloys the stacking-fault energy depends mainly on the number of valence electrons in the alloy. This implies that it is the energy contribution due to the scattering of the conduction electrons which decreases with increasing number of valence electrons. It is also striking that the slope of the curves for the copper and silver alloys should be similar in this region and this suggests, in agreement with recent experimental results for the pure metals (Shoenberg 1960), that the conduction electrons in these copper and silver alloys behave similarly.

The similar slopes of the curves of figs. 2 and 3 in the region of low solute-content enable us to estimate with more confidence than would otherwise be the case that the stacking-fault energies of copper and silver are in the vicinity of 40 erg cm^{-2} and 25 erg cm^{-2} respectively. This value for copper agrees well with Fullman's estimate quoted earlier. From fig. 4 we estimate that the stacking-fault energy of nickel is about 150 erg cm^{-2}. Although these stacking-fault energies can only be regarded as rough estimates it does not seem possible to reconcile them with the figures of 169 erg cm^{-2}, 43 erg cm^{-2} and 410 erg cm^{-2} quoted for copper, silver and nickel respectively by Seeger *et al.* (1959). Even when full allowance is made in our results for systematic errors of the type discussed in § 2 it does not seem probable that the figure for copper can be much higher than 60 erg cm^{-2}. The curves of fig. 2 would have to rise very steeply indeed for low solute-content alloys.

It does also seem probable that the method of estimating stacking-fault energies by observing whether loops or tetrahedra are formed on quenching is in error when based on simple energy considerations for defects of a given size. This method led to the high figure noted above for copper and also to an estimate of stacking-fault energy for Ni + 60% Co alloy of between 5 and 7×10^{-3} *Gb* (Mader and Simsch 1961). Both of these figures exceed our results by a factor of about 5 and it therefore appears that for some reason, probably connected with the rate of formation or shape of the dislocation loop, that the change to the tetrahedral configuration of stacking faults does not occur even though it is energetically favourable.

In the case of the nickel–cobalt alloys where an f.c.c. → h.c.p. transition occurs (at about 75% Co at room temperature) the stacking-fault energy is directly related to the phase change and must pass through zero at this composition, becoming negative for alloys of higher cobalt content. The curve of fig. 4 would indeed appear to extrapolate to zero at this composition. No such simple considerations apply to the copper and silver alloys since beyond the solid solution limit (at an electron-atom ratio between 1·36 and 1·41 in all cases) complex phases are formed. It is possible of course that stacking faults act as nuclei for these new phases and that the stacking-fault energy plays some role in the transition but at present we have no evidence of this. In the case of all the copper and silver alloys, however, hexagonal phases are eventually formed at still higher solute contents so that the stacking-fault energy can still be related to the relative stability of the f.c.c. and h.c.p. structures.

4.2. *Segregation Effects*

The dependence of stacking-fault energy on composition implies a chemical interaction between the solute atoms and the stacking fault so that the question of segregation of solute atoms to the fault must be considered. Segregation of this type was first proposed by Suzuki (1952) to explain the initial yield points of various alloys and has been analysed further in this connection by Suzuki (1956) and Flinn (1958). It has also been suggested as a possible explanation of various other yield and strain-rate phenomena observed during the deformation of alloy crystals (see for example Bolling 1959). Such a hypothesis however implies that segregation can take place at temperatures well below those at which solute diffusion by the usual process of the creation and migration of vacancies is operative. Thus, although there is no doubt that segregation will tend to take place in principle, the interesting questions of how and at what temperature it occurs are still unanswered.

All the measurements of stacking-fault energy reported here refer to specimens deformed at room temperature with no subsequent heat treatment. The authors have carried out several experiments to investigate the effects of such treatment on the size of the nodes. Ageing at 250°C for periods of 1 hour (after deformation at room temperature) produced no effect in any of the alloys studied (Cu + 7% Al, Cu + 4·5% Al, Cu + 30% Zn, Ni + 55% Co, Ni + 60% Co). In the case of the copper-aluminium alloys this result is in strong disagreement with the recent suggestion by Cahn and Davies (1960) (on the basis of x-ray small angle scattering results) that segregation takes place in these alloys at a temperature of about 200°C. Ageing experiments with the same five alloys were also carried out for times of between a few minutes and 1 hour at temperatures of 450°C and only in the case of the Cu + 7% Al alloy was any effect observed. With this alloy the nodes were observed to be smaller, indicating that the stacking-fault energy had risen during the ageing treatment from about 1·5 erg cm^{-2} to 5 erg cm^{-2}. This change was observed in specimens furnace cooled from 450°C and in specimens of the alloy quenched from 450°C. A possible interpretation is that solute atoms (already segregated at the fault) are leaving the fault for entropy reasons. However, there is no explanation for the absence of the effect in the other alloys and the observation that the specimens, for which the node size changed, showed a tendency to form pits during electropolishing was disquieting.

The apparent non-occurrence of segregation in the other copper alloys (Cu + 4·5% Al, Cu + 30% Zn) on ageing at 450°C where solute diffusion by creation and migration of vacancies is easy suggests that either segregation has already taken place at room temperature or else that the force of attraction between the solute atom and the fault is weak. Possible alternative processes of solute diffusion are:

(*a*) Diffusion involving the migration of single vacancies created during the deformation.

(*b*) Diffusion involving the migration of divacancies or other vacancy complexes created during the deformation.

(*c*) Diffusion of interstitial solute atoms created during the deformation.

(*d*) Pipe diffusion along dislocations. (It seems unlikely that this process would be an effective way of transferring solute atoms from the matrix to the vicinity of the stacking faults.)

In copper where E_m, the activation energy for vacancy migration, is quoted as 0·7 ± 0·1 ev (Kimura *et al.* 1959) segregation by process (*a*) could readily occur even at 0°C since a vacancy would make several jumps per second. It seems fairly improbable however that this process could be responsible for segregation at 0°C in nickel since even if E_m is as low as 1·0 ev (Sosin and Brinkman 1959) several hours would be needed for each jump and many of the specimens were examined in the microscope only 30 min after deformation. It therefore appears that process (*a*) can almost certainly be eliminated as a segregation mechanism in nickel since it would not be effective at the temperature of deformation and no segregation effects were observed even at higher temperatures. Segregation by process (*a*) may be ruled out in the case of copper and silver as well if we make the simplifying assumption that segregation occurs by the same mechanism in all the alloys.

We may conclude therefore, that although the possibility of segregation of solute atoms to stacking faults at room temperature or below still exists, it is unlikely to occur by any process involving the migration of single vacancies. If segregation does not occur at these temperatures we can conclude that solute atoms are only weakly attracted to stacking faults since it does not occur at higher temperatures either. A definite conclusion about the possibility of room temperature segregation could perhaps be reached if stacking-fault energies were measured after deformation at low temperatures without ageing at room temperature.

§ 5. CONCLUSIONS

By measuring the radius of curvature of extended dislocation nodes formed during deformation the stacking-fault energies have been determined for the solid solutions of aluminium and zinc in copper and silver and also for nickel–cobalt alloys over a range of compositions. The results suggest that the stacking-fault energies of copper, silver and nickel are about 40, 25 and 150 erg cm^{-2} respectively. The method is a powerful and direct way of measuring stacking-fault energies (provided they are not too high) and it should be possible to use it to obtain information about many other alloy systems. In practice, nodes with radii of curvature in the range 200 Å–4000 Å (or much more if the node lies in the plane of the foil) can be measured.

It is not known at present whether segregation of solute atoms to the stacking faults takes place or not, but the experiments suggest that if it does not occur at room temperature, then it does not occur at all, even at temperatures where diffusion of solute atoms can take place. Further experiments (particularly at low temperatures) are needed to settle this question.

ACKNOWLEDGMENTS

The authors are indebted to Professor N. F. Mott, F.R.S., Professor A. H. Cottrell, F.R.S. and to Dr. W. H. Taylor for their interest and encouragement and also to Professor J. Nutting, Dr. P. B. Hirsch and a number of colleagues for valuable advice and criticism. The gift of the nickel–cobalt alloys by the Mond Nickel Co. Ltd. is gratefully acknowledged. A. Howie thanks the Masters and Fellows of Trinity College for a Research Scholarship and the Masters and Fellows of Churchill College and I.C.I. Ltd. for Research Fellowships. P. R. Swann thanks I.C.I. Ltd. for a Research Grant.

REFERENCES

ATTREE, R. W., and PLASKETT, J. S., 1956, *Phil. Mag.*, **1,** 885.
BASINSKI, Z. S., 1959, *Phil. Mag.*, **4,** 393.
BILBY, B. A., GRINBERG, A., and SWINDEN, K. H., 1960, *Acta cryst.*, **13,** 1118.
BOLLING, G. F., 1959, *Phil. Mag.*, **4,** 537.
CAHN, R. W., and DAVIES, R. G., 1960, *Phil. Mag.*, **5,** 1119.
CHRISTIAN, J. W., and SPREADBOROUGH, J., 1957, *Proc. phys. Soc., Lond.* B, **70,** 1151.
FLINN, P. A., 1958, *Acta Met.*, **6,** 631.
FRIEDEL, J., 1953, *Les Dislocations* (Paris: Gauthier-Villars), p. 22.
FULLMAN, R., 1951, *J. appl. Phys.*, **22,** 448.
HEIDENREICH, R. D., and SHOCKLEY, W., 1948, *Report on Conference on Strength Solids* (London: The Physical Society), p. 57.
HIRSCH, P. B., 1959, *Internal Stresses and Fatigue in Metals* (New York: Elsevier), p. 139.
HIRSCH, P. B., HOWIE, A., and WHELAN, M. J., 1960, *Phil. Trans.* A, **252,** 499.
KIMURA, H., MADDIN, R., and KUHLMANN-WILSDORF, D., 1959, *Acta Met.*, **7,** 154.
KRÖNER, E., 1958, *Kontinuumstheorie der Versetzungen und Eigenspannungen* (Berlin: Springer), p. 164.
MADER, S., and SIMSCH, E., 1961, *Proceedings of the European Regional Conference on Electron Microscopy*, **1**, 379 (Delft: De Nederlandse Vereniging Voor Electronenmicroscopie).
SEEGER, A., 1956, *Dislocations and Mechanical Properties of Crystals* (New York: Wiley), p. 243.
SEEGER, A., BERNER, R., and WOLF, H., 1959, *Z. Phys.*, **155,** 247.
SHOENBERG, D., 1960, *Phil. Mag.*, **5,** 105.
SOSIN, A., and BRINKMAN, J. A., 1959, *Acta Met.*, **7,** 478.
SILCOX, J., and HIRSCH, P. B., 1959, *Phil. Mag.*, **4,** 72.
SUZUKI, H., 1952, *Sci. Rep. Inst. Tohoku Univ.* A, **4,** 455: 1956, *Dislocations and Mechanical Properties of Crystals* (New York: Wiley), p. 361.
THORNTON, P. R., and HIRSCH, P. B., 1958, *Phil. Mag.*, **3,** 738.
WHELAN, M. J., 1959, *Proc. roy. Soc.* A, **249,** 114.
WHELAN, M. J., HIRSCH, P. B., HORNE, R. W., and BOLLMANN, W., 1957, *Proc. roy. Soc.* A, **240,** 524.

The Occurrence of Dislocations in Crystals Grown from the Melt†

By S. Howe and C. Elbaum
Physics Department, Metals Research Laboratory,
Brown University, Providence, Rhode Island

[Received February 6, 1961]

Abstract

Single crystals of aluminium were grown by the Czochralski method at various rates. The crystals were carrot-shaped, about 4 cm long, tapering from a diameter of about 3 mm at the top to about 0·1 mm at the bottom. X-ray diffraction micrographs were taken of these specimens by means of Lang's technique, which is capable of revealing the dislocation structure in the interior of a crystal. It was found that the density of dislocations present in an as-grown crystal increases with both increasing diameter and rate of growth. For sufficiently small diameters (below about 0·3 mm) it was possible to grow crystals free of detectable dislocations. These experimental results are consistent with the idea that the majority of the initial dislocations are produced by the collapse of vacancy discs that are nucleated when a sufficient supersaturation of vacancies is reached in the crystal. Theoretical calculations of the supersaturation of vacancies that arise during crystal growth were made by considering the diffusion of these imperfections in a specimen cooled from the melting temperature. It is shown that the range of diameters below which the vacancy supersaturation is too small to nucleate a dislocation is of the same order of magnitude as the diameters of crystals found that contain no detectable dislocations.

§ 1. Introduction

Dislocations do not exist in thermal equilibrium with respect to any conceivable sources and sinks in a crystal, particularly with respect to external surfaces. It is therefore necessary to think of their occurrence in terms of kinetic mechanisms that would operate during growth. Five reasonable mechanisms have been proposed (Elbaum 1959):

(1) Propagation of dislocations into the growing crystal from the seed crystal.

(2) Shear strains arising from thermal strains or external mechanical constraints.

(3) Shear strains resulting from abrupt change in composition accompanied by changes in lattice parameter.

(4) Dendritic growth.

(5) The mechanism of collapsing vacancy discs.

---

† This work was sponsored by the Office of Naval Research under Contract No. Nonr 562(27).

By a judicious choice of growth technique and the use of high purity material, the effects of some of these mechanisms may be minimized. A study will be described in this paper of the mechanism of collapsing vacancy discs, as it is thought to be fundamentally the most important in creating dislocations in metal crystals grown from the melt.

§ 2. COLLAPSING VACANCY DISCS

In a crystal at its melting point, a certain number or vacancies exist in equilibrium with external surfaces and any other sources or sinks (such as dislocations) that may be present. Let us consider a cylindrical aluminium crystal whose only source and sink for vacancies is the external surface; no dislocations are assumed to be present. The concentration of vacancies in equilibrium with the surface, at the melting temperature, is given by

$$c_0 \cong \exp(-U_f/RT_0) \quad . \quad . \quad . \quad . \quad . \quad . \quad . \quad . \quad (1)$$

where U_f is the energy of formation of a vacancy (17 500 cal/mole (Bradshaw and Pearson 1957)) and T_0 ($=933$°K) is the melting temperature. If the temperature is suddenly lowered to $T_1 < T_0$, eqn. (1) states that a concentration of vacancies c_1 should now be in equilibrium with the surface. Since $c_1 < c_0$ it is apparent that at the instant the temperature is lowered, the concentration of vacancies in the crystal is greater than the new equilibrium value. The surface is now a sink for the excess vacancies which will begin migrating towards it. In a time t, vacancies will travel an approximate distance

$$x \simeq \sqrt{(Dt)} \quad . \quad . \quad . \quad . \quad . \quad . \quad . \quad . \quad . \quad (2)$$

where D is the diffusion coefficient for vacancies. Thus, the concentration of vacancies in the crystal will begin to approach the equilibrium value. It is apparent that if the crystal is large, or if D is very small ($D = D_0 \exp(-U_m/RT)$ where U_m is the activation energy for migration of vacancies) as will be the case if T_1 is rather low, then all of the excess vacancies in the centre of the crystal will not be able to reach the surface in a reasonably short time. In this case there will exist a supersaturation of vacancies in the crystal, of magnitude c_0/c_1. If other vacancy sinks are present, of course (such as dislocations), they may be able to reduce the vacancy supersaturation by absorbing the excess vacancies.

Frank (1950) was one of the first to describe how vacancies in supersaturation in a crystal could condense to form dislocation loops in crystals. Hitherto, the most direct support of the mechanism came from the experiments of Hirsch *et al.* (1958), who obtained electron micrographs of polycrystalline aluminium foils 0·075 mm thick quenched from 600°C into iced brine and then thinned by electropolishing; their pictures reveal many small dislocation loops.

It is difficult to determine from thermodynamic considerations the vacancy supersaturation needed to nucleate a vacancy disc, for the uncertainty in the difference between the free energies of a vacancy disc and a vacancy sphere is as great as or greater than the uncertainty in the value of the disc's surface energy. Once a vacancy disc has formed and collapsed to form a dislocation ring (Schoeck and Tiller 1960 show that a vacancy disc of radius $5\mathbf{b}$ or more may be considered to have collapsed), it is then possible to calculate the supersaturation necessary to keep the dislocation climbing. Since all dislocations formed by this mechanism must go through this early stage of growth, a lower limit can be obtained for the necessary vacancy supersaturation. The supersaturation that exists on cooling from a temperature T_0 to a lower temperature T_1 is given by

$$c_0/c_1=\exp\left[-\frac{U_f}{k}\left(\frac{1}{T_0}-\frac{1}{T_1}\right)\right]. \qquad (3)$$

The assumption made here is that the equilibrium concentration of vacancies with respect to external surfaces, c_0, that obtained at the melting point T_0 is frozen in; this estimate is, of course, an upper limit. Elbaum (1960) used the expression

$$\ln\frac{c_0}{c_1}=\frac{G\mathbf{b}^4}{4\pi(1-2\nu)rkT_1}\ln\left(\frac{r}{\mathbf{b}}+1\cdot 6\right)+\frac{1}{1+1\cdot 6\mathbf{b}/r} \qquad (4)$$

for the supersaturation of vacancies required to nucleate a dislocation loop of radius r. G is the shear modulus, ν is Poisson's ratio, k is Boltzmann's constant. $\mathbf{b}$ is the Burgers vector and T_1 is the temperature at which a concentration of vacancies c_1 is in thermal equilibrium with the external surface; T_1 (and thus c_1) is a function of r. Taking into account the temperature variation of the dislocation strain energy and expressing r in Burgers vectors, Elbaum (1960) finally derived an expression for the critical temperature T_c at which the vacancy supersaturation is great enough to form a dislocation loop of radius r:

$$T_c=\frac{1-\dfrac{A(G\mathbf{b}^3)_{T_R}}{U_f}(1+300(\beta+3\alpha))}{\dfrac{1}{T_0}+\dfrac{A(G\mathbf{b}^3)_{T_R}}{U_f}(\beta+3\alpha)} \qquad (5)$$

where A is a numerical factor that depends on the value chosen for r, and $(G\mathbf{b}^3)_{T_R}$ (which varies approximately as the strain energy per atomic plane of a dislocation) is taken at $T_R=300°\text{K}$. β is the temperature coefficient of the shear modulus (which is considered to decrease with temperature) and α is the linear coefficient of thermal expansion.

Elbaum (1960) made estimates of the maximum size to which a loop can grow once it has formed for a given value of the ratio of the temperature drop from the melting point, T_0-T_c, to the melting point, T_0, for several elements. The maximum size of a loop, $r_{\max}$, calculated by the above method, is so large for the case of aluminium that the actual size of dislocation loops originating from collapsed discs will not be determined by $r_{\max}$. The size will probably depend on the presence of other vacancy sinks in the crystal, in particular, on the presence of other dislocations. On the other hand, in the case of silicon and germanium, the values of $r_{\max}$ are so small that dislocations produced by collapsing vacancy discs will not attain sizes visible in an optical microscope. This suggests a reason why Dash (1958, 1959) was able to grow crystals essentially free of detectable dislocations.

In aluminium, the critical temperature T_c for a dislocation loop of radius $5\mathbf{b}$ to grow is 778°K. Substituting this value of T_c for T_1 in eqn. (3) yields a minimum vacancy supersaturation in the crystal of 6·6. Allowing for errors in the calculations of the minimum size of a dislocation loop (since there are uncertainties in the value of the surface energy of a vacancy disc), one may say that the minimum supersaturation required to nucleate a dislocation by the process of vacancy disc collapse is somewhat less than 10. The next step in showing that the collapsing vacancy disc mechanism is indeed possible is to calculate the vacancy supersaturation that exists in a crystal as it is cooled from the melting point, and thus obtain a lower limit to the diameter of a crystal for which no such supersaturation could be built up.

It is therefore desired to study the distribution of vacancies in a cylindrical aluminium crystal of radius A, whose temperature is lowered from the melting point T_0 to a lower temperature T according to some function of time.

The diffusion coefficient D is assumed to be a function of temperature only (and thus of time only) and not a function of concentration (this assumption is justified by the small overall concentration of vacancies). It is assumed that at any instant of time the temperature is the same throughout the crystal; that is, there are no temperature gradients. The initial concentration of vacancies in the crystal (when the temperature is T_0) is that which corresponds to equilibrium with the external surface; no other vacancy sources or sinks are assumed present. Thus, $c_0 = \exp(-U_f/RT_0)$, where c_0 is the equilibrium concentration of vacancies at T_0, U_f is the energy for formation of vacancies and R is the universal gas constant. As the temperature decreases with time in some fashion, the concentration of vacancies at the surface of the crystal is always assumed to be equal to the equilibrium value at the particular instantaneous temperature prevailing, or,

$$c(A, t) = c_A(t) = \exp(-U_f/RT). \quad . \quad . \quad . \quad . \quad (6)$$

The concentration of vacancies in the crystal as a function of distance from the origin and of time, for a given radius A for the above boundary conditions is the particular solution of the differential equation controlling the diffusion process. This equation, known as Fick's second law, may be written in cylindrical coordinates:

$$\frac{\partial c(r, t)}{\partial t} = D(t) \frac{\partial^2 c(r, t)}{\partial r^2} + \frac{1}{r} \cdot \frac{\partial c(r, t)}{\partial r}, \quad 0 \leqslant r \leqslant A \quad . \quad (7)$$

subject to the boundary conditions

$$\left.\begin{array}{lll} c(A,t)=c_A(t) & r=A, & t>0, \\ c(r,0)=c_0 & 0\leqslant r\leqslant A, & t=0. \end{array}\right\} \quad \ldots \quad (8)$$

The most likely functional dependence of temperature on time for crystal growth would be a relation of the form

$$T=T_0\exp(-\beta t) \quad \ldots \quad (9)$$

where T_0 is the melting temperature, t is the time and β is a coefficient that depends on the cooling rate. It was estimated that in 400 sec the temperature of the cylinder drops from 933°K (melting point of aluminium) to 588°K, a temperature at which the diffusion rate has dropped to a fairly low value; this yields a value of $\beta=1{\cdot}15\times10^{-3}\,\text{sec}^{-1}$.

An analytical approach to the solution was attempted, but with the temperature–time variation of eqn. (9), eqn. (7) could not be integrated in closed form. A linear temperature variation of the form $T=T_0-\beta' t$ was tried; eqn. (7) could still not be solved unless it was assumed that $U_\text{f}/U_\text{m}=2$, when it is, in reality 1·75 (Bradshaw and Pearson 1957). In view of all the assumptions made, it was decided that the analytical solution finally obtained was not a valid representation of the actual distribution of vacancies in a crystal cooled from the melting temperature. A finite difference solution was then evaluated in which the correct temperature–time relation was used with no further assumptions. These equations were solved using the IBM 7070 computer. The supersaturation of vacancies that exists in crystals of various diameters cooled from the melting temperature are plotted in figs. 1, 2 and 3† as a function of distance from the centre of the crystal expressed in fractions of a radius for various values of D_0 (where the diffusion coefficient $D=D_0\exp(-U_\text{m}/RT)$ and U_m is the activation energy for vacancy migration). D_0 usually lies somewhere between 0·1 and 0·01; its exact value for aluminium is not known. If the minimum supersaturation needed to nucleate a dislocation loop is around 10, then one may define a critical crystal diameter (for the cooling rate assumed) such that the vacancy supersaturation exceeds 10 if $d>d_\text{crit}$ where d is the diameter of the crystal. From figs. 1, 2 and 3 one may see that d_crit lies between 0·5 and 4 mm, depending on the exact value of D_0. If D_0 for aluminium is as low as 0·01, $d_\text{crit}\simeq 0{\cdot}5$ mm.

The above considerations suggest that the mechanism of collapsing vacancy discs is possibly of prime importance in producing dislocations in aluminium. It is apparent that in a crystal, the density of dislocaitons originating from collapsing vacancy discs will be a function of the supersaturation of vacancies that exists in the crystal as it is cooled from the melting temperature. The vacancy supersaturation depends, as has been shown above, on the length of time during which vacancies can move over appreciable distances; for high growth rates involving high cooling

---

† Figures 8–12 are shown as plates.

Fig. 1

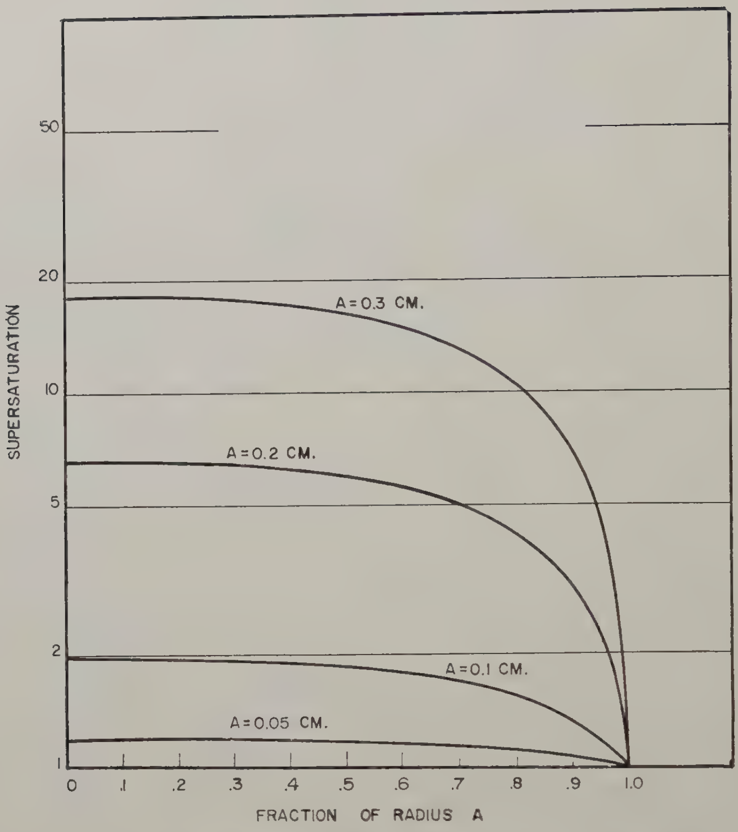

Supersaturation of vacancies in a cylindrical crystal cooled from 933°K to 588°K versus fraction of radius. (Radius of crystal in centimetres written beside each curve.) $D_0 = 1{\cdot}0\ \text{cm}^2\ \text{sec}^{-1}$.

rates, the diffusion coefficient will fall rapidly with falling temperature to a low value, preventing further diffusion. A large crystal diameter also maintains a vacancy supersaturation by not permitting vacancies to escape from the interior to the surface of the crystal before the diffusion rate becomes negligible. The following sections describe experiments wherein the dislocation structure in aluminium crystals grown from the melt by the Czochralski method was studied using an x-ray technique that reveals dislocations in the interior of a crystal.

§ 3. Experimental Procedure

The experiments consisted of two parts: growing the crystals, and examining their structure by means of x-ray diffraction pictures.

Fig. 2

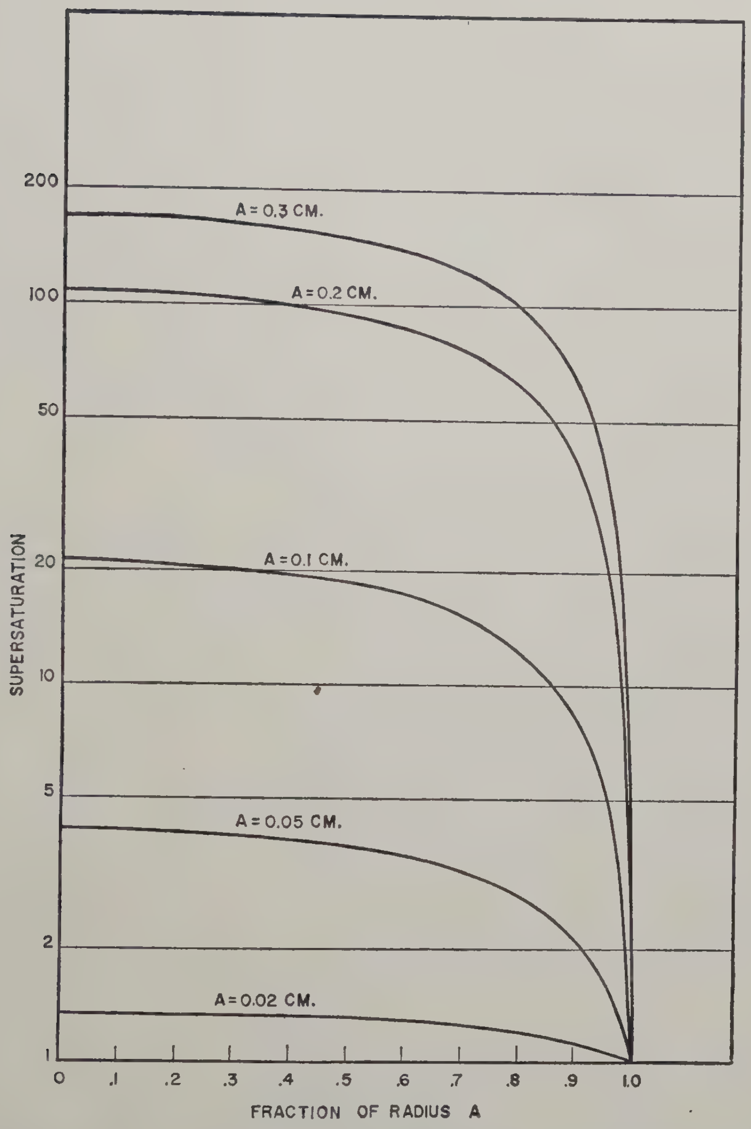

Supersaturation of vacancies in a cylindrical crystal cooled from 933°K to 588°K versus fraction of radius. (Radius of crystal in centimetres written beside each curve.) $D_0 = 0{\cdot}10$ cm^2 sec^{-1}.

3.1. *Growth of Crystals*

The choice of the particular crystal growing technique used in this research was dictated by certain requirements, the most important of which was the minimization of deformation due to constraints arising during

Fig. 3

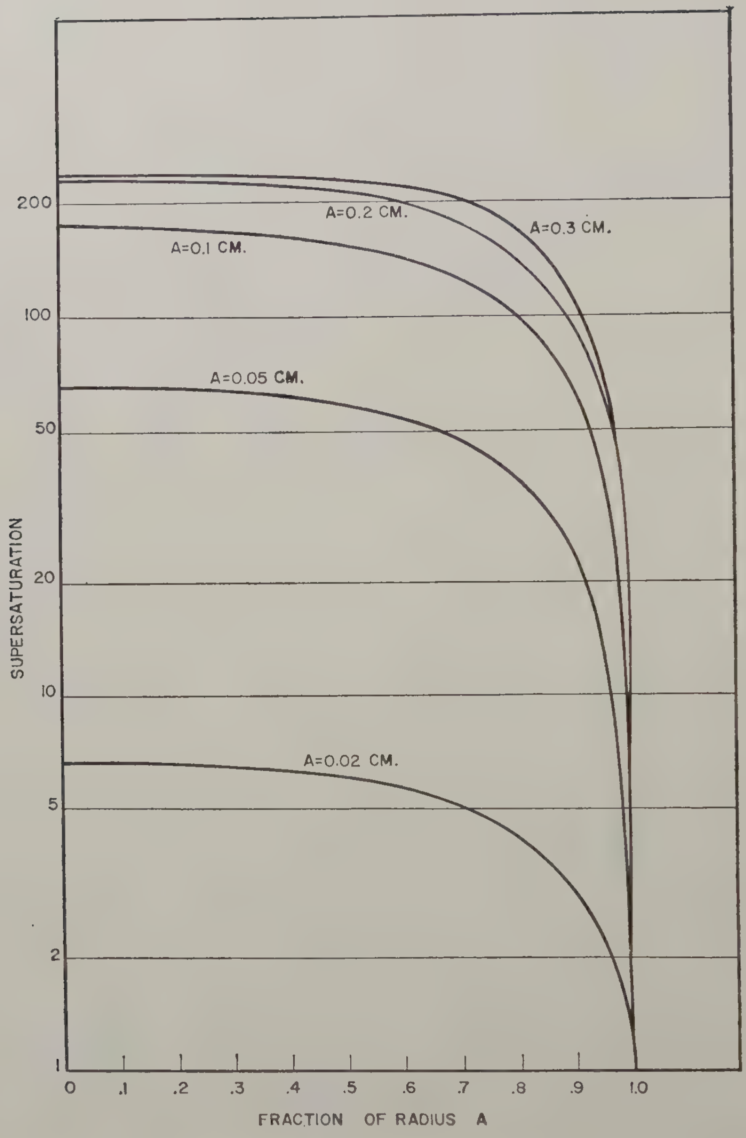

Supersaturation of vacancies in a cylindrical crystal cooled from 933°K to 588°K versus fraction of radius. (Radius of crystal in centimetres written beside each curve.) $D_0=0{\cdot}01$ cm^2 sec^{-1}.

growth, and from handling. This eliminated any form of Bridgman's technique which necessitates solidifying a crystal in a container, and is likely to introduce strains due to the constraint of the container walls. The Czochralski technique was chosen for several reasons: (1) The crystal need never be touched. (2) Control of orientation is easy. (3) The diameter of the crystal can be easily varied.

In order to study the variation of dislocation density with crystal diameter, tapered (carrot-shaped) crystals were grown; this shape could be obtained for a given pulling speed by correctly adjusting the melt temperature. The range of speeds used was from 0·4 mm/min to 5 mm/min; the growth process was performed in a helium atmosphere. The axis of the seed crystal was generally parallel to a $\langle 110 \rangle$ direction; this permitted diffraction from a $\{200\}$, $\{220\}$ and two $\{111\}$ planes. In some cases a random orientation resulted when the oxide layer prevented contact between the molten part of the seed and the melt; in one case a $\langle 111 \rangle$ seed crystal was used. The purities of aluminium used were 99·999% and zone-refined (12 to 13 passes) in order to study the effect of impurities on the dislocation density. In some cases, the specimens were electropolished in 95% methanol–5% perchloric acid cooled in a mixture of methanol–dry ice.

3.2. *X-ray Diffraction Technique*

An x-ray diffraction technique (Lang 1958, 1959) has been developed recently that enables one to see the dislocation structure in the interior of a crystal without damaging the specimen. In order to resolve individual dislocations by this technique the dislocation density must be of the order of 10^5 cm^{-2} or less. In the present set of experiments, molybdenum Kα_1 radiation at a voltage of 40 kv and an intensity of 20 mA was used. Ilford L 4 50 μ nuclear emulsion was employed to record the dislocation structure; with this film, the diffracted image could be magnified up to 80 × without a loss of detail. The dislocations appear in the diffraction image as dark areas or lines on a lighter background. This effect arises from an enhancement of diffracted intensity from a small volume surrounding the dislocation. Dislocation densities were determined by counting the number of dislocations in a given region of a crystal and dividing this number by the area. The dislocation density was then plotted against diameter and rate of growth.

§ 4. RESULTS

Figures 4 and 5 show dislocation density plotted against rate of growth (with the thickness of the crystal written beside each point) for the two purities of aluminium used; both curves show that the dislocation density rises with increasing rate of growth. The actual values of the dislocation densities are not too meaningful; more significant is the rising trend of the curves. There is probably an error of perhaps a factor of two or three in the number of dislocations counted, due to clustering (where estimates had to be made of the number of discernible dislocations) and poor resolution. However, the relative error in counts from one area to another of a given crystal or from one crystal to another is quite small, and was

Fig. 4

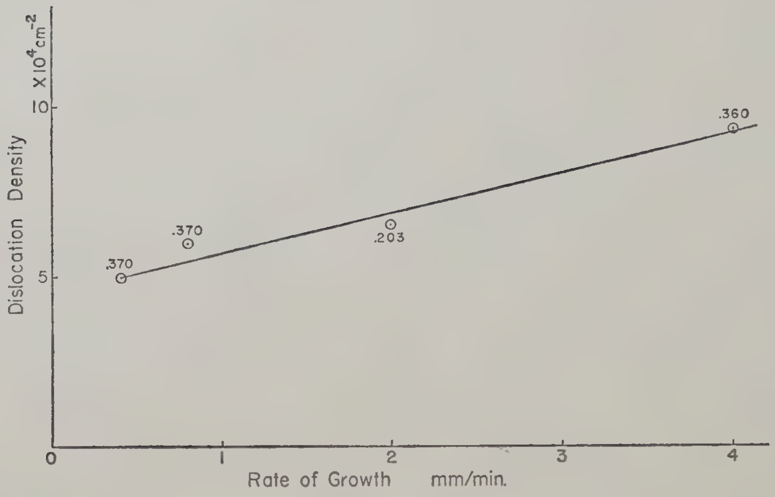

Plot of dislocation density versus rate of growth. Purity: 99·999% Al. (Diameter of crystal in millimetres written beside each point.)

Fig. 5

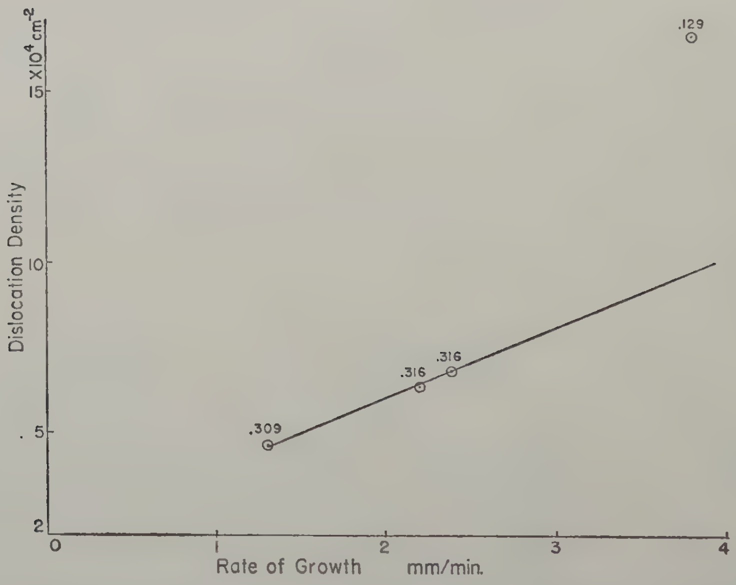

Plot of dislocation density versus rate of growth. Purity: zone-refined Al. (Diameter of crystal in millimetres written beside each point.)

Fig. 6

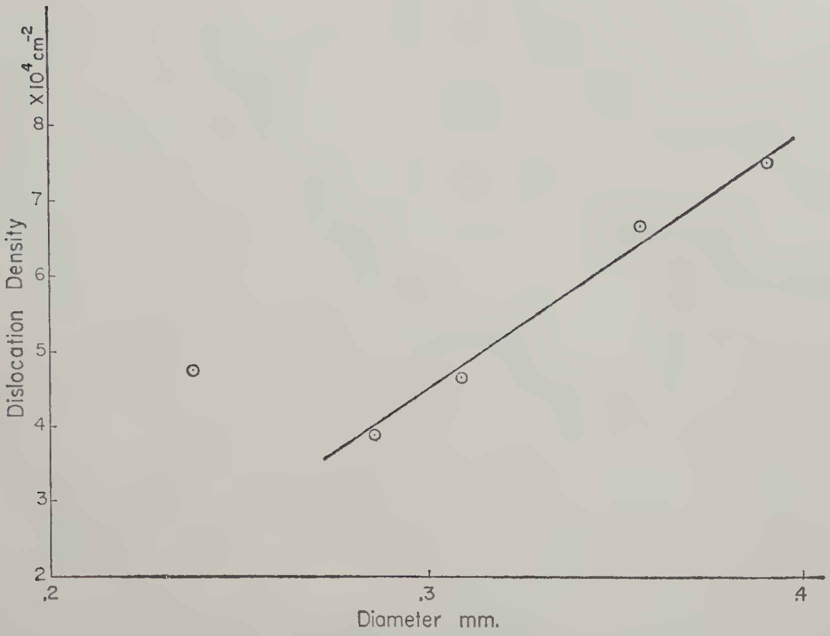

Plot of dislocation density versus crystal diameter. Purity: zone-refined Al. Rate of growth: 1·3 mm/min.

Fig. 7

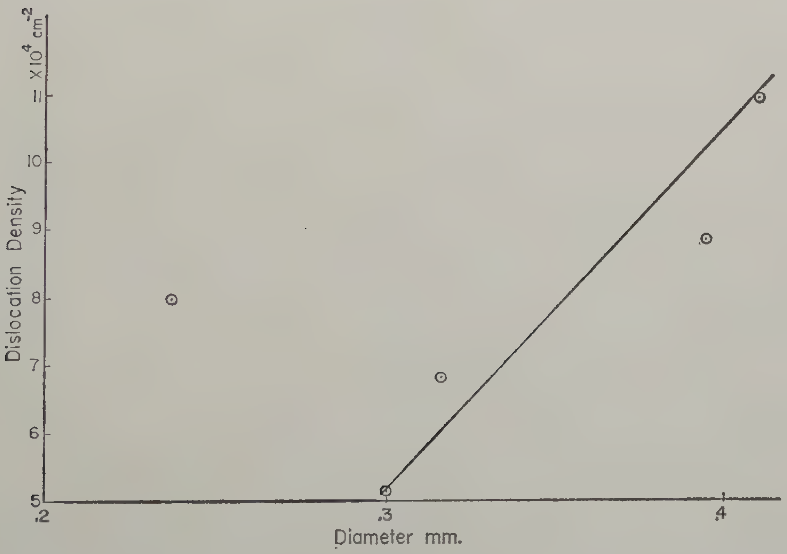

Plot of dislocation density versus crystal diameter. Purity: zone-refined Al. Rate of growth: 2·4 mm/min.

determined by having different individuals count the same area (this error is about 10% or less).

Figures 6 and 7 show dislocation density versus thickness for two rates of growth of zone-refined aluminium crystals. In both cases the dislocation density increases with increasing crystal diameter in the range of 0·3 to 0·4 mm. For larger diameters, the dislocation density is too great to enable one to resolve and count individual dislocations. For smaller diameters, the concept of density loses its significance. That is, if a region of a crystal contains only several scattered dislocations, the density would depend on how one chose the area; the density might have any value from zero to a large number in adjacent regions.

A study of many X-ray micrographs reveals the following pattern: in general, the thinnest region of a crystal contains very few dislocations in the form of isolated, dark, circular-shaped areas situated near the surface. With increasing diameter rather long dislocations appear in the centre. Away from the tip towards increasing diameter, their number increases; the dislocations become shorter, spreading out from the centre until, in the thickest regions of the crystal, the dislocations appear as dots covering the whole area (see fig. 8). One thin crystal (axial orientation parallel to a ⟨111⟩ direction) of diameter 0·2 mm containing a few surface dislocations (fig. 9) was electropolished. After the treatment, two new X-ray micrographs were taken by diffraction from two {220} planes 60° apart. Near the tip region in both pictures one sees a dense network of dislocations. Towards the tip, the number decreases sharply to a few scattered dislocations and drops to zero several millimetres from the tip (fig. 10). It was not possible in this case to compare identical locations in the crystal in the micrographs taken before and after electropolishing, since the amount of material removed is not known. A 'traverse' micrograph was taken of this particular crystal (for a 'traverse', both the crystal and the film are translated back and forth across the X-ray beam; because the slit has a finite width, this technique will reveal individual dislocations only if their number is extremely low. Otherwise, overlapping of the dislocation images will result). The traverse shows essentially the same features as the section micrographs described above (which merely reveal dislocations lying in or intersecting the diffracting plane), but establishes most definitely that the tip region is free of dislocations detectable by means of this technique; the traverse would reveal dislocations situated throughout the volume of the crystal, provided the Burgers vector of the dislocation is not parallel to the diffracting plane.

It is to be pointed out that this is the first recorded instance of a metal crystal grown from the melt having a large area free of detectable dislocations. Another crystal was grown of 99·999% pure aluminium that revealed a tip region containing a few scattered dislocations lying on the surface (fig. 11). After electropolishing (fig. 12) it was possible to compare similar regions of both micrographs (arrows point to similar regions). One sees that some of the surface dislocations have disappeared, and that regions are present which contain no dislocations.

§ 5. Discussion and Conclusions

It has been shown above that a necessary condition for vacancies to aggregate into discs and collapse is that there be a sufficient supersaturation of vacancies in the growing crystal. A minimum value for the supersaturation was calculated to be about 10; from calculations of the vacancy supersaturations reached in an aluminium crystal cooled from the melting point under the conditions of crystal growth described above, a critical diameter of about 0·5 mm was deduced, below which no dislocations should be produced by the collapsing vacancy disc mechanism. This is of the same magnitude as diameters of crystals for which the density of detectable dislocations is rapidly decreasing with decreasing diameter (figs. 6 and 7). The fact that the observed dislocation densities (figs. 4 and 5) increase with increasing rates of growth is consistent with the theory presented; a high growth rate implies that vacancies present in the interior of a crystal would not have time to diffuse out to the surface before the diffusion coefficient drops to a low enough value for the rate of diffusion to become negligible. It must be pointed out that the results of the experiments support the validity of the mechanism, but do not deny that other ways of forming dislocations either may be operating simultaneously or would operate under other growth conditions. We will now consider the operation of the other mechanisms mentioned in the introduction.

(1) Propagation of dislocations into the growing crystal from the seed crystal: It is apparent from fig. 11 (and from other x-ray micrographs not included in this paper) that the dislocation density does not change suddenly with a change in crystal diameter. This is consistent with the idea of dislocations propagating directly or growing by climb from one region of a crystal to another. If a dislocation line is at an angle to the crystal axis, it will eventually grow out to the surface of the crystal; only dislocations parallel to the axis of the crystal will continue growing indefinitely (even these dislocations can in principle climb and ultimately reach the surface of the crystal). This explains why adjacent regions of a crystal of the same diameter may have varying densities of dislocations; the last region to solidify will 'inherit' some of the dislocations from a previously solidified region. The propagation of dislocations from one region of a crystal to another is also an explanation of why the observed critical diameter (that diameter below which the vacancy supersaturation reached during growth is too small to nucleate dislocations by the mechanism of collapsing vacancy discs) is smaller than the theoretical value. Thus, a particular region of a crystal contains dislocations arising from two sources: those inherited from a previously grown part of the crystal and those created from collapsing vacancy discs.

(2) Shear strains arising from thermal strains or external mechanical constraints: Thermal and mechanical strains were probably reduced to a minimum by the use of the Czochralski technique, but the many dislocations that are situated near the surface may have been produced by mechanical stresses present during growth. These stresses might

arise from drag against the liquid of the oxide layer attached to the rotating crystal during growth. A torsional stress, which reaches a maximum at the surface of the crystal is thus introduced. The fact that these dislocations disappear after electropolishing proves that they lie on the surface.

(3) Shear strains resulting from abrupt changes in composition accompanied by changes in lattice parameter: Qualitatively, regions involving large impurity content differences are less likely to occur in crystals grown from zone-refined (high purity) materials. In these experiments, no significant difference was observed between values of the dislocation density in 99·999% aluminium or zone-refined aluminium. It thus appears, that this mechanism was not playing an important role.

(4) Dendritic growth: The crystals were grown by the Czochralski method, and did not solidify dendritically.

In conclusion, the results of the experiments performed in the course of the research are completely consistent with the idea that the mechanism of collapsing vacancy discs is responsible for creating most of the dislocations found in a metal crystal grown from the melt. It was also found that the crystal diameter for which no dislocations were detected, was somewhat less than the theoretical critical value; this is interpreted to mean that for a given vacancy supersaturation, the density of dislocations present contains two contributions: those created from collapsing vacancy discs and those inherited from the previously solidified part of the crystal.

Extensive regions of thin crystals were found to be free of dislocations when the diameter of the specimen was about 0·3 mm or less; this is the first recorded instance of the production of dislocation-free metal crystals by growth from the melt.

REFERENCES

Bradshaw, F. J., and Pearson, S., 1957, *Phil. Mag.*, **2,** 570.
Dash, W. C., 1958, *J. appl. Phys.*, **29,** 736; 1959, *Ibid.*, **30,** 459.
Elbaum, C., 1959, *Progr. Met. Phys.*, **8,** 203; 1960, *Phil. Mag.*, **5,** 669.
Frank, F. C., 1950, Symposium on the Plastic Deformation of Crystalline Solids, Mellon Inst., Pittsburgh.
Hirsch, P. B., Silcox, J., Smallman, R. E., and Westmacott, K. H., 1958, *Phil. Mag.*, **3,** 897.
Lang, A. R., 1958, *J. appl. Phys.*, **29,** 597; 1959, *Ibid.*, **30,** 1748.
Schoeck, G., and Tiller, W. A., 1960, *Phil. Mag.*, **5,** 43.

Theory of the Magnetic Properties of Igneous Rocks in Alternating Fields

By F. D. STACEY†
Geophysics Department, Australian National University, Canberra, Australia

[Received March 14, 1961]

ABSTRACT

Each magnetic grain in a rock contains ferromagnetic domains with a range of sizes, the small ones being magnetically harder and responding less readily to demagnetizing fields than the larger ones. By exposing a grain which has a thermoremanent magnetic moment to an alternating field, domains larger than a critical size are demagnetized, leaving the smaller domains unaffected. Domain size distributions are calculated for spherical and cubical grains and used to derive characteristic curves of the fraction of an initial thermoremanent magnetization which remains after demagnetization in a progressively increasing field. Coercive force, saturation remanence and anhysteretic magnetization are also calculated from the domain size distributions. Irregularities of grain shape are shown to lead to a pseudo-single domain behaviour which is responsible both for very hard components of thermoremanent moments and for the fact that small, randomly directed moments may be found to remain after rocks have been demagnetized in the highest fields.

§ 1. INTRODUCTION

THE technique of alternating field demagnetization of rocks is now an essential part of palaeomagnetic studies in a number of laboratories. Its use is based upon the observation that primary and secondary components in the natural remanence of rocks can often be distinguished. In most igneous rocks the secondary components are probably induced isothermally over long periods and are more readily destroyed than the original or primary thermoremanence (see for example Irving *et al.* 1961). In any physical description of the demagnetization process the important fact requiring explanation is that thermoremanent magnetization (TRM) is very resistant to demagnetization.

This paper extends the multidomain theory of magnetic grains in igneous rocks (Stacey 1958, 1959) to give a semi-quantitative description of the physical process of demagnetization of TRM. It may be regarded as a third-order calculation in the multidomain theory. To a useful approximation thermoremanent magnetization is a first-order effect, depending upon grain shape and the existence of a blocking temperature (Stacey 1958); grain size and domain structure have only secondary influences, provided the grains are true multidomains (as defined in § 6). The variation of domain structure with grain size is a second-order calculation and coercive force is a property described by such a calculation (Stacey 1959). To proceed further, specific consideration must be given to grain shape and domain structure, and in particular to the distribution of domain sizes within each grain. It is necessary for the explanation of alternating field demagnetization that the several domains in a single grain do not all have the same properties.

---

† Now Gassiot Fellow in Geomagnetism, Meteorological Research Unit, Huntingdon Road, Cambridge.

The detailed magnetic behaviour of rocks in alternating fields is so sensitive to grain shape that there is no possibility of deriving theoretically a demagnetization curve which fits the measured curve for the TRM of any rock. Magnetic grains are irregular in shape, whereas only simple geometrical shapes can be considered theoretically, even approximately. The calculations therefore indicate the broad features of demagnetization and other alternating field effects in terms of idealized spherical or cubical grains.

Irregularities in grain shape are particularly important when the grain size is small, i.e. less than about $1\,\mu$, but larger than $0{\cdot}03\,\mu$, which is roughly the upper limit for single domain grains. In this case magnetic properties may be substantially different from true multidomain behaviour and more like a superposition of single-domain properties upon the multidomain character. The essential feature is the appearance of permanent dipole moments which can be reversed but not destroyed by demagnetization, and the effect is therefore termed pseudo-single-domain behaviour (§ 6), which can occur in grains which are much too large to be true single domains.

The inapplicability of the simple multidomain theory to grains smaller than about $1\,\mu$ was pointed out by Stacey (1958, § 7 (5)). However, Verhoogen (1959) has questioned the fundamental basis of the multidomain theory on the grounds that some rocks are found to have single-domain-type properties; he suggested that the freedom of domain wall movements in a multidomain grain above its blocking temperature implies that energy barriers opposing domain wall motion must vanish and therefore that magnetocrystalline anisotropy and magnetostrictive energies also vanish, whereas it merely means that thermal activation provides sufficient energy to impel walls past the barriers (Stacey 1960 a). Verhoogen attributed the very hard components in the TRM of some rocks to the presence within normal, multidomain-sized grains of small, single-domain inclusions, which are chemically and physically indistinguishable parts of the grains except for the presence of very strong, local stress concentrations which cause them to act independently as regards their magnetic properties. Even if this is possible, the fact that the single domains would be completely embedded in the magnetically softer matrix would neutralize their properties. The single domains would be magnetically screened by the matrix so that TRM would still be acquired by grains as a whole. Further, if alignment of the moments of the single domains in a grain were produced (the application of a strong field appears to be the only method) then the aligned moments would give rise to a self-demagnetizing field in the grain as a whole and so would tend to magnetize the matrix in the opposite direction. During demagnetization the domain structure of the matrix would adjust itself to produce zero internal field, i.e. zero total moment, without affecting the inclusions. Thus the remanence and magnetic hardness of the single-domain volumes would not be apparent. These difficulties are only partly avoided by supposing that the single domains represent a phase separation of finely divided but strongly magnetic material in a less magnetic matrix, as in dispersion-hardened alloys (Stoner and Wohlfarth 1948), and other difficulties are introduced. The hard components of TRM, which Verhoogen considered, are readily explained in terms of the theory of very small multidomain grains of irregular shape (§ 6).

In this paper consideration is given only to the properties of strongly magnetic minerals, magnetite and the titanomagnetites, which normally occur in igneous rocks. Haematite, which is frequently a constituent of sedimentary rocks is quite different and cannot be treated in the same way.

§ 2. DOMAIN STRUCTURES OF SPHERICAL AND CUBICAL GRAINS

The domain structure of a magnetic grain in its lowest energy state in zero external field can, in principle, be determined by minimizing the total magnetic energy. The more important energy contributions which must be balanced in such a calculation are magnetostatic (due to free poles), magnetocrystalline, magnetostrictive and domain wall energies. In practice the simultaneous consideration of all four energies is impossible, so that a probable model of the domain structure is first set up and can then be adjusted to minimize the energy contributions in pairs. Stacey (1959) showed that if the domain structures of magnetite grains are assumed to be controlled mainly by magnetostrictive and domain wall energies, then the domains take the form of rods of square cross sections. For irregular or spherical grains the magnetostatic and anisotropy energies must be appreciable but in view of the agreement between calculated and observed coercive forces (Stacey 1959, fig. 1) it is reasonable to assume that the rod model is nevertheless applicable to magnetite grains.

2.1. *Spherical Grains*

In spherical grains the rod model takes the form shown in fig. 1 (*a*), the spacing of domain walls being determined by balancing wall energy with the energies of domain end-effects. A grain in the demagnetized state has no overall self-demagnetizing field, so that one part of the grain can have no influence on the domain structure of any other part more than one or two domain-widths away. Thus the energy balance of each part of the grain is locally adjusted, the widths of the domains being determined by their lengths, as in the original rod model calculation (Stacey 1959), the result of which may be used directly. The critical field, H_{cr}, required to move a domain wall past potential barriers whose heights are characteristic of the length of the wall, l, is given by

Fig. 1

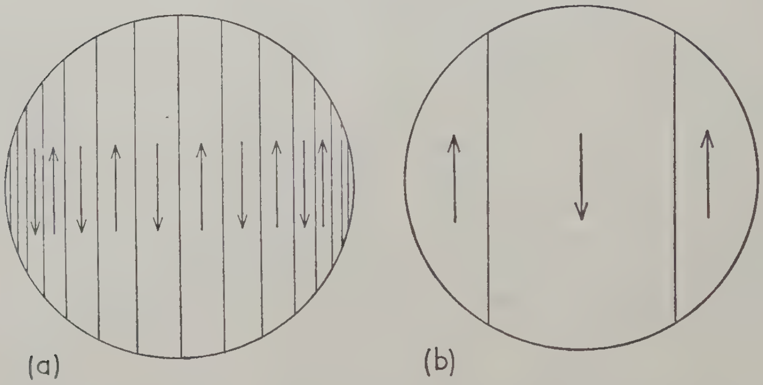

(*a*) Rod model of the domain structure of a spherical grain of magnetite in the virgin state.

(*b*) Regions of net magnetization in a grain which has been magnetized to saturation in the upward direction and then placed in a downward directed field equal to the coercive force, producing zero total moment.

$$H_{cr} \propto l^{-3/4}. \qquad (1)$$

Compared with the central part of a grain the magnetic energy balance causes the domains of the outer parts to be narrower and magnetically harder, as a consequence of their shortness. Within each grain there is therefore a spectrum of critical fields controlled by (1). In a grain of diameter d and volume V, there is a volume v which contains domains shorter than l, where

$$v = (\pi/6)l^3,$$

so that

$$v/V = (l/d)^3. \qquad (2)$$

If the largest, central domains of length d have a critical field $H_{cr\,0}$, the spectrum of critical fields is obtained by substituting (1) in (2) from which

$$\frac{v}{V}=\left(\frac{H_{\mathrm{cr}}}{H_{\mathrm{cr}\,0}}\right)^{-4}, \text{ for } H_{\mathrm{cr}}/H_{\mathrm{cr}\,0}\geqslant 1. \quad . \quad . \quad . \quad . \quad (3)$$

Equation (3) gives the volume fraction v/V of spherical grains for which the critical field is greater than H_{cr}. For $H_{\mathrm{cr}}/H_{\mathrm{cr}\,0}\leqslant 1$, $v/V=1$. Equation (3) is the starting point of the demagnetization calculations (§ 3).

As a consequence of the domain structure indicated in fig. 1 (*a*), the central region of a spherical grain can be magnetized (and demagnetized) more easily than the outer parts. After magnetization to saturation and the application of a smaller field in the opposite direction, as in the measurement of coercive force, the grain therefore contains regions of net magnetization as shown in fig. 1 (*b*), in which the downward directed domains are larger than the upward directed domains in the central region and the upward directed domains are larger in the outer parts. However, this domain structure does not affect the variation of coercive force with grain size.

2.2. *Cubical Grains*

The interest in grains of cubical shape is not that they represent any better approximation to the actual shapes of naturally occurring magnetic grains than do the spheres considered above but that they indicate very clearly the strong dependence of certain magnetic properties upon grain shape and even upon the orientation of the domains with respect to the shape. In a cube there are an infinite number of possible orientations the three principal cases being:

(i) domains parallel to cube edges,
(ii) domains parallel to face diagonal,
(iii) domains parallel to body diagonal,

Consideration of the geometry of each case gives the distribution of domain lengths, from which the spectrum of critical fields is obtained. These spectra are:

Case (i) all domains have the same critical field,

Case (ii) $v/V=(H_{\mathrm{cr}}/H_{\mathrm{cr}\,0})^{-8/3}$, ... (4)

Case (iii) $v/V=(H_{\mathrm{cr}}/H_{\mathrm{cr}\,0})^{-8/3}(3-2(H_{\mathrm{cr}}/H_{\mathrm{cr}\,0})^{-4/3})$. . . . (5)

§ 3. ALTERNATING FIELD DEMAGNETIZATION OF TRM IN SPHERICAL AND CUBICAL GRAINS

In this section it is assumed that each grain considered is demagnetized by the application of an alternating field in a direction parallel to its domains (which is the most effective direction). A rock specimen containing magnetic grains in which the crystallographic axes and domain directions are randomly oriented can be demagnetized by rotating it about two mutually perpendicular axes simultaneously, at frequencies unrelated to one another and to the field (as in the experiments of Irving *et al.* 1961). In this way the grains are presented to the field in all possible orientations and the field therefore acts on each grain in the direction of its domains or very near to it. The calculations therefore refer to this method of demagnetization. Certain effects arising from the demagnetization of stationary specimens are considered in § 5.

3.1. *Spherical Grains*

When a spherical grain is given a small TRM the domains in the direction of net magnetization are all enlarged at the expense of their reversed neighbours, so that the net magnetization is uniformly distributed through the grain. Subjection to an increasing alternating field induces no irreversible domain wall movements until the effective field acting on the grain reaches $H_{\mathrm{cr}\,0}$, when it becomes just sufficient to demagnetize the central region, i.e. to rearrange the domain walls, making the net magnetization of the region zero. With further increase in the

Fig. 2

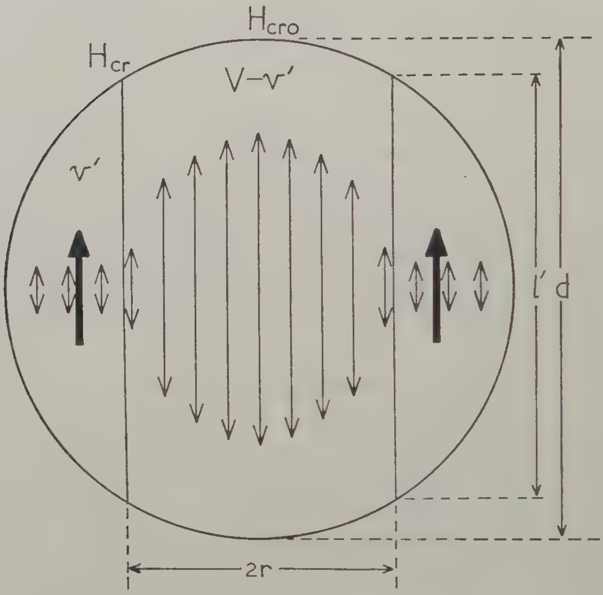

Partial demagnetization of a spherical grain. Heavy arrows in outer region indicate remaining TRM, light arrows indicate alternating magnetization induced by the applied field and show the form of its variation within the grain. The heavy arrows are not to scale as TRM is normally much smaller than the induced magnetization under these conditions.

applied field to a peak value H the demagnetized region spreads outwards to a radius r, at which the critical field required to move the domain walls H_{cr}' is equal to the effective field acting at r (applied field, H, less self-demagnetizing fields due to polarization of the grain).

A grain in such a partially demagnetized state is shown in fig. 2, in which the remaining TRM of the grain is carried by the volume outside radius r, where

$$\left(\frac{2r}{d}\right)^2 = 1 - \left(\frac{v'}{V}\right)^{2/3}, \qquad \qquad (6)$$

d being the grain diameter and V its total volume as before. Since the original TRM was uniformly distributed through the grain the fraction remaining, M/M_0, is given by

$$M/M_0 = v'/V. \qquad \qquad (7)$$

The induced magnetization, indicated by the light arrows in fig. 2, is due both to reversible and to irreversible movements of domain walls. Thus the field H_{cr}' acting at r is given by

$$H_{\text{cr}}' = H - N\chi H_{\text{cr}}' - H_{\text{D}}. \qquad \qquad (8)$$

In eqn. (8) χ is the low-field intrinsic susceptibility, i.e. that contribution to susceptibility which is due to small displacements of domain walls, which do not take them across potential barriers and do not produce remanence, and N is the demagnetizing factor appropriate to the reversibly induced moment, $(\chi H_{\text{cr}}')$ being the reversible moment. Although not strictly correct it is assumed for simplicity that the reversible moment is uniform over the whole grain, so that $N = \frac{4}{3}\pi$ at all points. H_{D} is that part of the self-demagnetizing field which is due to polarization of the central (demagnetized) region by irreversible movements of domain walls. Since, at any point inside radius r the critical field H_{cr} is less than the effective field H_{cr}' acting at r, the irreversible polarization is controlled by $(H_{\text{cr}}' - H_{\text{cr}})$ at each point, and is superimposed upon the reversible polarization. This means simply that the irreversible polarization has just such a magnitude that the self-demagnetizing field reduces the effective field at each point in the central region to the value of H_{cr} at that point, this being the maximum field which the domain walls can withstand. Thus the field H_{D}, acting at radius r is due to an alternating moment M' in the central region, being given by

$$M' = \int_V^{v'} \frac{H_{\text{cr}}' - H_{\text{cr}}}{N'}(-dv), \qquad \qquad (9)$$

N' being the demagnetizing factor of the central region, which is for this purpose adequately regarded as a uniformly magnetized prolate ellipsoid of length d and width $2r$. Substituting for H_{cr} in terms of v from (3) we obtain an expression for M' which integrates directly to give

$$M' = \frac{VH_{\text{cr}\,0}}{N'}\left[\left(\frac{v'}{V}\right)^{-1/4} + \frac{1}{3}\left(\frac{v'}{V}\right)^{3/4} - \frac{4}{3}\right]. \qquad \qquad (10)$$

Then the field H_{D} due to M' is given approximately by

$$H_{\mathrm{D}}=\frac{M'}{((d/2)^2+r^2)^{3/2}}. \qquad (11)$$

Substituting for r from (6) and noting that $V=\frac{4}{3}\pi(d/2)^3$, we obtain

$$H_{\mathrm{D}}=\frac{4\pi}{3V}\cdot\frac{M'}{(2-(v/V')^{2/3})^{3/2}}. \qquad (12)$$

Equation (8) may be rewritten

$$\frac{1}{1+N\chi}\cdot\frac{H}{H_{\mathrm{cr}\,0}}=\frac{H_{\mathrm{cr}}'}{H_{\mathrm{cr}\,0}}+\frac{1}{1+N\chi}\cdot\frac{H_{\mathrm{D}}}{H_{\mathrm{cr}\,0}}.$$

Now $(H_{\mathrm{cr}}'/H_{\mathrm{cr}\,0})=(v'/V)^{-1/4}$ from (3) and H_{D} is given by (12) where M' has the form (10). Making these substitutions an expression is obtained for $H/H_{\mathrm{cr}\,0}$ in terms of (v'/V), which is then expressed in terms of (M/M_0) according to (7). Thus the final equation for the demagnetization of TRM in spherical grains is

$$\frac{1}{1+N\chi}\cdot\frac{H}{H_{\mathrm{cr}\,0}}=\left(\frac{M}{M_0}\right)^{-1/4}+\frac{1}{3D'(1+N\chi)}\cdot\frac{[(M/M_0)^{-1/4}+\frac{1}{3}(M/M_0)^{3/4}-\frac{4}{3}]}{[2-(M/M_0)^{2/3}]^{3/2}} \qquad (13)$$

where, for convenience $D'=N'/4\pi$. Equation (13) gives the peak value H of the alternating field required to reduce the TRM of a spherical grain to a fraction M/M_0 of its initial value, in terms of the constant $H_{\mathrm{cr}\,0}$ and the intrinsic low field susceptibility χ. It is convenient to consider the characteristic field for alternating field demagnetization to be

$$H_0=H_{\mathrm{cr}\,0}\,(1+N\chi) \qquad (14)$$

which is the field below which no demagnetization occurs.

The two limiting forms of (13) are plotted in fig. 3, curves 2 and 3. The procedure for plotting curve 3 was to select a series of values of $(d/2r)$ for which corresponding values of D' have been tabulated by Stoner (1945). Values of (v'/V) and hence (M/M_0) are given by (6) and used directly in (13) to find (H/H_0). Physically the two limits represented by these curves are that for very large χ the self-demagnetization due to irreversibly induced moments is negligible compared with that due to the reversible moments and for very small χ the reversible moments are negligible and the irreversible moments become important. The intrinsic susceptibility χ, used in this section is the susceptibility in the direction of the domains, for which the symbol $\chi_{\parallel}$ is used in § 5. $\chi_{\parallel}$ is related in an inverse manner to $H_{\mathrm{cr}\,0}$ and is hence not an independent constant, although no quantitative relationship between them is known. Both $\chi_{\parallel}$ and $H_{\mathrm{cr}\,0}$ are also related to the coercive force H_{c}, which is considered in § 4.

3.2. *Cubical Grains*

Demagnetization curves for cubical grains with $\chi\rightarrow\infty$ (negligible self-demagnetizing effects due to irreversible domain wall movements) follow directly from eqns. (4) and (5), if it is assumed that TRM is uniformly distributed through a cube, since in this case $v'/V = M/M_0$, as for spherical grains. This is the approximation used to plot curves 4 and 5 of fig. 3. Curve 1 is trivial since it assumes simply that all the domains are alike. Equation (7) is not exactly valid for cubes because the factor N which controls TRM (Stacey 1958) is not constant over the whole volume and TRM is therefore not uniformly distributed, but (7) is a useful approximation. Curves for cubes with $\chi \rightarrow 0$, in which the self-demagnetizing fields lead to terms corresponding to the second one in (13) have not been plotted on fig. 3. The curves are readily obtained by approximating the central demagnetized regions to ellipsoids, as in the case of spherical grains, and lie above the curves for $\chi \rightarrow \infty$. However, the nature of the approximation is such that this result is only of qualitative interest.

Fig. 3

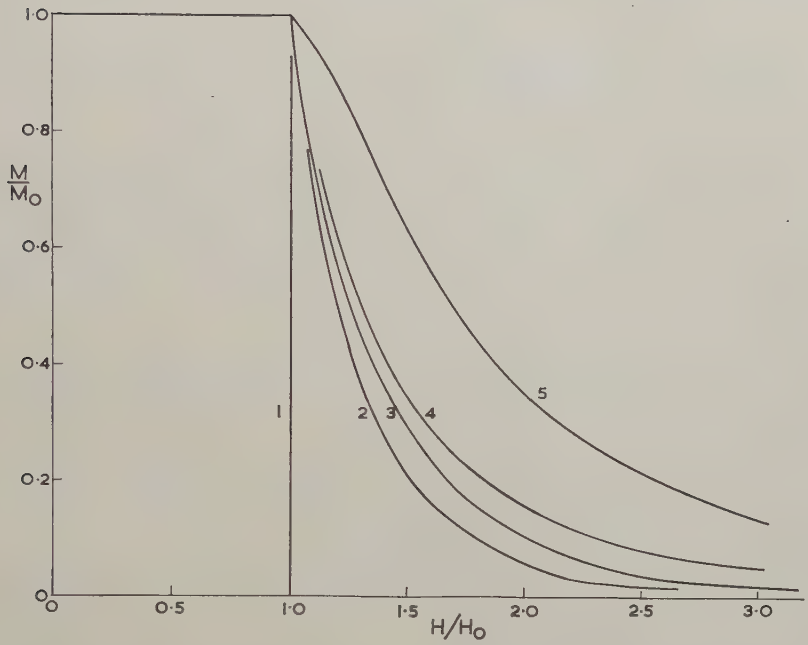

Alternating field demagnetization. Theoretical curves for (1) cube with domains parallel to cube edge; (2) sphere, assuming high intrinsic, low-field susceptibility, χ; (3) sphere, assuming $\chi \rightarrow 0$; (4) cube with domains parallel to a face diagonal, $\chi \rightarrow \infty$; (5) cube with domains parallel to a body diagonal, $\chi \rightarrow \infty$.

The variety of shapes of the curves of fig. 3 shows clearly that demagnetization is very dependent upon grain shape. Demagnetization of the irregular grains occurring in rocks can therefore not be calculated quantitatively but the physical principles must be the same as for the simple shapes and the general form of curves of demagnetization of TRM must be similar. The more irregular a grain is, the less sharp becomes its demagnetization curve. Observed demagnetization curves are spread out by several other factors including grain size distributions which have the effect of superimposing curves with different characteristic fields H_0. Many rocks contain intergrown and exsolved minerals which are even more complicated and can only be discussed qualitatively.

§ 4. COERCIVE FORCE, SATURATION REMANENCE AND ANHYSTERETIC MAGNETIZATION OF SPHERICAL GRAINS

4.1. *Coercive Force*

The measurement of the coercive force of a single grain, by the application of fields parallel to its domain directions, produces the state of magnetization indicated in fig. 1 (*b*), the total moment being zero, so that

$$\int_V^0 I(-dv)=0, \qquad (15)$$

where I is the magnetization at any point. Since the grain is subjected to a downwards directed field H_c, the effective field at any point is

$$H_{cr}=H_c-N'I, \qquad (16)$$

N' being the demagnetizing factor appropriate to the region in question. Equation (16) expresses the fact that at each point the domains are supporting a field equal to the critical field H_{cr}. Then

$$I=(H_c-H_{cr})/N'. \qquad (17)$$

It is difficult to specify an appropriate value for N', but (15) can be integrated by assuming that N' is effectively constant over the whole grain. Substituting for H_{cr} from (17) and (3) and integrating (15) we obtain

$$-\frac{V H_{cr\,0}}{N'}\left[\frac{H_c}{H_{cr\,0}}\left(\frac{v}{V}\right)-\frac{4}{3}\left(\frac{v}{V}\right)^{3/4}\right]_{v=V}^{0}=0,$$

whence

$$H_c=\tfrac{4}{3}H_{cr\,0}. \qquad (18)$$

When an assembly of grains, uniform in size but with randomly oriented crystallographic axes is considered, an additional numerical factor is included. It is assumed that during the measurement of coercive force the domains of each grain are re-aligned to the easy direction of magnetization which is nearest to the direction of the applied field. Consider a grain in which the domains make an angle α to the direction of the field H_c, equal to the coercive force of the whole assembly. Its magnetic moment will be

$$M=\beta(H_c\cos\alpha-\tfrac{4}{3}H_{cr\,0}), \qquad (19)$$

where β depends upon grain volume, intrinsic susceptibility and the demagnetizing factor, but is an arbitrary constant for the present purpose. The component of M in the field direction is

$$M \cos \alpha = \beta(H_c \cos^2 \alpha - \tfrac{4}{3} H_{cr\,0} \cos \alpha), \quad \ldots \quad (20)$$

but for the whole assembly

$$\overline{M \cos \alpha} = 0,$$

so that from (20),

$$H_c = \tfrac{4}{3} H_{cr\,0} \frac{\overline{\cos \alpha}}{\overline{\cos^2 \alpha}} . \quad \ldots \quad (21)$$

Taking values of $\overline{\cos \alpha}$ and $\overline{\cos^2 \alpha}$ from the Appendix, we obtain

$$H_c = 1{\cdot}57\, H_{cr\,0}. \quad \ldots \quad (22)$$

Slightly different factors would apply to other grain shapes.

4.2. *Saturation Remanence*

For a single grain, the saturation remanence per unit volume is

$$I_{RS} = \frac{1}{V} \int_V^0 I(-dv), \quad \ldots \quad (23)$$

where, at any point,

$$I = H_{cr}/N. \quad \ldots \quad (24)$$

Substituting for H_{cr} as before and integrating, we obtain

$$I_{RS} = \tfrac{4}{3} \frac{H_{cr\,0}}{N} .$$

For an assembly of grains the saturation remanence of an individual grain must be multiplied by the mean cosine of the angle between the individual moments and the total moment, $\overline{\cos \alpha}$. Assuming these to be the minimum possible angles, since the grains have been exposed to a strong field to saturate them, $\overline{\cos \alpha}$ is given in the Appendix, so that

$$I_{RS} = \tfrac{4}{3} \frac{H_{cr\,0}}{N} \overline{\cos \alpha} = 1{\cdot}14 \frac{H_{cr\,0}}{N} = 0{\cdot}726 \frac{H_c}{N}. \quad \ldots \quad (25)$$

Equation (25) thus expresses the saturation remanence of an assembly of grains of uniform size in terms of the coercive force of the whole assembly.

4.3. *Anhysteretic Magnetization*

Anhysteretic magnetization is induced in a rock when it is exposed to a small, steady field h, superimposed upon an alternating field H which is gradually reduced to zero. The interesting case is saturation anhysteretic magnetization, induced when the alternating field is initially strong enough to saturate the grains, and is applied parallel to h. Figure 2 may be used to represent a grain undergoing anhysteretic magnetization, when H has been reduced to the point at which irreversible domain wall movements no longer occur outside radius r. The outer domains then carry an anhysteretically induced moment represented by the heavy arrows. The effective field acting at radius r oscillates between the values

$$\frac{(H+h)-H_{\mathrm{D}+}}{1+N\chi} \text{ and } \frac{(H-h)-H_{\mathrm{D}-}}{1+N\chi},$$

where $H_{\mathrm{D}+}$ and $H_{\mathrm{D}-}$ are the self-demagnetizing fields due to the moments induced irreversibly by external fields $(H \pm h)$. The net effective steady field acting at r is thus

$$h' = \tfrac{1}{2} \cdot \frac{1}{1+N\chi}\,(2h-(H_{\mathrm{D}+}-H_{\mathrm{D}-})) . \quad . \quad . \quad . \quad . \quad (26)$$

The self-demagnetizing fields may be treated exactly as in § 3, and examination of the numerical data shows that for spherical grains dH_{D}/dH is approximately constant over the whole range of interest and equal to about 0·2, so that

$$(H_{\mathrm{D}+}-H_{\mathrm{D}-}) \approx 0{\cdot}2(2h),$$

whence

$$h' = 0{\cdot}8h/(1+N\chi). \quad . \quad . \quad . \quad . \quad . \quad . \quad . \quad (27)$$

Thus the saturation anhysteretic magnetic moment per unit volume is

$$I_{\mathrm{AR}} = h'/N, \quad . \quad . \quad . \quad . \quad . \quad . \quad . \quad . \quad . \quad (28)$$

where h' is given by (27). It is therefore significantly smaller than the TRM induced in the same field h.

§ 5. ANISOTROPY OF SUSCEPTIBILITY INDUCED BY ALTERNATING FIELDS

Intrinsic magnetic anisotropy of rocks is due to alignment of grain elongations (shape anisotropy) and crystallographic axes (magnetocrystalline anisotropy); as a special case of shape anisotropy, fabric effects due to the stringing together of magnetic grains in lines or planes may also be considered. Stacey (1960 b) showed that such intrinsic anisotropies are conveniently measured by means of a torquemeter, with which it is possible to distinguish the types of anisotropy. Graham (1954) developed a sensitive apparatus for measuring anisotropy of magnetic susceptibility which is an alternative method of examining magnetic anisotropy and has been used by Balsley and Buddington (1960) and Fuller (1960). An important difference is that the susceptibility method is sensitive to induced anisotropy as well as to the intrinsic anisotropies. This is a disadvantage when slight intrinsic anisotropies are being measured; however it appears that useful information about the fundamental magnetic processes occurring in rocks can be obtained from measurements of induced anisotropy.

Induced anisotropy results from the alignment of magnetic domains and is caused by the exposure of rock specimens to magnetic fields and possibly to several other effects including the application of stresses. It arises by virtue of the differences between the magnetic properties of grains parallel and perpendicular to their domain directions. A similar effect has been observed in bulk metals by Jackson *et al.* (1958), whose results give a useful qualitative agreement with the explanation here advanced more specifically for rocks.

The intrinsic low-field susceptibility of the material of a grain measured parallel to its domain directions, $\chi_{\|}$, is a measure of the ease with which the 180° domain walls may move. Such domain wall movements allow the growth of favourably oriented domains at the expense of their oppositely magnetized neighbours; in sufficiently low fields the movements are reversible and do not take the walls past potential barriers, but simply displace them from the centres of the potential wells between the barriers. $\chi_{\|}$ is inversely related to the barrier heights and therefore to coercive force, but the relationship is not known quantitatively. The susceptibility measured perpendicular to the domain directions, $\chi_{\perp}$, is due to quite a different magnetization process. The application of a small field H perpendicular to the domains causes the magnetization of the domains to turn towards the field direction by an angle θ while the positions of the walls remain stationary. This gives a magnetization $I_S \sin\theta$ perpendicular to the walls, I_S being the saturation magnetization, and causes the appearance of magnetocrystalline energy by virtue of the deflection of the domains out of the easy directions. The total energy is

$$E=|\tfrac{2}{3}K_1+\tfrac{2}{9}K_2|\sin^2\theta-HI_S\sin\theta, \quad . \quad . \quad . \quad . \quad (29)$$

K_1 and K_2 being the magnetocrystalline anisotropy constants. Since θ is determined by the condition $dE/d\theta=0$, this gives

$$\chi_{\perp}=\frac{I_S\sin\theta}{H}=\frac{I_S{}^2}{|\tfrac{4}{3}K_1+\tfrac{4}{9}K_2|}. \quad . \quad . \quad . \quad . \quad . \quad . \quad (30)$$

Normally $\chi_{\|}$ is somewhat larger than $\chi_{\perp}$.

In an assembly of grains with domain directions randomly oriented the effective intrinsic susceptibility is

$$\chi=\tfrac{1}{3}(\chi_{\|}+2\chi_{\perp}), \quad . \quad . \quad . \quad . \quad . \quad . \quad . \quad . \quad . \quad (31)$$

being the same in all directions. The effective susceptibility is changed in value and becomes anisotropic when a stationary rock specimen in which there is no alignment of grain elongations or crystallographic axes, is subjected to an alternating field which is gradually reduced to zero from a value high enough to saturate the specimen. After this treatment the domains of each grain lie in the nearest easy direction of magnetization to the direction in which the field was applied. The susceptibility in the direction of the alternating field becomes

$$\chi_1=\chi_{\|}\overline{\cos^2\alpha_1}+\chi_{\perp}(1-\overline{\cos^2\alpha_1}), \quad . \quad . \quad . \quad . \quad . \quad . \quad (32)$$

and the susceptibility in any perpendicular direction is

$$\chi_p=\tfrac{1}{2}\{\chi_{\|}(1-\overline{\cos^2\alpha_1})+\chi_{\perp}(1+\overline{\cos^2\alpha_1})\}, \quad . \quad . \quad . \quad . \quad . \quad (33)$$

where $\overline{\cos^2\alpha_1}$ is the mean square direction cosine of the directions of the domains with respect to the direction in which the alternating field was applied.

In magnetite the easy directions of magnetization are [111] crystal axes, and $\overline{\cos^2 \alpha_1} = 0{\cdot}728$ (see Appendix), so that (32) and (33) give the induced anisotropy of susceptibility χ_l/χ_p in terms of the fundamental ratio $\chi_\parallel/\chi_\perp$,

$$\frac{\chi_l}{\chi_p} = \frac{0{\cdot}728\,\chi_\parallel/\chi_\perp + 0{\cdot}272}{0{\cdot}136\,\chi_\parallel/\chi_\perp + 0{\cdot}862}. \quad . \quad . \quad . \quad . \quad . \quad . \quad . \qquad (34)$$

Then using (31) and (34) absolute values of $\chi_\parallel$ and $\chi_\perp$ may be calculated from the absolute intrinsic susceptibility χ of the isotropic rock and the induced anisotropy ratio χ_l/χ_p. Thus the factor $I_S{}^2/|\frac{4}{3}K_1 + \frac{4}{9}K_2|$ can be estimated in terms of susceptibility measurements only, or alternatively a known value of this factor may be used to estimate the absolute intrinsic susceptibility from the anisotropy ratio.

In measuring the intrinsic susceptibility of the material comprising the magnetic grains of a rock, account must be taken of the demagnetizing factors of the grains. The susceptibilities considered above are all intrinsic to the magnetic material and are related to the observed susceptibilities by the usual expression

$$\chi_0 = \frac{v\chi}{1+N\chi}, \quad . \quad . \quad . \quad . \quad . \quad . \quad . \quad . \quad . \qquad (35)$$

where χ_0 is the observed susceptibility corresponding to an intrinsic susceptibility χ, when the volume fraction of magnetic mineral present is v, which is assumed to be small so that grain interactions can be neglected. N is the effective demagnetizing factor. For an assembly of spheres, $N = \frac{4}{3}\pi$ but in rocks the grains are better represented by ellipsoids. Stacey *et al.* (1960) suggested that in igneous rocks a good approximation would be general ellipsoids with dimension ratios 1·65 : 1·45 : 1, although the middle figure is not very reliable. As the nearest simple case we may take an isotropic assembly of grains to be equivalent to an assembly of oblate ellipsoids with a dimension ratio $b : a = 1{\cdot}5 : 1$ and randomly oriented axes. The demagnetizing factors are then $N_a = 4\pi\ (0{\cdot}466)$ and $N_b = 4\pi\ (0{\cdot}267)$ and as an approximation $1/N = 1/N_a + 2/N_b$ so that an effective value of N is 3·91 compared with 4·19 for an assembly of spheres. It is doubtful whether this difference is significant in view of other uncertainties in determining intrinsic susceptibilities.

§ 6. PSEUDO-SINGLE-DOMAIN BEHAVIOUR OF FINE GRAINS OF IRREGULAR SHAPES

In the foregoing sections consideration is given only to spherical or other simple geometrical grains, which are much larger than the critical size for single-domain behaviour and have perfect multidomain properties. A perfect multidomain grain may be defined as a grain whose lowest magnetic energy state in zero field is a state of zero total moment. Perfect multidomains may still have remanence but are not then in their lowest energy states. Naturally occurring magnetic grains are not regular in shape and frequently a single rock sample contains grains with a wide range of sizes. The irregularities of shape are particularly important in the smaller grains because they result in departures from perfect multidomain character, i.e. the lowest magnetic energy states of the grains in zero external field are states of finite magnetic moments. Such grains are therefore considered to have pseudo-single-domain properties superimposed upon their multidomain characters.

A simple example is the wedge-shaped two-domain grain, shown in fig. 4, which is too large to be a single domain but only large enough to have two domains with moments M_1 and M_2 as shown. The position of minimum energy of the domain wall is determined by the balance of wall energy and magnetostatic energy due to surfaces of polarity at the ends of the domains. Qualitative considerations are sufficient to show that the minimum energy occurs at a position such that $M_2 > M_1$. The domain wall energy, being proportional to wall area, decreases as the wall moves to the left in the figure. The magnetostatic energy also has a minimum left of the position at which $M_1 = M_2$, because the shorter domain on the left experiences a stronger self-demagnetizing field and therefore has a

Fig. 4

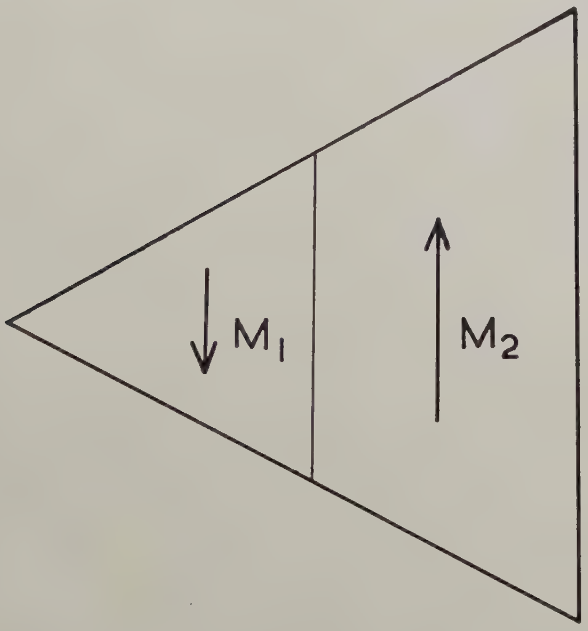

Magnetization in a wedge-shaped two-domain grain.

higher magnetostatic energy than the domain on the right; this energy is reduced by a limited leftward displacement of the wall. The effect is to give the grain a permanent dipole moment $(M_2 - M_1)$ which is responsible for pseudo-single-domain properties. While this example is particularly simple, it is evident that permanent dipole moments must be normal in very small grains and may even be due to small irregular protuberances on larger grains; pseudo-single-domain properties, superimposed upon multidomain properties, must be expected in rocks in which an appreciable fraction of the magnetic minerals occur as grains smaller than about 1 micron in diameter. The permanent dipole moments are necessarily very much smaller than the saturation moments of the grains, but can have an important effect on TRM.

The fact that single-domain-type properties can be due to grains as large as one micron, while true single domains (in which the permanent moments are equal to the saturation moments) are smaller than about 0·03 micron, is of considerable interest in rock magnetism. Verhoogen (1959) has pointed out that a compromise between the single-domain and multidomain theories appears to be necessary to explain the properties of some rocks; the data quoted in his paper is used here to support the pseudo-single-domain approach to this problem. For convenience in comparing it with the data, the multidomain theory of TRM (Stacey 1958) may be rewritten as follows, using the original notation:

TRM per unit volume of magnetic mineral is given by

$$I_0 = \frac{H_E}{N} \cdot \frac{\sigma_R}{\sigma_B} - N\chi I_0 . \qquad (36)$$

The first term of (36) is equivalent to Verhoogen's eqn. (5) except that in the latter the factor J_{SO}/J_S was accidentally inverted. The second term is the susceptibility correction (Stacey 1958, § 4), which allows for the fact that with magnetization I_0 a grain experiences a self-demagnetizing field $(-NI_0)$ which produces a reversed moment. χ is the intrinsic susceptibility, which is generally unknown, but

$$Q = \frac{I_0(1+N\chi)}{\chi H_E}, \qquad (37)$$

Q being the ratio of TRM acquired in a small field to the moment induced at room temperature in the same field. This is a quantity which is frequently measured in experimental work on rock magnetism. Combining (36) and (37) we obtain

$$I_0 = \frac{H_E}{N}\frac{\sigma_R}{\sigma_B} \cdot \frac{Q}{Q+\sigma_R/\sigma_B} . \qquad (38)$$

The data in Verhoogen's table 1 may be used as a test of the reliability of (38) and the relevant figures are given in the table below, together with the estimates of TRM from (38). The ratio (σ_R/σ_B) of spontaneous magnetization at room temperature to the value at the blocking temperature is generally about 3, but for the material in column 4 of the table, the Curie point is so low that (σ_R/σ_B) could not be much greater than 2, as noted in the table.

Properties of powdered magnetic minerals in controlled grain sizes. Figures quoted by Verhoogen (1959) from Roquet (1954) and Uyeda (1958), with calculated values of TRM by multidomain theory

Material	Fe_3O_4	$\begin{Bmatrix} 0{\cdot}11\ Fe_2TiO_4 \\ 0{\cdot}89\ Fe_3O_4 \end{Bmatrix}$	$\begin{Bmatrix} 0{\cdot}67\ Fe_2TiO_4 \\ 0{\cdot}33\ Fe_3O_4 \end{Bmatrix}$
Grain size (μ)	0·1	100	10
Curie point (°c)	582	550	123
TRM in 2 oersteds by experiment (e.m.u./cm³)	9·1	0·77	0·69
Q (eqn. (24))	17	2·2	4·8
Assumed (σ_R/σ_B)	3	3	2
TRM in 2 oersteds from eqn. (25) (e.m.u./cm³)	1·2	0·61	0·70

The TRM of the large grains listed in columns 3 and 4 of the table agrees excellently with (38); the uncertainty in estimating (σ_R/σ_B) is sufficient to explain the small differences. The very small grains of column 2 behave quite differently, as would be expected from their small size. The pseudo-single-domain nature of the TRM of the very fine material is confirmed by Roquet's (1954) observation that its TRM was not proportional to field but approached saturation in quite low fields. When an assembly of grains with permanent moments μ acquires TRM by alignment in a field H, the TRM is proportional to H for $\mu H/kT_B \ll 1$ and saturates when $\mu H/kT_B \gg 1$, k being Boltzmann's constant and μ is measured at the blocking temperature T_B. The range of fields in which saturation becomes apparent depends upon the material but 10 oersteds may be sufficient in many materials. The measurement of TRM therefore provides two tests for pseudo-single-domain effects, which must be invoked to explain any TRM which is much larger than indicated by (38) and is not proportional to the inducing field at low fields.

The observations indicate that pseudo-single-domain effects are associated only with small grains. However, it is possible that permanent dipole moments occur on all grains more or less independently of their sizes, being relatively less important for the larger grains.

During demagnetization of small grains the first process is the movement of domain walls to their equilibrium or minimum energy positions, that is the multidomain contribution to TRM is destroyed, leaving the permanent moments unaffected. The pseudo-single-domain TRM is only destroyed by randomizing the permanent moments. In the wedge shown in fig. 4 this would require the application of a field of strength sufficient to reverse both the domains of the grain, which is clearly greater than the field required to move the domain wall to the left or right. The permanent moments of grains are therefore responsible for magnetically hard components of TRM which are of particular interest in palaeomagnetism, although it must be expected that in most cases the multidomain component is much larger.

There is a further interesting consequence of the pseudo-single-domain behaviour which arises in demagnetization experiments. During complete demagnetization the permanent dipole moments are randomized, so that in a rock sample with n grains each of permanent moment μ, one must expect to observe a randomly directed moment of average value about $(n^{1/2}\mu)$ after demagnetization in the highest fields. Observations of such random moments have evidently been made by Irving *et al.* (1961). The effect is not consistent with perfect multidomain behaviour, because each perfect multidomain grain has zero moment in its demagnetized state.

§ 7. Discussion

There can be little doubt that magnetic grains in most igneous rocks are multidomains, but a quantitative description of their properties is difficult to give an account of the structural complexity of the grains. In this paper simple models are used to explain some of the important magnetic properties on the basis of conventional domain theory. Several predictions are made which will provide tests for the essential validity of the theory. An approximate magnitude is calculated for saturation anhysteretic magnetization; saturation remanence is shown to be determined by coercive force (which is also related directly to the characteristic field of alternating field demagnetization). The induction of anisotropy of susceptibility by alternating fields is a consequence of multidomain structure and measurements of induced anisotropy of powdered magnetite, for which the factor $(I_S{}^2/|\frac{4}{3}K_1+\frac{4}{9}K_2|)$ is known could provide an accurate test of the theory. Two further consequences of multidomain structure are considered qualitatively.

Stacey (1960 b) and Stacey *et al.* (1960) found that the anisotropies of several types of igneous rocks which were examined were due to the alignment of elongations of magnetic grains and that the crystallographic axes of cubic magnetic minerals were randomly oriented and uncorrelated with the grain elongations. TRM in an anisotropic rock is stronger in the direction of the grain elongations than in the perpendicular directions because the demagnetizing factors of grains are smaller in the directions of their long axes. Also it follows from the considerations of domain structure in § 2 that grains in which the domains are parallel to the long axes are magnetically softer and are therefore more easily demagnetized than are grains of the same size and shape, but in which the domains are perpendicular to the long axes. Thus when a rock is cooled in a field at an angle θ to its axis of anisotropy it acquires TRM at an angle $\phi < \theta$, but by demagnetization ϕ is increased. A quantitative estimate of the change in ϕ is of considerable interest in palaeomagnetism, but it has not been found possible to make useful calculations of this effect. Firstly it is not known whether the domain pattern in a cooling rock favours alignment with grain elongations; secondly calculations of changes in ϕ depend upon the differences in demagnetization curves parallel and perpendicular to the axis of anisotropy and these curves were shown in § 3 to depend very strongly upon the precise grain shape. Only experiments will be able to show whether, during demagnetization, ϕ reaches θ or overshoots it. However, if the multidomain theory is correct at all the change in direction of TRM occurring in an anisotropic rock during demagnetization must be such as to offset the deflection of TRM by the intrinsic anisotropy, at least qualitatively (Stacey 1960 b).

Another interesting consequence of the multidomain structure of magnetic grains in rocks is the slight dependence of TRM upon cooling rate. Above the blocking temperature T_B the domain walls in a grain are thermally excited past the potential barriers, which prevent movements below T_B. Above T_B a grain thus has a magnetic moment in equilibrium with the external field (Stacey 1958). Quite apart from the fact that blocking temperature is actually a range of temperatures because the domain walls in a grain have different areas and activation energies, the value of T_B is dependent upon the rate of cooling, because thermally activated domain wall motion is a rate process (Stacey 1960 a). The blocking temperatures T_{B1} and T_{B2} corresponding to cooling rates T_1' and T_2' are approximately related by the equation

$$\frac{1}{T_{B2}} - \frac{1}{T_{B1}} = \frac{k}{E} \ln\left(\frac{T_1'}{T_2'}\right), \quad . \quad . \quad . \quad . \quad . \quad . \quad . \quad (39)$$

where E is potential barrier energy and k is Boltzmann's constant. Slower cooling thus causes a lowering of blocking temperature, reduction of the ratio (σ_R/σ_B) and hence a smaller TRM. The effect may be appreciable when the natural magnetic moments of very large igneous bodies are considered and brings an additional unknown into any attempt to guess the magnitude of the primeval earth's field from the magnitudes of the natural moments of rocks. It may be noted that in single domain grains the effect is exactly opposite since lower blocking temperature results in higher moments μ of the grains and therefore increases the factor $(\mu H/kT_B)$, producing stronger alignment.

APPENDIX

Mean and mean square direction cosines of the nearest easy directions of magnetization with respect to a fixed direction in an assembly of grains with randomly oriented crystallographic axes.

Cubic grains with positive and negative magnetocrystalline anisotropy constants K_1 have easy directions of magnetization parallel to [100] and [111] crystallographic axes. In magnetite K_1 is negative and the easy direction is [111].

The calculation of mean and mean square direction cosines of the angles between nearest easy directions of magnetization and a fixed direction in a random assembly of grains is equivalent to calculating the cosines for random directions with respect to the nearest easy direction in a fixed cube. We consider a cube of side $2d$ centred at the origin of a coordinate system, the sides being parallel to the x, y, z axes. A line emerging from the face $(z=d)$ at (x, y, d) makes angles ϕ with the z axis ([100] axis) and ψ with the body diagonal $(x=y=z)$ ([111] axis), where

$$\cos\phi=\frac{d}{(d^2+x^2+y^2)^{1/2}},$$

$$\cos\psi=\frac{d+x+y}{3(d^2+x^2+y^2)^{1/2}}.$$

It is sufficient to integrate over one quarter-face since all other quarter-faces present simple repeats of the same geometry. The mean and mean square direction cosines are then:

$$\begin{array}{ll} \text{For } K_1 \text{ positive} & \left\{\begin{aligned} \overline{\cos^2\alpha} &= \frac{6}{\pi}\int_0^d\int_0^d \frac{\cos^3\phi\,dx\,dy}{(d^2+x^2+y^2)}=0{\cdot}701, \\ \overline{\cos\alpha} &= \frac{6}{\pi}\int_0^d\int_0^d \frac{\cos^2\phi\,dx\,dy}{(d^2+x^2+y^2)}=0{\cdot}818. \end{aligned}\right. \\ \text{([100] easy)} & \\ \text{For } K_1 \text{ negative} & \left\{\begin{aligned} \overline{\cos^2\alpha} &= \frac{6}{\pi}\int_0^d\int_0^d \frac{\cos^2\psi\cos\phi}{(d^2+x^2+y^2)}\,dx\,dy=0{\cdot}728, \\ \overline{\cos\alpha} &= \frac{6}{\pi}\int_0^d\int_0^d \frac{\cos\psi\cos\phi}{(d^2+x^2+y^2)}\,dx\,dy=0{\cdot}858_5. \end{aligned}\right. \\ \text{([111] easy)} & \end{array}$$

References

Balsley, J. R., and Buddington, A. F., 1960, *Amer. J. Sci.*, **258A, 6.**

Fuller, M. D., 1960, *Nature, Lond.*, **186,** 791.

Graham, J. W., 1954, *Bull. geol. Soc. Amer.*, **65,** 1257.

Irving, E., Stott, P. M., and Ward, M. A., 1961, *Phil. Mag.*, **6,** 225.

Jackson, R. C., Lee, E. W., and Troughton, A. G. H., 1958, *Brit. J. appl. Phys.*, **9,** 495.

Roquet, J., 1954, *Ann. Geophys.*, **10,** 282.

Stacey, F. D., 1958, *Phil. Mag.*, **3,** 1391; 1959, *Ibid.*, **4,** 594; 1960 a, *Aust. J. Phys.*, **13,** 599; 1960 b, *J. geophys. Res.*, **65,** 2492.

Stacey, F. D., Joplin, Germaine, and Lindsay, J., 1960, *Geofis. pur. appl.*, **47,** 30.

Stoner, E. C., 1945, *Phil. Mag.*, **36,** 803.

Stoner, E. C., and Wohlfarth, E. P., 1948, *Phil. Trans.*, **240,** 599.

Uyeda, S., 1958, *Japan. J. Geophys.*, **2,** 1.

Verhoogen, J., 1959, *J. geophys. Res.*, **64,** 2441.

The Force on a Moving Dislocation

By F. R. N. Nabarro
University of the Witwatersrand, Johannesburg†

[Received September 26, 1960]

Abstract

There is a close formal similarity between the equations of elasticity with anti-plane strain and the equations of electrodynamics in two dimensions, the screw dislocation being the counterpart of the line charge. This similarity has led to the suggestion that there is a specific ‘ Lorentzian ’ force on a dislocation which moves through a medium which is itself in motion. This is the analogue of the magnetic force on a moving charge. The equations of a linear continuum can be satisfied whether such a force exists or not. A non-linear model based on that of Peierls is constructed, and an approximate solution of a problem is presented which, if the approximations made are justified, demonstrates that this ‘ Lorentzian ’ force on a dislocation does not exist.

§ 1. Introduction

Frank (1949) first showed that there were strong formal analogies between the dynamics of a screw dislocation and the dynamics of a particle in the special theory of relativity, the velocity of light in the latter theory being replaced by the velocity of shear waves in the former. Eshelby (private communication 1950, 1953), by an extension of this formal analogy, suggested that a dislocation line which moved through a medium which was itself in motion might experience a force proportional to its velocity through the medium, analogous to the Lorentz force on a moving charge. A physical interpretation of this result was given by Nabarro (1951), and a simpler discussion by Eshelby (1956).

Interest in the nature of this force has been revived in discussions and correspondence with Gilman, Frank and Eshelby. Gilman has suggested that the existence of a Lorentzian force on a fast-moving dislocation may be a factor in explaining the observation of Johnston and Gilman (1960) that a dislocation loop may be expanded slowly in lithium fluoride without producing further dislocations, while an equal expansion in a shorter time leads to profuse multiplication of dislocations. On the other hand, Frank has given reasons for doubting the physical reality of the Lorentzian force, and has proposed a paradox which appears to show that the existence of the Lorentzian force on a dislocation leads to a conflict with the Principle of Special Relativity. The present approach is based on the idea that a linear field theory cannot determine the equation of motion of its singularities. Accordingly, arguments based on a linear theory show that the motion induced by this force will be in accordance with the laws of mechanics, if it occurs, but leave open the possibility that it may not occur, or show that it is difficult to see what processes will induce this motion, but do not show that the existence of the motion is in conflict with the general laws of nature. The arguments in favour of the real existence of the force show that if the motion in the direction of the force occurs, external tractions have to be applied to maintain the prescribed velocities. When the motion occurs, these external agents do work, and we are accustomed to say that if a given motion of a dislocation allows external agents to do work, then a force acts on the dislocation in the direction of that motion. The arguments against the real existence of the force rest on the appearance of a term V, which is apparently the *absolute* velocity of the medium in the neighbourhood of the dislocation. Such a uniform velocity cannot affect the internal motions of a system.

---

† On leave at Cavendish Laboratory, Cambridge.

The nature of the force is such that if one part of a crystal is slipping over another by the spreading of loops of dislocations over a glide plane, and the crystal as a whole is moving in the same direction as one of the edge elements of each loop is moving, both screw elements of each loop tend to deviate towards the same side of the glide plane. Although the edge elements could leave the glide plane only by climb, a similar Lorentzian force acts on them, and, to simplify the sign conventions, we shall consider a two-dimensional case in which only edge dislocations are moving.

§ 2. THE LINEAR THEORY

We consider the crystal of fig. 1. To avoid difficulties connected with the transport of matter in the climb of dislocations, we suppose the gliding of the upper part of the crystal over the lower with relative velocity v to be effected by the movement of equal numbers of positive and negative edge dislocations in opposite directions. We suppose that in a given frame of reference the upper and lower parts of the crystal have velocities in the x direction of $V+\frac{1}{2}v$ and $V-\frac{1}{2}v$ respectively, while the glide plane is at a height ζ above the middle of the crystal. The three quantities V, v and ζ specify the motion of the crystal, but not its shape, which depends on the past values of $v(t)$ and $\zeta(t)$. The coordinates are thus rheonomic.

We neglect any resistance to the motion of the dislocations. The initial rates of change of V, v and ζ then depend on the constraints which are imposed on the motion. We shall consider constraints of three kinds: (i) free motion, (ii) linear motion with conservation of linear momentum and (iii) linear motion with v and V maintained constant.

(i) We first consider the crystal to be moving freely in space. Then its kinetic energy, its linear momentum along Ox and its angular momentum around Oy must be conserved. These three conditions ensure that V, v and ζ remain constant, so that there is no Lorentzian force.

When the crystal travels freely the conservation of angular momentum ensures that the relative velocity v continues to be directed along the x axis. If the conditions of constancy of kinetic energy and of linear momentum are replaced by other conditions, the condition of constancy of angular momentum can generally be satisfied only if the glide plane is allowed to rotate about the y axis. We therefore replace the condition of constancy of angular momentum by the condition of constant zero angular velocity of the glide plane. We do this by arranging that the upper and lower surfaces of the crystal are guided by frictionless planes at $z = \pm\frac{1}{2}a$. The forces exerted by the planes $z = \pm\frac{1}{2}a$ do no work and have no component in the Ox direction, so that kinetic energy and momentum along Ox are still conserved. They may introduce stresses into the crystal which exert forces on the dislocations, but these forces act in opposite directions on dislocations of opposite signs, whereas the Lorentzian force acts in the same direction on dislocations of opposite signs when they are moving in opposite directions.

Fig. 1

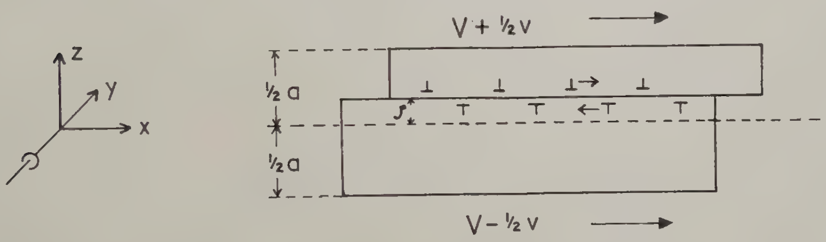

Glide of a crystal. The mean velocity of the crystal is V, the relative velocity of the upper and lower parts v. The thickness of the crystal is a, and the glide plane lies a distance ζ above the middle of the crystal.

(ii) Having replaced the 'natural' condition of constant angular momentum by the condition of constant angular velocity which was implicit in the statement of the problem, we proceed to replace the 'natural' condition of constant kinetic energy by the condition of constant relative velocity v which is stated in the problem. We may do this by means of a mechanical device which is attached to the two parts of the crystal, but is not anchored to a fixed frame of reference. This device can alter the kinetic energy of the crystal, but cannot alter its linear momentum. The linear momentum is proportional to $(\frac{1}{2}a-\zeta)(V+\frac{1}{2}v)+(\frac{1}{2}a+\zeta)(V-\frac{1}{2}v)$. Thus, if the initial values of V, v and ζ are V_0, v_0 and ζ_0, the conditions of the experiment are now given by

$$v = v_0$$

$$(\tfrac{1}{2}a-\zeta)(V+\tfrac{1}{2}v)+(\tfrac{1}{2}a+\zeta)(V-\tfrac{1}{2}v) = (\tfrac{1}{2}a-\zeta_0)(V_0+\tfrac{1}{2}v_0)+(\tfrac{1}{2}a+\zeta_0)(V_0-\tfrac{1}{2}v_0). \quad (1)$$

These lead to

$$V = V_0 + (\zeta-\zeta_0)v_0/a \quad (2)$$

and a kinetic energy T given by

$$2T/\rho S = (\tfrac{1}{2}a - \zeta)(V + \tfrac{1}{2}v)^2 + (\tfrac{1}{2}a + \zeta)(V - \tfrac{1}{2}v)^2$$

or

$$2aT/\rho S = a^2 V_0^2 - 2a\zeta_0 V_0 v_0 + \zeta_0^2 v_0^2 + (\tfrac{1}{4}a^2 - \zeta^2)\, v_0^2. \quad . \quad . \quad (3)$$

where ρ is the density of the crystal and S the area of the glide plane.

In accordance with the usual definition of the force on an elastic singularity (such as a group of dislocations), we say that if the movement of the glide plane in a given direction allows the applied forces to do work, then a force acts on the glide plane in this direction. In the present problem the work done by the applied forces appears as kinetic energy. The only term in (3) which depends on ζ is the last. This does not contain V_0, so that the motion of the glide plane cannot be used to determine the absolute velocity V_0. In fact the glide plane is in stable equilibrium in the middle of the crystal, and, if displaced, tends to move back to the middle, a satisfactorily 'relativistic' result.

(iii) Let us finally replace the 'natural' condition of constancy of linear momentum by the condition V = constant which is stated in the problem. This condition cannot be expressed in terms of the internal state of the crystal, but only with respect to an external reference system. It is now possible to vary ζ if linear momentum is no longer conserved. This requires a force in the Ox direction to act on the crystal as a whole, and this force must react on the fixed reference system. Once we recognize that the imposed conditions of the experiment require external forces to act, we see that the situations (a) and (b) in fig. 2 are not identical, any more than the conditions are identical if we require a rifle not to recoil when a bullet is fired at 7×10^4 cm sec^{-1} or if we require the rifle to recoil at 7×10^4 cm sec^{-1}

Fig. 2

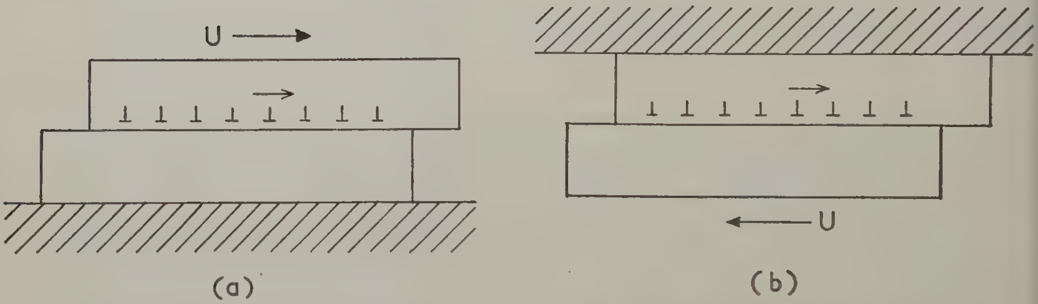

The upper half of a crystal glides with velocity U to the right with respect to the lower half, the motion being caused by a procession of positive edge dislocations moving from left to right. In (a) the bottom of the crystal is fixed and top moves to the right, while in (b) the top of the crystal is fixed while the bottom moves to the left.

while the bullet is held fixed. In fact under the imposed conditions $V=V_0$, $v=v_0$ the kinetic energy is given by

$$2T/\rho S=(\tfrac{1}{2}a-\zeta)(V_0+\tfrac{1}{2}v_0)^2+(\tfrac{1}{2}a+\zeta)(V_0-\tfrac{1}{2}v_0)^2$$
$$=aV_0{}^2+\tfrac{1}{4}av_0{}^2-2\zeta V_0v_0. \qquad (4)$$

If V_0 and v_0 have the same sign, T is increased by decreasing ζ, and conversely, so that the system gains kinetic energy from its constraining mechanisms when the slip plane moves to increase the volume of material which is moving fastest with respect to the system of reference in which V is prescribed. By expressing v_0 in terms of the number and velocity of the dislocations moving in the glide plane it is easily shown that $\partial T/\partial\zeta$ represents a force on each dislocation equal to $b\rho V_0v_0$, where b is the Burgers vector.

As was to be expected from the fact that only linear mechanics is used, this calculation does not lead to a unique conclusion. We have shown that if the glide plane does change in the way predicted by the force which has just been calculated, the equations of mechanics will be satisfied. If the glide plane does not change, the equations of mechanics are still satisfied. Similarly we may suppose that the free motion of fig. 2 (*a*) is perturbed by a force applied to the upper block in that direction of its motion U. Then the equations of mechanics may be satisfied either by the glide plane moving downwards to increase the mass of the moving block, or by an acceleration of the block rigidly over the existing glide plane. Conversely it is strange that the internal behaviour of the crystal should depend on its mean velocity with respect to the reference system against which the applied force reacts, but the crystal is not an isolated system to which a principle of relativity can be applied. If the crystal and the massive reference system are treated as a single closed system, V is an internal coordinate, and neither the presence nor the absence of a force depending on it violates the ideas of relativity.

§ 3. THE NON-LINEAR THEORY

We attempt to resolve the question by constructing a non-linear model in which two screw dislocations of opposite sign lie in the plane $y=vt$, and the Peierls condition is applied between planes $y=vt\pm\tfrac{1}{2}b$. The dislocations are held in equilibrium against their natural attraction by an applied shear stress p_{yz}. There is an analogous electromagnetic problem in which two line charges are held in equilibrium by an electric field E_x. In both problems we may calculate the external field which is necessary to maintain equilibrium when the singularities are at rest, and then enquire how this stress is altered when the singularities move in the y direction with speed v. In both cases the Lorentz contraction increases the stress or electric field with which each singularity attracts the other by a factor $(1-v^2/c^2)^{-1/2}$, and, if there were no other effects, the external stress would have to be increased by this amount in order to maintain equilibrium. In the electromagnetic case the moving charges each move in a magnetic field produced by the motion of the other. This results in a repulsion between the charges which, to lowest order in v, is $-v^2/c^2$ times their attraction when at rest. To this order the total attraction between them is multiplied by a factor $1-v^2/2c^2$, and the external field E_x required to maintain equilibrium is therefore reduced by this factor. The velocity-dependent terms in the interaction reverse the effect of the Lorentz contraction of the static field.

The function w which exactly satisfies the Peierls condition between the planes $y=vt\pm\frac{1}{2}b$ and exactly satisfies the elastic equation of motion outside these planes is given by

$$\begin{aligned}\frac{2\pi w}{b} = {} & \tan^{-1}\frac{y+\frac{1}{2}b(\sec\delta-1)\operatorname{sgn}(y-vt)-vt}{\rho(x-l)} \\ & -\tan^{-1}\frac{y+\frac{1}{2}b(\sec\delta-1)\operatorname{sgn}(y-vt)-vt}{\rho(x+l)} \\ & +(y/b)\sin\delta+\tfrac{1}{2}(\delta-\sin\delta)\operatorname{sgn}(y-vt), \quad . \quad . \quad . \quad . \quad . \quad (5)\end{aligned}$$

where

$$\rho=(1-v^2/c^2)^{1/2} \quad . \quad . \quad . \quad . \quad . \quad . \quad . \quad . \quad . \quad (6)$$

and

$$\delta=\tfrac{1}{2}\sin^{-1}(b/\rho l). \quad . \quad . \quad . \quad . \quad . \quad . \quad . \quad . \quad (7)$$

The distance between the dislocations, $2l$, is independent of v. The external stress at large distances which maintains equilibrium is

$$p_{yz}=(\mu/2\pi)\sin\delta.$$

If the dislocations are far apart so that their cores do not overlap, δ is small, and $\sin\delta=b/2\rho l$. Thus the external stress is proportional to ρ^{-1}, which corresponds to the effect of the Lorentz contraction alone and the absence of velocity-dependent forces which would lead to a total equilibrating stress proportional to ρ. The calculation is not wholly convincing, because it fails to consider the mechanisms by which the dislocations can move in the y direction and, more seriously, by which the state of being non-Hookean between the planes $y=vt\pm\frac{1}{2}b$ can propagate.

§ 4. CONCLUSION

The existence or non-existence of a Lorentzian force on a dislocation which moves in a medium which is itself in motion can be proved only by constructing a non-linear model of a dislocation. We have obtained an approximate solution for such a model, and, in this solution, the Lorentzian force is absent. It is possible, but hardly likely, that it would appear in an exact solution.

ACKNOWLEDGMENTS

The ideas presented in this paper have been developed as a result of stimulating discussions with Professors F. C. Frank and J. J. Gilman, and Drs. J. D. Eshelby and F. Kroupa.

REFERENCES

ESHELBY, J. D., 1953, *Phys. Rev.*, **90**, 248; 1956, *Solid State Physics*, **3**, 79.
FRANK, F. C., 1949, *Proc. phys. Soc., Lond.* A, **62**, 131.
JOHNSTON, W. G., and GILMAN, J. J., 1960, *J. appl. Phys.*, **31**, 632.
NABARRO, F. R. N., 1951, *Proc. roy. Soc.* A, **209**, 278.

Elastic Self- and Interaction Energies of Dislocation Jogs

By F. Kroupa† and L. M. Brown
Cavendish Laboratory, Cambridge, England

[Received February 27, 1961]

Abstract

An elastic calculation shows that there is an interaction between two jogs or kinks on an infinite straight dislocation line. For jogs sufficiently far apart, the interaction potential varies as the reciprocal of the distance between them, and as the product of their lengths. Formulae are also obtained for the self energies of jogs.

Recent papers on plasticity have emphasized the role of jogs on dislocation lines in limiting the velocity a dislocation can achieve under a given applied stress (Mott 1960, Hirsch 1960, Gilman and Johnston 1960). Such theories are based on calculations of the rate at which jogs are created by forest cutting, and the rate at which they are annihilated by glide or climb. Two important quantities are required for these calculations: the *self-energy* of a jog, E_S, and the *interaction energy* between two jogs, E_I. We shall calculate these quantities using the model of a dislocation familiar in the classical isotropic theory of elasticity. We shall assume that both jogs are perpendicular to an infinite straight dislocation line.

The method is illustrated in fig. 1. When the loop 2 is added to a straight dislocation 1 with the same Burgers vector **b**, the resulting configuration is that of a dislocation line containing two ‘ antiparallel ’ jogs. The total elastic energy E of the dislocation with two such jogs is given by

$$E = E_1 + E_2 + E_{12} \qquad \ldots \ldots \ldots \quad (1)$$

where E_1 and E_2 are the self-energies of the dislocation line and loop respectively, and E_{12} is the interaction energy between them.

The ‘ double jog energy ’, E_{jj}, can be defined as

$$E_{jj} = E - E_1 = E_2 + E_{12}. \qquad \ldots \ldots \ldots \quad (2)$$

It can be divided into two parts. That part which does not depend on the distance r between jogs, is twice the self-energy of one jog E_S. The part dependent on r is precisely the interaction energy between the two jogs, E_I. Thus

$$E_{jj} = 2E_S + E_I(r). \qquad \ldots \ldots \ldots \quad (3)$$

---

† On leave from the Institute of Physics, Prague.

The Burgers vector **b** can be resolved into three components (fig. 1): b^P, perpendicular to the plane of the jogs; b^S in the direction of the straight dislocation (such that it is screw); and b^E in the plane of the jogs but perpendicular to the straight dislocation (such that it is edge). We shall treat these cases separately. E_S and E_I for a general Burgers vector **b** are given as sums

$$E_S = E_S{}^P + E_S{}^E + E_S{}^S;\ E_I = E_I{}^P + E_I{}^E + E_I{}^S$$

for

$$\mathbf{b} = \mathbf{i}b^E + \mathbf{j}b^P + \mathbf{k}b^S. \qquad (4)$$

Fig. 1

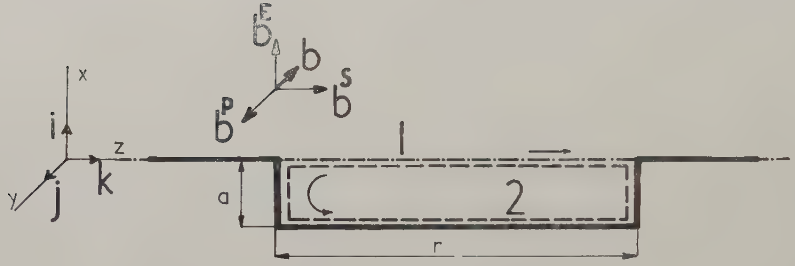

The self-energy of a rectangular loop can be calculated by the method of Yoffe (1960). For a prismatic loop, with its Burgers vector b^P normal to the loop plane, we have:

$$E_2{}^P = \frac{\mu(b^P)^2}{2\pi(1-\nu)}\left\{a\log\frac{2a}{\epsilon} + r\log\frac{2r}{\epsilon} - \frac{a}{2}\log\frac{\sqrt{(a^2+r^2)}+a}{\sqrt{(a^2+r^2)}-a}\right.$$
$$\left. - \frac{r}{2}\log\frac{\sqrt{(a^2+r^2)}+r}{\sqrt{(a^2+r^2)}-r} + 2\sqrt{(a^2+r^2)} - 2(a+r)\right\} \qquad (5)$$

where μ is the shear modulus, ν is Poisson's ratio, and ϵ is the core cut-off radius, $\epsilon \approx b$. The length of the loop is r, and its width is a.

For a glide loop, with its Burgers vector parallel to the side a, we find

$$E_2{}^E = \frac{\mu(b^E)^2}{2\pi}\left\{a\left[\log\frac{2a}{\epsilon} - \frac{1}{2}\log\frac{\sqrt{(a^2+r^2)}+a}{\sqrt{(a^2+r^2)}-a} + \frac{\sqrt{(a^2+r^2)}}{a} - \frac{a+r}{a}\right]\right.$$
$$\left. + \frac{r}{1-\nu}\left[\log\frac{2r}{\epsilon} - \frac{1}{2}\log\frac{\sqrt{(a^2+r^2)}+r}{\sqrt{(a^2+r^2)}-r} + \frac{\sqrt{(a^2+r^2)}}{r} - \frac{a+r}{r}\right]\right\}. \qquad (6)$$

The self-energy $E_2{}^S$ of a similar loop, with its Burgers vector b^S parallel to r, can be found by interchanging r and a in the above formula.

The interaction energies are easily found by computing the work required to make the loop in the stress-field of the infinite dislocation. In the prismatic case we find for instance:

$$E_{12}{}^P = -\frac{\mu(b^P)^2}{2\pi(1-\nu)}\, r\log\frac{a}{\epsilon}. \qquad (7)$$

The interaction $E_{12}{}^{\mathrm{E}}$ is given by eqn. (7) when the superscript P is replaced by E. $E_{12}{}^{\mathrm{S}}$ is given by (7), replacing P by S and omitting the factor $(1-\nu)^{-1}$. The double jog energy, $E_{\mathrm{jj}}{}^{\mathrm{P}}$, is given by eqn. (2), using eqns. (5) and (7), and similarly for $E_{\mathrm{jj}}{}^{\mathrm{E}}$ and $E_{\mathrm{jj}}{}^{\mathrm{S}}$.

Dividing E_{jj} up as in eqn. (3), one finds for the self-energies

$$\left.\begin{aligned} E_{\mathrm{S}}{}^{\mathrm{P}} &= \frac{\mu(b^{\mathrm{P}})^2 a}{4\pi(1-\nu)}\left[\log\frac{2a}{\epsilon}-2\right], \\ E_{\mathrm{S}}{}^{\mathrm{E}} &= \frac{\mu(b^{\mathrm{E}})^2 a}{4\pi}\left[\log\frac{2a}{\epsilon}-\frac{2-\nu}{1-\nu}\right], \\ E_{\mathrm{S}}{}^{\mathrm{S}} &= \frac{\mu(b^{\mathrm{S}})^2 a}{4\pi(1-\nu)}\left[\log\frac{2a}{\epsilon}-2+\nu\right]. \end{aligned}\right\} \quad . \quad . \quad . \quad . \quad . \quad (8)$$

Note that these elastic energies all become zero for a jog length $a \approx 4\epsilon$. Thus, for small jogs, or jogs of from one to four or five Burgers vectors long, the elastic approximation breaks down, and most of the jog energy must be considered to come from atomic arrangements in the core of the dislocation. Our formulae are therefore useful only for long jogs.

When $a/r \ll 1$ so that powers of a/r greater than one can be neglected, we find for the interaction energies:

$$\left.\begin{aligned} E_{\mathrm{I}}{}^{\mathrm{P}} &= -\frac{\mu(b^{\mathrm{P}})^2}{8\pi}\left[\frac{1}{1-\nu}\right]\frac{a^2}{r}, \\ E_{\mathrm{I}}{}^{\mathrm{E}} &= -\frac{\mu(b^{\mathrm{E}})^2}{8\pi}\left[\frac{1-2\nu}{1-\nu}\right]\frac{a^2}{r}, \\ E_{\mathrm{I}}{}^{\mathrm{S}} &= -\frac{\mu(b^{\mathrm{S}})^2}{8\pi}\left[\frac{1+\nu}{1-\nu}\right]\frac{a^2}{r}. \end{aligned}\right\} \quad . \quad . \quad . \quad . \quad . \quad . \quad (9)$$

The total force on a single jog can be found from differentiating the above expressions with respect to r. In all cases, the jogs attract one another with a force which falls off with distance as r^{-2}. The force also increases as the square of the jog length. Two antiparallel jogs behave thus as equal and opposite electrical charges.

The method used above cannot be applied directly to calculate the interaction energy between antiparallel jogs of different length, or between parallel jogs. For the general case, when both jogs are perpendicular to the dislocation line, but have different lengths and lie on different planes making the angle α with each other (fig. 2), the dislocation with two jogs can be composed from a straight dislocation 0, and two semi-infinite loops 1 and 2. The total energy E of the jogged dislocation is the sum of the self- and interaction energies

$$E = E_0 + E_1 + E_2 + E_{01} + E_{02} + E_{12}.$$

Only the interaction energy E_{12} between two semi-infinite loops 1 and 2 depends on the distance r between the two jogs. Thus

$$E_{\mathrm{I}} = E_{12}(r).$$

To calculate this interaction energy, we must know the stress field of the loop 1. This can readily be found using the expressions for stresses of an infinitesimal loop (Kroupa 1962) at the point (0, 0, z) and integrating over the area of the loop. Since we are only interested in the case where $r \gg a_1$, $r \gg a_2$, we can treat the widths of the loops as infinitesimal, effectively replacing all double integrals by single integrals. In this way, the interaction energy is found to be, for general **b**

$$E_{\mathrm{I}} = E_{12} = -\frac{\mu}{8\pi(1-\nu)}\left\{[(b^{\mathrm{P}})^2+(b^{\mathrm{S}})^2(1+\nu)+(b^{\mathrm{E}})^2(1-2\nu)]\cos\alpha - 2\nu b^{\mathrm{P}} b^{\mathrm{E}} \sin\alpha\right\}\frac{a_1 a_2}{r} . \qquad (10)$$

Fig. 2

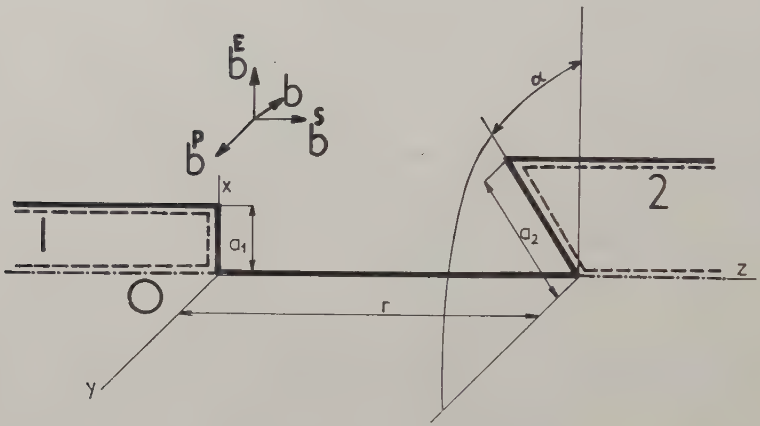

For $\alpha = 0$ and $a_1 = a_2$, eqn. (10) reduces to the special case of antiparallel jogs of length a (eqns. (4) and (9)). When the jogs are parallel, $\alpha = \pi$, $\cos\alpha = -1$, $\sin\alpha = 0$; the interaction energy is positive, and the jogs repel one another. Thus the analogy with electric charges is very close in that unlike (antiparallel) jogs attract, and like (parallel) jogs repel, provided that the jogs are in the same plane, and far apart.

ACKNOWLEDGMENTS

Our thanks are due to Dr. J. D. Eshelby, who independently obtained formulae (9), and kindly compared the results with us. We also acknowledge the encouragement of Professor N. F. Mott, F.R.S., and Dr. W. H. Taylor. We are grateful to Dr. P. B. Hirsch for reading the manuscript and helpful discussion. Financial support is gratefully acknowledged from the British Council (F.K.) and from the Admiralty (L.M.B.).

REFERENCES

GILMAN, J. J., and JOHNSTON, W. G., 1960, *J. appl. Phys.*, **31,** 687.
HIRSCH, P. B., 1960, Congress on Crystallography, Cambridge.
KROUPA, F., 1962 (to be published).
MOTT, N. F., 1960, *Trans. Amer. Inst. min.* (*metall.*) *Engrs*, **218,** 962.
YOFFE, E. H., 1960, *Phil. Mag.*, **5,** 161.

Intensity of the Cosmic Radiation at Great Depths Underground

By J. C. Barton
Northern Polytechnic, London

[Received April 17, 1961]

Abstract

The cosmic ray intensity was measured in a mine using a combined scintillation counter and Geiger counter telescope. It was shown that this apparatus could discriminate effectively against local γ-radiation. The intensities at 1660 m.w.e. and 3280 m.w.e. were 3×10^{-5} and 10^{-6} of that at the surface; no cosmic ray events were observed at 5050 m.w.e. The results suggest a steepening of the energy spectrum in the region of 10^{12} ev. The most probable energy loss of μ-mesons which had a mean energy of about 3×10^{11} ev was found to be not significantly higher than that of minimum ionizing particles.

§ 1. Introduction

Progress in the measurement of the intensity of cosmic rays deep underground has been remarkably slow, although it has always been recognized that such information would be of considerable interest. Since the review article of Barrett *et al.* (1952), which showed that data on the intensity were then established down to a depth close to 2000 m.w.e., no further satisfactory results have been published. There appear to be two major difficulties which have to be surmounted. Firstly, there are only a small number of mines which are of sufficient depth and are sunk in rock of low radioactive content. (The alternative technique of working in the deep oceans presents considerable technical problems which have not yet been solved in an economically feasible manner.) Secondly, it is necessary to measure a very feeble flux of mesons in the presence of γ-radiation from the surrounding rock. Even in a mine of relatively low radioactive content the ratio of the flux of mesons to that of γ-rays is less than 10^{-9} at a depth equivalent to a few thousand metres of water; such a ratio would be regarded as troublesome in an accelerator or pile experiment and is even more so when working away from a laboratory. An attempt made using a Geiger counter telescope in 1956 and reported recently (Barton and Michaelis 1961) failed for this reason. A new apparatus was therefore designed which would make the identification of cosmic ray events more definite, and readings were obtained with this apparatus in the summer of 1960. So far, only a small number of readings have been obtained but these are being reported now as it may be some time before a more satisfactory set of data is available.

§ 2. APPARATUS

This was a modification of that used earlier (Barton 1956) with the middle tray of Geiger counters replaced by a large scintillation counter, fig. 1. The block of plastic phosphor, of size 53·0 cm × 15·0 cm × 3·0 cm, was viewed through a short light guide (at one end) by two type 51 AVP photomultipliers. The optical arrangement was dictated by the need to fit the scintillation counter into the same space as the Geiger counters which had been replaced. As a result the uniformity of response was slightly poorer than that obtained with the rather similar counter for which full information was published recently (Barnaby and Barton 1960). A block diagram of the circuits used, which were much more complicated than those used before, is shown in fig. 2. The fast coincidence between the two photomultipliers was included as an additional precaution against spurious events.

Fig. 1

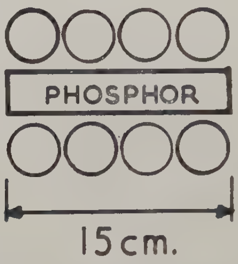

Section through apparatus.

The magnitude of the pulses from the last dynodes of the two photomultipliers, connected in parallel, was measured by a 'ringing coil' type pulse height analyser. The damped oscillation of a tuned circuit, excited by the incoming pulse, was amplified and then passed to a simple integral discriminator which triggered once each cycle until the oscillation had decayed below a certain fixed level. In this manner a chain of pulses was produced whose number was proportional to the logarithm of the height of the original pulse. This number was converted into binary form and, together with the hodoscope data from the eight Geiger counters, was recorded on fourteen tracks on magnetic tape moving at 2·5 cm hour^{-1}. With this type of analyser the width of each channel is proportional to the pulse height accepted by it. In this particular analyser the incremental channel width, which could be controlled by the resistance across the tuned circuit, was set at 10% and was found experimentally to be uniform from the second to at least the fortieth channel.

Fig. 2

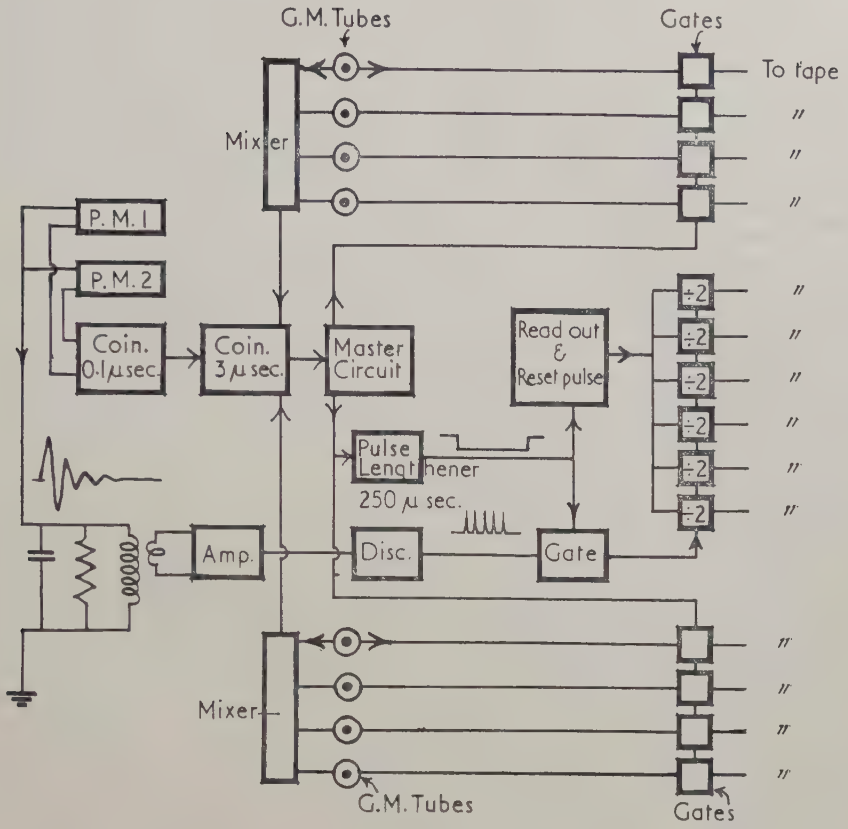

Block diagram of circuits.

The e.h.t. supply for the counters and photomultipliers was provided by a voltage converter circuit derived from that given by Hooker and Light (1956). A corona stabilizer was included in a feed-back loop to control the oscillator and resulted in a stability of 0·1% for the changes in battery voltage and ambient temperature which were encountered under operating conditions.

The apparatus contained a total of 80 transistors which consumed in all rather less than 100 mw. All the circuits were operated from ‘Mallory’ type dry cells which provided a satisfactorily uniform voltage. The most critical stage, the discriminator in the pulse height analyser, was further stabilized by a Zener diode. Both batteries and tape recorder could operate for up to five weeks at a time without attention. Laboratory experiments showed that the counting rate of the apparatus was independent of temperature within the range 10°c to 40°c. There was a slight dependence of pulse height on temperature, and the results have been corrected for this effect whenever the temperature underground was different from that at the surface: the correction necessary was a difference of only one or two channels.

§ 3. OBSERVATIONS

Most of the data was obtained during a visit to the Lake Shore Gold Mine, Northern Ontario, in the summer of 1960. This mine is situated at latitude 48° 9′ N, longitude 80° 3′ W; the surface of the mine is 320 m above sea level and does not vary by more than 30 m for several miles in any direction.

The rock of the Canadian Shield in the region of this mine, except for the thin ore-bearing fissures, is almost entirely syenite–porphyry of density 2·73, mean $Z = 11{\cdot}7$ and mean $Z/A = 0{\cdot}50$ (Thomson 1948); one foot of rock is thus 'equivalent' to 0·83 m of water.

In the first set of experiments the apparatus was operated at the surface and at depths of 2000 ft and 6075 ft. Histograms of pulse height data from all the events recorded are presented in fig. 3, where the data have been grouped into pairs of channels. The data obtained at sea level and at 2000 ft show the characteristic 'Landau' shape, though the asymmetry is less striking than if the pulse heights had been plotted instead of their logarithms. On the other hand the 15 events registered at 6075 ft appear to be of an entirely different character since the mean pulse height is only

Fig. 3

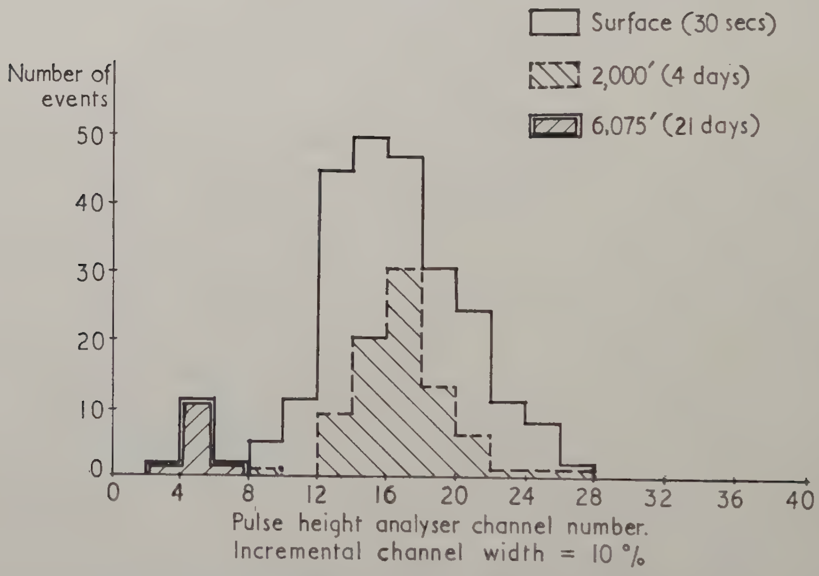

Pulse height histograms for first series of experiments.

of the order of one-third of that recorded elsewhere. Further information can be obtained by examining the Geiger counter hodoscope records. If only one counter has been discharged in each tray the inclination to the vertical of the particle trajectory can be determined. Those events in which more than one counter is discharged in either or both trays are referred to as multiple events, although in a proportion of cases a single particle may be responsible. The resulting analysis is given in table 1.

Allowing for the appropriate statistical and geometric weighting factors it is found that the results at the surface are consistent with the expected approximately $\cos^2\theta$ distribution.

The results for 2000 ft indicate a more collimated distribution and a higher proportion of multiples. Both these effects are to be expected and should be even more noticeable at 6075 ft. Instead the events at the latter depth appear to be more widely spread in angle and include no example of a multiple event. This strengthens the suggestion made above that the events here are of a different nature.

Table 1. Hodoscope results for first series of experiments

	Mean projected inclination to vertical 0°	23°	41°	53°	Multiple events	Total
Surface	88	94	28	3	17	230
2000 ft	33	30	4	1	15	83
6075 ft	2	7	5	1	0	15

Table 2. Hodoscope results for second series of experiments

	Mean projected inclination to vertical 0°	23°	41°	53°	Multiple events	Total
Surface	76	92	26	2	22	218
3950 ft log $h \leqslant 13$	93	131	76	18	2	320
3950 ft log $h \geqslant 18$	1	3	1	0	4	9

In order to investigate the nature of these other events more closely the apparatus was adjusted so that all the scintillation counter pulses were larger but the minimum signal required to trigger the master coincidence circuit was smaller. Histograms then obtained at the surface and at a depth of 3950 ft are shown in fig. 4.

The distribution for the events recorded at the surface is not significantly different from that obtained before, but is shifted to a higher mean value. The two events with a very small pulse height are probably due to particles passing close to the end of the apparatus as the Geiger counters were several centimetres longer than the block of scintillation phosphor. The events at 3950 ft clearly divide into two groups of which the lower one can be compared to that registered at 6075 ft but, owing to the different discriminating requirements, is very much more striking. The hodoscope data are presented separately for each group in table 2.

Fig. 4

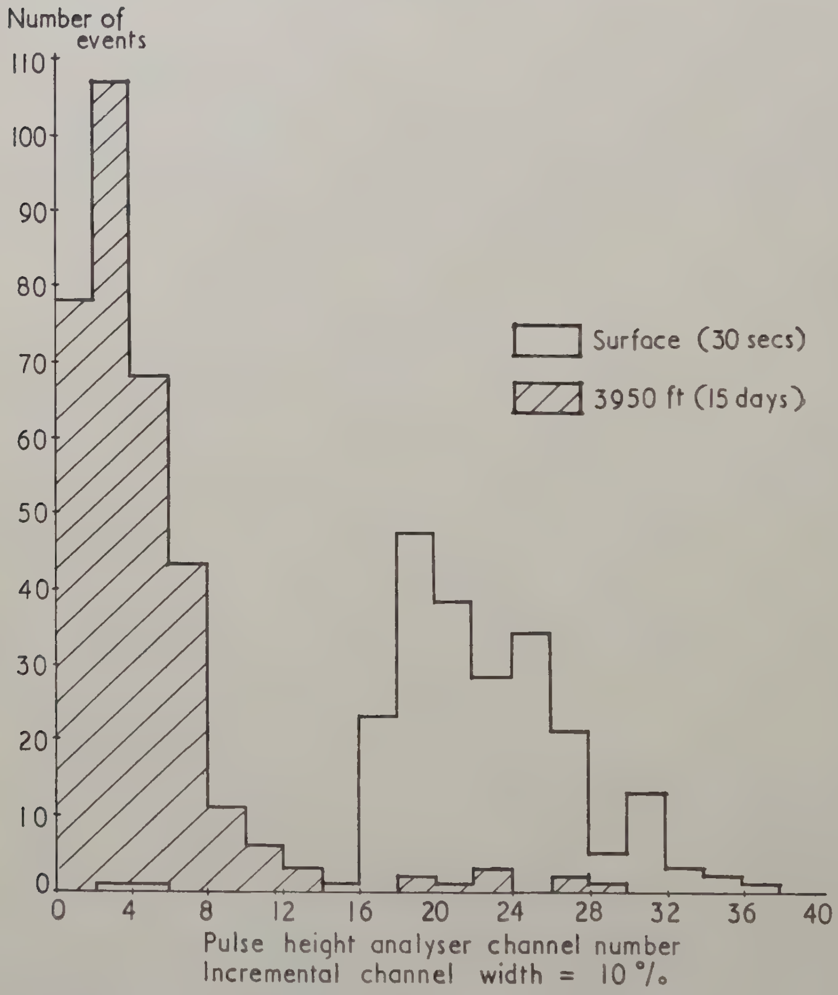

Pulse height histograms for second series of experiments.

It can be shown that the smaller pulse height events at 3950 ft are compatible with an isotropic distribution. These events are clearly similar to those recorded in the earlier experiment (Barton and Michaelis 1961) using a three-fold Geiger counter telescope. The evidence presented there leads to the conclusion that such events were due to γ-radiation from the surrounding rock. Only the other nine events are to be interpreted as due to cosmic rays, for which the high proportion of multiple events is not unexpected. By making a similar analysis of the results at 6075 ft it follows that all the events at that depth can be attributed to the effects of γ-rays, and that there is no evidence for any cosmic rays there. This means that it is only possible to deduce an upper limit for the cosmic ray intensity.

There is one other point of interest about table 2. Among the γ-ray events recorded at 3950 ft there were two events in which two counters were discharged in one tray. This means that, including the scintillation counter, a total of four counters was discharged. In the earlier investigation of Barton and Michaelis (1961) no evidence was found for four-fold coincidences due to γ-rays but it would not have been possible to exclude a very low rate of such events.

The results for the cosmic ray events in the two sets of experiments are combined in table 3. The mean channel number (i.e. the mean of the logarithm of the pulse height) has been adjusted for the second experiment so that it can be compared directly with the first series of experiments. Also the number of multiple events has been reduced to take account of the proportion which can be attributed to a single particle passing through two counters in a tray.

Table 3. Summarized results

	Time	Counts	Normalized rate	Mean channel number	Corrected number of multiples	Proportion of multiple events
Surface	60 sec	448	1	$16{\cdot}1 \pm 0{\cdot}2$	22	5%
2000 ft	4 days	83	$(3{\cdot}2 \pm 0{\cdot}4) \times 10^{-5}$	$16{\cdot}6 \pm 0{\cdot}4$	13	16%
3950 ft	15 days	9	$(9 \pm 3) \times 10^{-7}$	$16{\cdot}9 \pm 1{\cdot}2$	4	45%
6075 ft	21 days	0	$< 10^{-7}$	—	0	—

§ 4. ANALYSIS

The mean channel number, used in table 3, is convenient as an easily observed quantity but is not of direct physical significance. A more detailed analysis of the histograms of pulse heights, in the manner suggested by Barnaby (1961), does give rather similar results. The increase in the most probable pulse height between the surface and 2000 ft was found to be $5 \pm 3\%$ and between the surface and 4000 ft $11 \pm 5\%$.

There is a possibility of a small additional systematic error so that any rise in the energy loss might be between 0 and 10% at 2000 ft and between 0 and 20% at 4000 ft. The minimum energies of the mesons which penetrate to these depths are at least 5×10^{11} ev and $1{\cdot}4 \times 10^{12}$ ev respectively. The mean energy at the underground location of those mesons which succeed in penetrating can only be estimated very crudely since the values depend on the shape of the energy spectrum; estimates of 3×10^{11} ev and 6×10^{11} ev are in accord with the spectrum deduced here.

Recently Barnaby (1961) has shown that between 10^9 ev and 10^{10} ev there can be no increase in the most probable energy loss greater than 1%, in agreement with the predictions of Sternheimer's (1956, 1959) theory. The present data suggest that any increase at higher energies must be very gradual.

The result is not at variance with the increase in the proportion of multiple events underground. These would be expected to contribute mostly to the high energy tail of the Landau distribution and have relatively little effect on the most probable energy loss. There are not sufficient of these events to enable any detailed deductions to be made but the increased number can readily be explained by the increasing importance of electromagnetic interactions by μ-mesons in this energy range. (The contribution from multiple penetrating particles, either surviving from air showers or else produced locally, is extremely small.) Figure 5, which includes additional results obtained at shallower depths, shows that the cross section for these interactions is consistent with a dependence on the logarithm of the meson energy, as predicted theoretically (see, e.g.,

Fig. 5

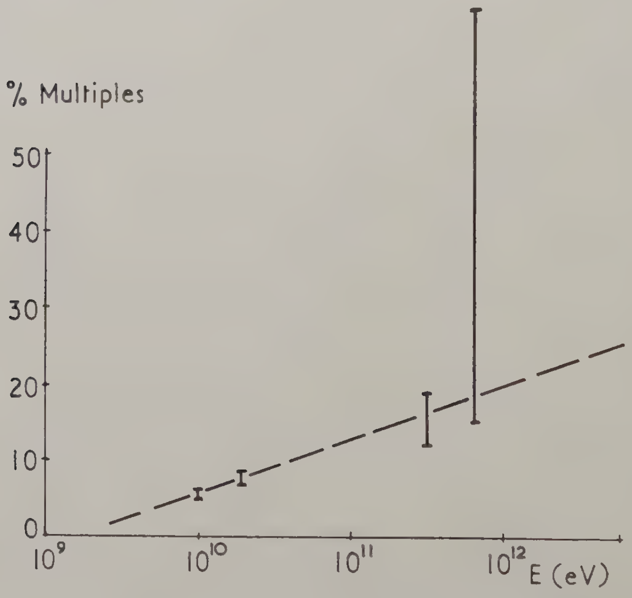

Proportion of multiple events.

Fowler and Wolfendale 1958). Not all the soft component at sea level is in equilibrium with the μ-meson beam so that the results obtained at the surface are not directly comparable and have been omitted from fig. 5.

The total intensity data of table 3 need two corrections in order to construct a range spectrum of μ-mesons. Firstly, mesons which miss the apparatus may nevertheless be recorded through secondary particles produced in the rock close to the apparatus. The importance of this effect will be proportional to the number of multiple events but it is hard to calculate the necessary numerical factor; it must be between 0 and 1

Fig. 6

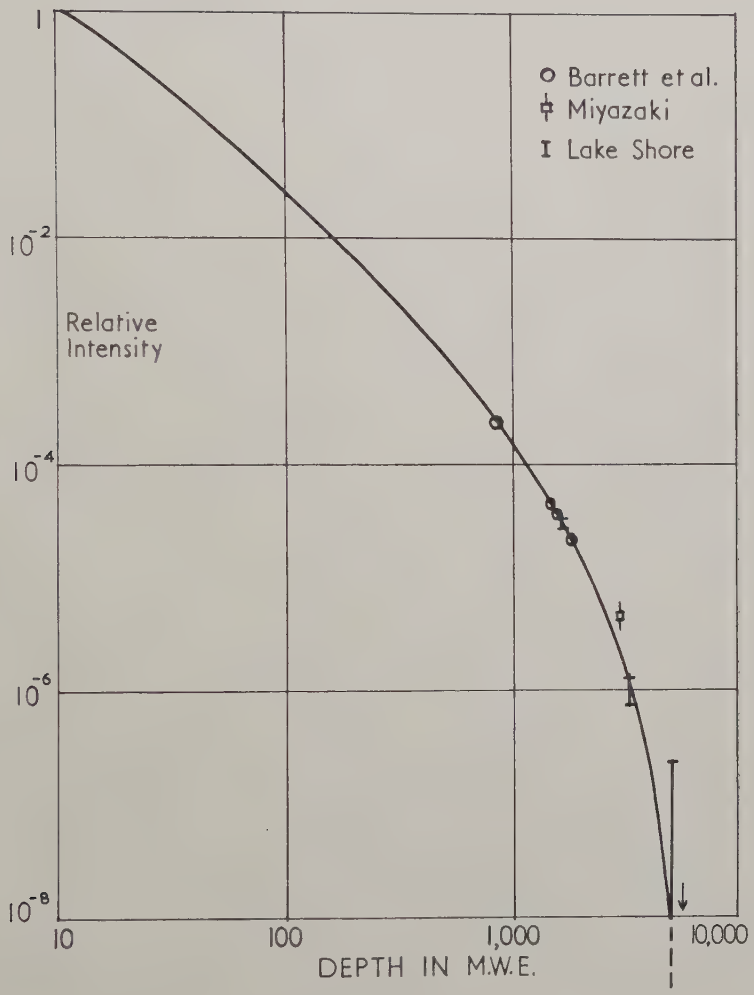

Intensity–depth curve.

so that to adopt a value of $\frac{1}{2}$ will be reasonable and sufficient for the immediate purpose. Secondly, the vertical intensity is not quite proportional to that measured with a wide angle telescope because of the increasing collimation of the μ-meson beam with depth underground. The angular distribution results of Bollinger (1951) are sufficient to enable an adequate estimate of this factor to be made.

The corrected results are plotted as a function of 'water equivalent' depth in fig. 6 together with other available data for the intensity at great depths. The upper limit for the intensity at 5050 m.w.e. has been chosen so that the probability of the true rate being greater is 16% (Regener 1951). The agreement is seen to be good except that the measurement of Miyazaki (1949) at 3000 m.w.e. is not consistent with the new results. There are several reasons for not being surprised at this discrepancy. Miyazaki's results were obtained with a simple telescope of Geiger counters which, as shown by Miesowicz and Massalski (1950) and by Barton and Michaelis (1961), could be sensitive to local radioactivity. The reported 75% decrease in intensity on inserting 100 cm of lead in the telescope suggests that there was some such effect. Also the data are only reported very briefly and there appears to be a discrepancy between the results for two separate experiments.

The intensities measured at various inclinations to the vertical at one depth by Bollinger (1951) can be plotted on an intensity–depth curve, as is done in his thesis. However, estimates made in this way cannot be compared easily with results obtained directly by measurements at different depths because the effects of meson interaction and decay are different in the two cases. Allowing for this factor, and the uncertainties in it, there seems to be adequate agreement between the two sets of results. Neither set has sufficient accuracy for it to be possible to make any useful deductions about the problem of the proportion of K to π-mesons among the parents of the μ-mesons.

To convert the intensity–depth curve to an integral energy spectrum it is necessary to assume the form of the range–energy relationship for high energy μ-mesons, which in turn is obtained from their rate of energy loss. The results for depths less than 1000 m.w.e. have been analysed recently by Ashton (1961) so will not be considered here.

It has been customary (Barrett *et al.* 1952, Ashton 1961) to assume that the rate of energy loss is something like

$$\frac{dE}{dx} = 2{\cdot}05 + 0{\cdot}175 \log_{10} \frac{E}{10^3 + \dfrac{11{\cdot}3 \times 10^6}{E}} + 3{\cdot}0 \times 10^{-6} E \text{ Mev g}^{-1}\text{ cm}^2.$$

Unfortunately there is considerable uncertainty about the correct value for the numerical coefficient in the third term. Although the total cross sections for the various processes (bremsstrahlung, pair production and nuclear) are fairly well established experimentally (Avan 1956, 1958), neither theory nor experiment provides reliable estimates of the partial cross sections when the energy transfer is large. These rarer high energy interactions do not contribute appreciably to the total cross section but may make a large difference to the mean rate of energy loss. This applies especially to the theoretical estimate by Kessler and Kessler (1957) of the nuclear interaction cross section. It is therefore possible that the third term may need to be anything up to twice as large as given above.

A further uncertainty arises because the energy loss can no longer be considered as a continuous process once the additional energy loss terms, particularly the bremsstrahlung, become important. The problem is then analogous to that of β-ray absorption and it is necessary to consider the effects of straggling. This has been treated theoretically for μ-mesons by Mandò and Sona (1953) and by Rozenthal and Strel'tsov (1958); their assumptions and numerical results are rather different but they agree in predicting that the intensity at a given depth will be rather greater than that calculated without allowing for straggling.

If the energy loss relationship is given correctly by the expression adopted by Barrett *et al.*, any high energy transfers are sufficiently rare that it should be reasonable to ignore the correction for straggling. If, however, the second term has been underestimated then the number of high energy transfers is correspondingly larger and the effect of straggling may no longer be negligible. Assuming that at least the sign of the effect is given correctly by the theories, then it will tend to mitigate the larger rate of energy loss.

The data have been plotted as an energy spectrum in fig. 7 for both low and high values of the energy loss expression. The true spectrum should lie between the two curves and, as explained above, is unlikely to be very close to that drawn for the higher value. It is therefore probable that the exponent of the energy spectrum is increasing at energies above 5×10^{11} ev. This result is not in disagreement with the sea-level measurements of the momentum spectrum (Ashton *et al.* 1960), where the exponent of the spectrum was found to be approximately constant, since the statistical accuracy of their results is not sufficient to rule out an appreciable change at energies greater than 5×10^{11} ev. An indication of the steepening of the meson energy spectrum at very high energies has also been reported by Duthie *et al.* (1961) from the analysis of the spectrum of π^0 mesons which produce electron–photon cascades in nuclear plates exposed near the top of the atmosphere. The results in the paper suggest an absolute magnitude of the spectrum exponent which is larger than that which would be deduced from fig. 7, but subsequent work by the same group (Perkins, private communication) leads to a meson spectrum which is in agreement with that deduced from the underground observations.

The lack of any cosmic ray events during the 21 days of observation at the greatest depth is of interest in setting an upper limit to the cross section for the interaction of neutrinos. As far as neutrinos emitted by the sun are concerned the limit is much higher than the recently observed value, but for neutrinos produced by cosmic ray decay processes there is the possibility that, due to a resonance in the cross section at high energy, the cross section may be very much higher. An estimate of the possible rate which would be expected on account of anti-neutrinos has been given by Glashow (1960). It has already been pointed out (Barton 1960) that the present observations put the upper limit within the region predicted by Glashow. Unfortunately neither the statistical weight of the observations nor the uncertainties in the theoretical treatment allow any definite conclusion to be drawn.

Fig. 7

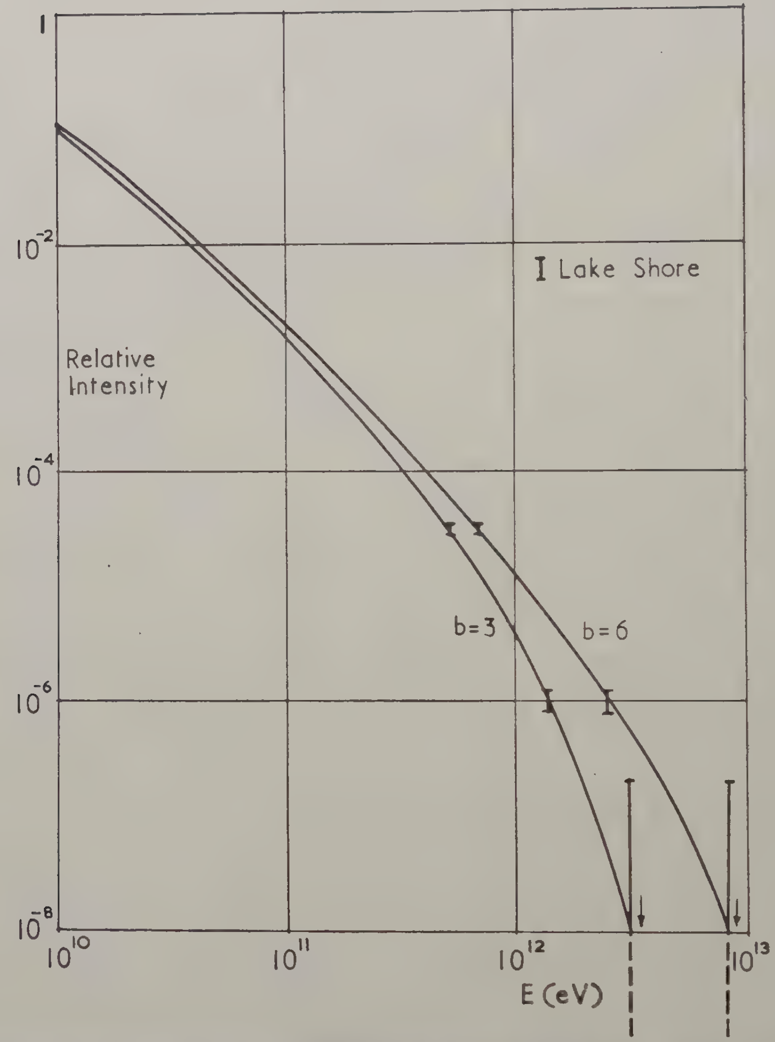

Integral spectra of μ-mesons. *b* is the coefficient of the third term in energy loss expression.

§ 5. CONCLUSIONS

1. The intensity of the cosmic radiation at a depth of 3280 m.w.e. is about one-millionth of that at the surface and at 5050 m.w.e. it is unlikely to be more than one ten-millionth.

2. The most probable rate of energy loss of μ-mesons is not more than 10% greater at 3×10^{11} ev and 20% at 6×10^{11} ev than at 10^9 ev, and may be the same.

3. The proportion of secondary particles increases slowly with the energy of the mesons.

4. The energy spectrum of μ-mesons appears to become steeper a energies greater than 5×10^{11} ev.

ACKNOWLEDGMENTS

The observations at Lake Shore were made possible and effective by the most helpful cooperation of Mr. W. T. Robson, the Mine Superintendent, and Mr. C. Purvis, the Chief Engineer.

The expenses of travelling to Canada were met by a grant from the Royal Society.

I am most grateful to Dr. E. P. George for first stimulating my interest in this problem and to Dr. M. E. Pillow, Professor J. D. Bernal, F.R.S., and Professor G. D. Rochester, F.R.S., for their support.

The apparatus was constructed with the skilled assistance of Mr. R. F. Benham and Mr. W. F. Carter.

REFERENCES

ASHTON, F., 1961, *Proc. phys. Soc., Lond.*, **77,** 587.

ASHTON, F., BROOKE, G., GARDENER, M., HAYMAN, P. J., JONES, D. G., KISDNASAMY, S., LLOYD, J. L., TAYLOR, F. E., WEST, R. H., and WOLFENDALE, A. W., 1960, *Nature, Lond.*, **185,** 364.

AVAN, L., 1956, *Ann. Phys., Paris*, **1,** 1870; 1958, *Ibid.*, **3,** 123.

BARNABY, C. F., 1961, *Proc. phys. Soc., Lond.*, **77,** 1149.

BARNABY, C. F., and BARTON, J. C., 1960, *Proc. phys. Soc., Lond.*, **76,** 745.

BARRETT, P. H., BOLLINGER, L. M., COCCONI, G., EISENBERG, Y., and GRINSEN, K., 1952, *Rev. mod. Phys.*, **24,** 133.

BARTON, J. C., 1956, *J. sci. Instrum.*, **33,** 308; 1960, *Phys. Rev. Letters*, **5,** 514.

BARTON, J. C., and MICHAELIS, E. G., 1961, *Proc. phys. Soc., Lond.*, **77,** 377.

BOLLINGER, L. M., 1951, Ph.D. Thesis, Cornell University, Ithaca, N.Y.

DUTHIE, J. G., FISHER, C. M., FOWLER, P. H., KADDOURA, A., PERKINS, D. H., and PINKAU, K., 1961, *Phil. Mag.*, **6,** 89 and 113.

FOWLER, G. N., and WOLFENDALE, A. W., 1958, *Prog. Cosmic Ray Phys.*, **4,** 107.

GLASHOW, S. L., 1960, *Phys. Rev.*, **118,** 316.

HOOKER, P. M., and LIGHT, L. H., 1956, *Mullard tech. Commun.*, **2,** 157.

KESSLER, P., and KESSLER, D., 1957, *C. R. Acad. Sci., Paris*, **244,** 1896.

MANDÒ, M., and SONA, P. G., 1953, *Nuovo Cim.*, **10,** 1275.

MIESOWICZ, M., and MASSALSKI, J. M., 1950, *Acta phys. polon.*, **10,** 274.

MIYAZAKI, 1949, *Phys. Rev.*, **76,** 1733.

REGENER, V. H., 1951, *Phys. Rev.*, **84,** 161.

ROZENTHAL and STREL'TSOV, 1958, *J. exp. theor. Phys.*, **35,** 1440.

STERNHEIMER, R. M., 1956, *Phys. Rev.*, **103,** 511; 1959, **115,** 137.

THOMSON, J. E., 1948, Ontario Department of Mines, 57th Annual Report, 57, V, 1.

Electron Theory of Interaction between Point Defects in Metals

By G. K. Corless and N. H. March
Department of Physics, The University, Sheffield

[Received March 24, 1961]

Abstract

By employing a simple model of point charges in a uniform electron gas, it is shown how interaction energies between imperfections (for example, impurity–vacancy or vacancy–vacancy interactions) may be evaluated within the framework of low-order perturbation theory. Close contact may be established throughout with the earlier investigation of Alfred and March (1957), in which, however, a restrictive assumption that the perturbing potential was slowly varying had to be made. Our work now removes this assumption completely and provides a firm basis for the so-called 'electrostatic model' of the interaction between imperfections. In view of the long-range oscillations in the electrostatic potential around a defect, the interaction energy also has an oscillatory behaviour as a function of distance.

The relevance of our work to the Lazarus theory of impurity diffusion in metals is discussed. In this case, the numerical results are in fair agreement with those of the earlier treatment, and lend further support to the Lazarus theory. Also the investigation of Seeger and Bross (1956) on the di-vacancy may be critically examined by comparison with the present findings. It then appears that the terms in the total interaction energy which these earlier workers have omitted may be large. Indeed, in our calculations they are sufficient to change the sign of the interaction. It is finally pointed out that the present theory may have relevance in the interpretation of the results of Biondi and Rayne (1959, Rayne 1961) on optical absorption in Cu–Zn and Cu–Ge alloys.

§ 1. Introduction

We develop here a theory of the interaction between defects in metals, based on careful study of an admittedly over-simplified model. Thus we adopt the uniform gas approximation for the matrix metal, and assume that the point defects may be simulated by embedding appropriate point charges in the gas. Departures from such a model, particularly the use of Bloch waves rather than plane waves, and hence a non-uniform periodic density, for the conduction electrons in the unperturbed metal certainly require full investigation, but at present appear to lead to major complications.

We shall refer briefly here to a few of the numerous applications to which our interaction energy calculations are highly relevant. Lazarus (1954) developed a theory of impurity diffusion in metals based on a calculation of the interaction energy between an impurity and a vacancy (for a review of diffusion in metals, see Lazarus 1960). While Lazarus's earlier treatment was open to certain objections, particularly with regard to the neglect of correlation effects in diffusion (see, for example, Bardeen and Herring 1952, Manning 1958) and to the calculation of the energy of movement, the recent reformulation of the theory by Le Claire (1961) appears to go some way towards removing these unsatisfactory features. The other application of our work which we consider in some detail is to discuss the stability of the di-vacancy and to make an analysis of the earlier calculation of Seeger and Bross (1956).

The present work has been made possible by recent progress in the general theory of defects in metals (March and Murray 1960, 1961). While, in this earlier work, explicit results were obtained only for a single imperfection in an infinite metal, a full perturbation development of the Dirac density matrix was presented, and this is applicable to a general perturbing potential. We show here how considerable progress can be made in the two-centre case† (for example, impurity–vacancy or vacancy–vacancy complexes), using a first-order approximation. Our results reduce to the first-order treatment of Alfred and March (1957) when the assumption of a slowly varying potential is made. While these workers obtained the same final result as Lazarus for the interaction energy, it was clear that his original argument was valid only because of a major cancellation of the kinetic energy terms with part of the potential energy. We shall show by a quite general first-order argument that this cancellation occurs, independently of any assumption concerning the spatial variation of the potential.

§ 2. DENSITY MATRICES AND KINETIC ENERGY DENSITY

Following March and Murray (1961), we write for the Dirac density matrix $\rho(\mathbf{r}, \mathbf{r}_0, k)$, where $k^2=2E$, with E denoting the Fermi energy:

$$\rho(\mathbf{r}, \mathbf{r}_0, k)=\rho_0+\rho_1+\rho_2+0(V^3) \qquad . \quad . \quad . \quad . \quad (2.1)$$

where V is the perturbing potential energy. We then have the equations defining ρ_0, ρ_1 and ρ_2 as

$$\rho_0=\frac{k^2 j_1(k|\mathbf{r}-\mathbf{r}_0|)}{\pi^2 \quad |\mathbf{r}-\mathbf{r}_0|}, \qquad . \quad . \quad . \quad . \quad . \quad . \quad (2.2)$$

$$\rho_1=-\frac{k^2}{2\pi^3}\int d\mathbf{r}_1 \frac{V(\mathbf{r}_1) j_1(k|\mathbf{r}_1-\mathbf{r}_0|+k|\mathbf{r}-\mathbf{r}_1|)}{|\mathbf{r}_1-\mathbf{r}_0||\mathbf{r}-\mathbf{r}_1|}, \qquad . \quad . \quad . \quad . \quad . \quad (2.3)$$

$$\rho_2=\frac{k^2}{4\pi^4}\int\int d\mathbf{r}_1 d\mathbf{r}_2 \frac{V(\mathbf{r}_1)V(\mathbf{r}_2) j_1(k|\mathbf{r}_1-\mathbf{r}_0|+k|\mathbf{r}_2-\mathbf{r}_1|+k|\mathbf{r}-\mathbf{r}_2|)}{|\mathbf{r}_1-\mathbf{r}_0||\mathbf{r}_2-\mathbf{r}_1||\mathbf{r}-\mathbf{r}_2|}. \qquad (2.4)$$

We note first that the kinetic energy T is given by

$$T=-\tfrac{1}{2}\int d\mathbf{r}[\nabla_{\mathbf{r}}^2\rho]_{\mathbf{r}_0=\mathbf{r}}. \qquad . \quad . \quad . \quad . \quad . \quad . \quad (2.5)$$

---

† The generalization to M centres is readily achieved, as shown in Appendix 1.

Using (2.2)–(2.4) we then find by straightforward calculation:

$$\nabla_{\mathbf{r}}^2\rho_0 = \frac{k^4}{\pi^2}\frac{j_1''(k|\mathbf{r}-\mathbf{r}_0|)}{|\mathbf{r}-\mathbf{r}_0|}, \quad . \quad . \quad . \quad . \quad (2.6)$$

$$\nabla_{\mathbf{r}}^2\rho_1 = \frac{2k^2}{\pi^2}\frac{V(\mathbf{r})j_1(k|\mathbf{r}-\mathbf{r}_0|)}{|\mathbf{r}-\mathbf{r}_0|}$$

$$-\frac{k^4}{2\pi^3}\int d\mathbf{r}_1\,\frac{V(\mathbf{r}_1)j_1''(k|\mathbf{r}-\mathbf{r}_1|+k|\mathbf{r}_1-\mathbf{r}_0|)}{|\mathbf{r}-\mathbf{r}_1||\mathbf{r}_1-\mathbf{r}_0|}, \quad . \quad . \quad . \quad (2.7)$$

$$\nabla_{\mathbf{r}}^2\rho_2 = \frac{k^4}{4\pi^4}\int\!\!\int d\mathbf{r}_1\,d\mathbf{r}_2\,\frac{V(\mathbf{r}_1)V(\mathbf{r}_2)j_1''(k|\mathbf{r}_1-\mathbf{r}_0|+k|\mathbf{r}_2-\mathbf{r}_1|+k|\mathbf{r}-\mathbf{r}_2|)}{|\mathbf{r}_1-\mathbf{r}_0||\mathbf{r}_2-\mathbf{r}_1||\mathbf{r}-\mathbf{r}_2|}$$

$$-\frac{k^2}{4\pi^4}\int d\mathbf{r}_1\,\frac{V(\mathbf{r}_1)V(\mathbf{r})4\pi j_1(k|\mathbf{r}_1-\mathbf{r}_0|+k|\mathbf{r}-\mathbf{r}_1|)}{|\mathbf{r}_1-\mathbf{r}_0||\mathbf{r}-\mathbf{r}_1|}. \quad . \quad . \quad (2.8)$$

Evaluating (2.6), (2.7) and (2.8) at $\mathbf{r}_0=\mathbf{r}$, and inserting the results in (2.5) we find

$$T = \frac{k^5}{10\pi^2}\int d\mathbf{r} - \frac{k^3}{2\pi^2}\int d\mathbf{r}_1 V(\mathbf{r}_1)$$

$$+\frac{k^4}{2\pi^3}\int\!\!\int d\mathbf{r}_1\,d\mathbf{r}_2\,V(\mathbf{r}_1)V(\mathbf{r}_2)\left[\frac{j_1'(2k|\mathbf{r}_2-\mathbf{r}_1|)}{2k|\mathbf{r}_2-\mathbf{r}_1|}+\frac{4j_1(2k|\mathbf{r}_2-\mathbf{r}_1|)}{(2k|\mathbf{r}_2-\mathbf{r}_1|)^2}\right]. \quad (2.9)$$

At this stage we make use of the relation that to $0(V^2)$ the displaced charge $\rho-\rho_0$ is given by

$$\rho-\rho_0 = -\frac{k^2}{2\pi^3}\int d\mathbf{r}_1 V(\mathbf{r}_1)\,\frac{j_1(2k|\mathbf{r}-\mathbf{r}_1|)}{|\mathbf{r}-\mathbf{r}_1|^2}$$

$$+\frac{k^2}{4\pi^4}\int\!\!\int d\mathbf{r}_1\,d\mathbf{r}_2\,\frac{V(\mathbf{r}_1)V(\mathbf{r}_2)j_1(k|\mathbf{r}_1-\mathbf{r}|+k|\mathbf{r}_2-\mathbf{r}_1|+k|\mathbf{r}-\mathbf{r}_2|)}{|\mathbf{r}_1-\mathbf{r}||\mathbf{r}_2-\mathbf{r}_1||\mathbf{r}-\mathbf{r}_2|} \quad (2.10)$$

and integrating (2.10) with respect to $\mathbf{r}$ we find

$$\int d\mathbf{r}(\rho-\rho_0) = -\frac{k}{\pi^2}\int d\mathbf{r}_1 V(\mathbf{r}_1)$$

$$+\frac{k}{2\pi^3}\int\!\!\int d\mathbf{r}_1\,d\mathbf{r}_2\,\frac{V(\mathbf{r}_1)V(\mathbf{r}_2)j_0(2k|\mathbf{r}_2-\mathbf{r}_1|)}{|\mathbf{r}_2-\mathbf{r}_1|}+0(V^3). \quad (2.11)$$

Thus, using (2.11) we may rewrite (2.9) in the form

$$T = \frac{k^5}{10\pi^2}\int d\mathbf{r} + \frac{k^2}{2}\int d\mathbf{r}(\rho-\rho_0) + \frac{k^4}{\pi^3}\int\!\!\int d\mathbf{r}_1\,d\mathbf{r}_2\,\frac{V(\mathbf{r}_1)V(\mathbf{r}_2)j_1(2k|\mathbf{r}_2-\mathbf{r}_1|)}{(2k|\mathbf{r}_2-\mathbf{r}_1|)^2}. \quad (2.12)$$

§ 3. INTERACTION ENERGIES BETWEEN DEFECTS

We turn now to deal with the energies of interaction between two defects, carrying charges Z_1 and Z_2. We obtain the interaction energy by considering the changes in total energy as we bring the imperfections from infinity to the near-neighbour distance a.

The basic equation of the perturbation theory of March and Murray (1960) for the perturbing potential V, to first-order in V, is

$$\nabla^2 V(\mathbf{r}) = \frac{2k^2}{\pi^2}\int d\mathbf{r}_1 V(\mathbf{r}_1)\frac{j_1(2k|\mathbf{r}-\mathbf{r}_1|)}{|\mathbf{r}-\mathbf{r}_1|^2} \quad . \quad . \quad . \quad . \quad (3.1)$$

where k is the magnitude of the wave vector at the Fermi surface. This equation reduces to the Mott form

$$\nabla^2 V = q^2 V, \quad q^2 = 4k/\pi \quad . \quad . \quad . \quad . \quad (3.2)$$

when V is slowly varying in space. It will be seen that the superposition property of (3.2), exploited by Alfred and March (1957) in their two-centre work, is also valid for (3.1), and thus, within the first-order approximation, no new calculation of the density and potential for the defect complex under consideration is required. Thus, if charges Z_1 and Z_2 are situated at $\mathbf{a}_1$ and $\mathbf{a}_2$ respectively, and if V_{Z1} and V_{Z2} represent the one-centre potentials as given by March and Murray (1961), then the two-centre potential may be written as

$$V(\mathbf{r}) = V_{Z1}(\mathbf{r}-\mathbf{a}_1) + V_{Z2}(\mathbf{r}-\mathbf{a}_2). \quad . \quad . \quad . \quad . \quad (3.3)$$

We now proceed to obtain the desired kinetic energy change from (2.12), and in doing so we note that if we measure changes from the unperturbed gas state and use charge normalization requirements, only the third term on the right-hand side of (2.12) needs to be considered. We have then, for the complex Z_1Z_2 at separation $a = |\mathbf{a}_2 - \mathbf{a}_1|$, the contribution from this term as

$$\frac{k^4}{\pi^3}\int\int d\mathbf{r}_1 d\mathbf{r}_2 [V_{Z1}(\mathbf{r}_1-\mathbf{a}_1) + V_{Z2}(\mathbf{r}_1-\mathbf{a}_2)][V_{Z1}(\mathbf{r}_2-\mathbf{a}_1) + V_{Z2}(\mathbf{r}_2-\mathbf{a}_2)] \times j_1(2k|\mathbf{r}_2-\mathbf{r}_1|)^2. \quad (3.4)$$

The one-centre terms are now seen to correspond to the kinetic energy changes at infinite separation of Z_1 and Z_2 and thus the kinetic energy change ΔT is given by

$$\Delta T = \frac{k^4}{\pi^3}\int\int d\mathbf{r}_1 d\mathbf{r}_2 \frac{V_{Z1}(\mathbf{r}_1-\mathbf{a}_1)V_{Z2}(\mathbf{r}_2-\mathbf{a}_2)j_1(2k|\mathbf{r}_2-\mathbf{r}_1|)}{(2k|\mathbf{r}_2-\mathbf{r}_1|)^2}$$
$$+ \frac{k^4}{\pi^3}\int\int d\mathbf{r}_1 d\mathbf{r}_2 \frac{V_{Z2}(\mathbf{r}_1-\mathbf{a}_2)V_{Z1}(\mathbf{r}_2-\mathbf{a}_1)j_1(2k|\mathbf{r}_2-\mathbf{r}_1|)}{(2k|\mathbf{r}_2-\mathbf{r}_1|)^2}. \quad . \quad . \quad . \quad (3.5)$$

We turn next to the evaluation of the potential energy change ΔU in this approximation. As we are working in a Hartree framework, we have that the potential energy of the gas with charges Z_1 and Z_2 at $\mathbf{a}_1$ and $\mathbf{a}_2$ is

$$\int d\mathbf{r}\rho(\mathbf{r})V_0(\mathbf{r}) + \tfrac{1}{2}\int d\mathbf{r}_1 d\mathbf{r}_2 \frac{\rho(\mathbf{r}_1)\rho(\mathbf{r}_2)}{|\mathbf{r}_2-\mathbf{r}_1|} + \frac{Z_1Z_2}{|\mathbf{a}_2-\mathbf{a}_1|} \quad (3.6)$$

where

$$V_0(\mathbf{r}) = -\frac{Z_1}{|\mathbf{r}-\mathbf{a}_1|} - \frac{Z_2}{|\mathbf{r}-\mathbf{a}_2|} = V_0(\mathbf{r}-\mathbf{a}_1) + V_0(\mathbf{r}-\mathbf{a}_2)$$

and

$$V(\mathbf{r}_1) = V_0(\mathbf{r}_1) + \int d\mathbf{r}_2 \frac{\rho(\mathbf{r}_2)}{|\mathbf{r}_2-\mathbf{r}_1|}.$$

Clearly (3.6) may now be expressed as

$$\tfrac{1}{2}\int d\mathbf{r}\rho(\mathbf{r})V(\mathbf{r})+\tfrac{1}{2}\int d\mathbf{r}\rho(\mathbf{r})V_0(\mathbf{r})+\frac{Z_1Z_2}{|\mathbf{a}_2-\mathbf{a}_1|}. \qquad (3.7)$$

Using (2.1) for $\rho(\mathbf{r})$, adopting the superposition potential energy (3.3), and omitting unperturbed and one-centre terms we immediately find to second order in V,

$$\Delta U=\tfrac{1}{2}\int d\mathbf{r}\rho_{1Z1}(\mathbf{r}-\mathbf{a}_1)V_{Z2}(\mathbf{r}-\mathbf{a}_2)+\tfrac{1}{2}\int d\mathbf{r}\rho_{1Z2}(\mathbf{r}-\mathbf{a}_2)V_{Z1}(\mathbf{r}-\mathbf{a}_1)$$

$$+\frac{Z_1Z_2}{|\mathbf{a}_2-\mathbf{a}_1|}-\frac{Z_1}{2}\int d\mathbf{r}\frac{\rho_{1Z1}(\mathbf{r}-\mathbf{a}_1)}{|\mathbf{r}-\mathbf{a}_2|}-\frac{Z_2}{2}\int d\mathbf{r}\frac{\rho_{1Z2}(\mathbf{r}-\mathbf{a}_2)}{|\mathbf{r}-\mathbf{a}_1|}, \quad . \quad . \quad (3.8)$$

where ρ_{1Z1} and ρ_{1Z2} are related to V_{Z1} and V_{Z2} by the Poisson equation

$$\nabla^2V_{Zi}(\mathbf{r}-\mathbf{a}_i)=-4\pi\rho_{1Zi}(\mathbf{r}-\mathbf{a}_i), \quad i=1,2. \qquad (3.9)$$

Using (3.9) is it easily shown that (3.8) reduces to the form

$$\Delta U=-\frac{Z_1}{2}V_{Z2}(|\mathbf{a}_1-\mathbf{a}_2|)-\frac{Z_2}{2}V_{Z1}(|\mathbf{a}_2-\mathbf{a}_1|)$$

$$+\tfrac{1}{2}\int d\mathbf{r}\rho_{1Z1}(\mathbf{r}-\mathbf{a}_1)V_{Z2}(\mathbf{r}-\mathbf{a}_2)+\tfrac{1}{2}\int d\mathbf{r}\rho_{1Z2}(\mathbf{r}-\mathbf{a}_2)V_{Z1}(\mathbf{r}-\mathbf{a}_1). \qquad (3.10)$$

But from (2.3) we may write

$$\rho_{1Zi}(\mathbf{r}-\mathbf{a}_i)=-\frac{k^2}{2\pi^3}\int d\mathbf{r}_1\frac{V_{Zi}(\mathbf{r}_1-\mathbf{a}_i)j_1(2k|\mathbf{r}_1-\mathbf{r}|)}{|\mathbf{r}_1-\mathbf{r}|^2} \qquad (3.11)$$

and it may then be shown readily that (3.5) has the form

$$\Delta T=-\tfrac{1}{2}\int d\mathbf{r}\,\rho_{1Z1}(\mathbf{r}-\mathbf{a}_1)V_{Z2}(\mathbf{r}-\mathbf{a}_2)$$

$$-\tfrac{1}{2}\int d\mathbf{r}\,\rho_{1Z2}(\mathbf{r}-\mathbf{a}_2)V_{Z1}(\mathbf{r}-\mathbf{a}_1). \quad . \quad . \quad . \quad (3.12)$$

Thus, adding (3.10) and (3.12) we are left with the final simple result

$$\Delta E=\Delta T+\Delta U=-\frac{Z_1}{2}V_{Z2}(|\mathbf{a}_1-\mathbf{a}_2|)-\frac{Z_2}{2}V_{Z1}(|\mathbf{a}_2-\mathbf{a}_1|). \qquad (3.13)$$

We now demonstrate directly the connection with the earlier treatment given by Alfred and March (1957). As pointed out in § 3, the basic eqn. (3.1) of the first-order treatment reduces to the Mott eqn. (3.2) in the slowly varying potential limit, and the appropriate one-centre solution is

$$V_{Zi}(r)=-\frac{Z_i}{r}\exp(-qr). \quad . \quad . \quad . \quad . \quad (3.14)$$

Thus, from (3.13) we then find

$$\Delta E=\frac{Z_1Z_2\exp(-qa)}{a} \quad . \quad . \quad . \quad . \quad . \quad . \quad . \quad (3.15)$$

which is just Lazarus's formula. A numerical comparison of the predictions of (3.13) and (3.15) will be made later.

§ 4. Impurity Diffusion in Metals

In the Lazarus theory, as modified by Le Claire, the energy of movement is calculated using a model for the saddle-point configuration which was originated by Huntington (1942). The model consists of a linear three-centre configuration of point charges, $-\frac{1}{2}$, Z, $-\frac{1}{2}$, the half-vacancies being separated from the impurity by distances $(11/16)a$ in the Huntington approximation (see Le Claire 1961 for detailed reasons for this choice). The M-centre calculation of Appendix 1 immediately gives the desired result, which, in Le Claire's notation, may be written quantitatively as

$$\Delta H_2 + \Delta E = -\tfrac{1}{2} V_Z(11a/16) + Z V_{-1/2}(11a/16). \qquad (4.1)$$

Substituting $V_Z(r)$ as given by the slowly varying potential approximation in (4.1), we find

$$\Delta H_2 + \Delta E = -\frac{Z}{(11/16)a} \exp(-11qa/16). \qquad (4.2)$$

This differs from Le Claire's result only by a factor α of the order of unity, α being Z dependent (see Alfred and March 1956). The introduction of α may be thought of as an attempt to introduce higher order perturbation corrections (see also the remarks of § 6) and is necessary if curvature in the activation energy versus Z plot is to be explained. In our approximation, α is simply unity.

We record in the table results for divalent impurities in copper, as calculated from (3.13) and (3.15) for ΔE, and from (4.1) and (4.2) for $\Delta H_2 + \Delta E$. It will be seen that the results of our treatment provide a fair numerical justification of the formulae used previously. In view of this, and the crude approximation involved in the choice of the saddle-point model, it does not seem necessary at this stage to rework the predictions of the theory of impurity diffusion as presented by Le Claire (1961), although eventually numerical revision may become desirable.

Results for various energy terms for divalent impurities in copper

Impurity–vacancy interaction energy ΔE ($a = 4{\cdot}8$ atomic units)

(1) From eqn. (3.13): $\Delta E = -0{\cdot}0028$ ($-0{\cdot}076$ ev)

(2) From Lazarus formula (3.15): $\Delta E = -0{\cdot}0021$ ($-0{\cdot}057$ ev)

Energy $\Delta H_2 + \Delta E$, *for saddle-point configuration described by Huntington's model* (see § 4)

(1) From eqn. (4.1): $\Delta H_2 + \Delta E = -0{\cdot}0095$ ($-0{\cdot}26$ ev).

(2) From eqn. (4.2): $\Delta H_2 + \Delta E = -0{\cdot}0128$ ($-0{\cdot}35$ ev).

§ 5. Stability of Di-vacancy: Comparison with the Calculation of Seeger and Bross

The existence of the di-vacancy is important in a number of fields (see, for example, Lomer 1959). As Lomer points out, the stability of the di-vacancy does not seem established beyond doubt, although recent work (Weizer and Girifalco 1960) suggests on both theoretical and experimental grounds that it should be stable.

The only calculation which considers the electronic distribution round the di-vacancy, prior to our work, is that of Seeger and Bross (1956). However, their work on the di-vacancy is incomplete, in the same sense that the work of Fumi (1955) on the formation energy of a vacancy was incomplete. While some justification can be given for the partial cancellation of the terms in the energy omitted by Fumi (Lidiard and Tharmalingham, private communication) for the single-centre problem, no consideration has as yet been given to this point for the di-vacancy.

In order to throw light on this point, we shall now attempt to cast our treatment into a form which parallels the calculation of Seeger and Bross. We note first that these workers, following Fumi, focus attention only on changes in eigenvalue sums for model potentials chosen to satisfy the Friedel sum rule. It is clear then that their calculations are not complete, in that Coulomb corrections are not properly accounted for. In our work, on the other hand, we have used the full energy expressions within a Hartree framework.

We consider then, at this stage, the change in eigenvalue sum using our model of the di-vacancy. The potential energy term in the eigenvalue sum for a complex Z_1Z_2 is

$$\int d\mathbf{r}\,\rho(\mathbf{r})V(\mathbf{r}) \qquad (5.1)$$

and we now invoke the superposition theorem to obtain

$$\int d\mathbf{r}[\rho_{1Z1}(\mathbf{r}-\mathbf{a}_1)+\rho_{1Z2}(\mathbf{r}-\mathbf{a}_2)-\rho_0][V_{Z1}(\mathbf{r}-\mathbf{a}_1)+V_{Z2}(\mathbf{r}-\mathbf{a}_2)]. \qquad (5.2)$$

Again, separating out unperturbed, one-centre, and two-centre terms, the potential energy contribution to the change in eigenvalue sum is clearly

$$\Delta U_{\text{eigenvalue}}=\int d\mathbf{r}[\rho_{1Z1}(\mathbf{r}-\mathbf{a}_1)V_{Z2}(\mathbf{r}-\mathbf{a}_2)+\rho_{1Z2}(\mathbf{r}-\mathbf{a}_2)V_{Z1}(\mathbf{r}-\mathbf{a}_1)]. \qquad (5.3)$$

From the Mott approximate solution (3.14) we obtain the result, for $Z_1=Z_2=-1$

$$-q\exp(-qa). \qquad (5.4)$$

(5.3) has been obtained numerically, as it seemed of interest to know how the energy change was built up from potential and kinetic contributions. We obtain

$$\Delta U_{\text{eigenvalue}}=-0{\cdot}0074 \text{ atomic units}=-0{\cdot}20\,\text{ev},$$

whereas (5.4) yields $-0{\cdot}26$ ev.

Also, from (3.12) it follows that

$$\Delta T=-\tfrac{1}{2}\Delta U_{\text{eigenvalue}}=0{\cdot}10\,\text{ev},$$

and hence

$$\Delta E_{\text{eigenvalue}}=-0{\cdot}10\,\text{ev},$$

whereas using the approximate solution (3.14) the result is $-0{\cdot}13$ ev. Since $\Delta E_{\mathrm{eigenvalue}}$ is just the quantity which Seeger and Bross take as a measure of the binding energy, these calculations would then indicate stability of the di-vacancy, and our result of 0·1 ev is to be compared with their value of 0·3 ev. Unfortunately, our estimate of the total energy change ΔE is given by (3.13) and is $\Delta E = 0{\cdot}076$ ev. This indicates repulsion and we see that in the present framework even the sign of the interaction is changed when we use the eigenvalue sum as a measure of the binding energy. Our work therefore must cast serious doubt on the validity of the Seeger–Bross energy; as even if we adopt our Coulomb correction of 0·18 ev and their eigenvalue sum, their binding energy is reduced to 0·12 ev.

§ 6. HIGHER APPROXIMATIONS

There is little doubt that, even within the framework of the present model, higher approximations should eventually be considered. Thus, the one-centre calculations of March and Murray (1960, 1961) show that the electron density given by the first-order eqn. (3.1), while containing all the essential features of the problem, is not capable of complete quantitative accuracy. The framework developed by these workers is general enough however so that the second-order corrections can be estimated in principle, and this is under discussion for the one-centre case (March and Murray, to be published). The calculations for the present problem are, unfortunately, very formidable indeed, the main obstacle being the loss of the superposition property when terms of $0(V^2)$ are included in (3.1). Thus, entirely new calculations of the two-centre potential and density would be required. However, such a calculation was in fact carried through completely by Alfred and March (1957) for a divalent impurity and a vacancy in Cu, in the simpler case when the potential is assumed slowly varying, and this enables us to draw some tentative conclusions.

Thus, the full computations of Alfred and March referred to above showed that while a result was obtained in quite reasonable numerical agreement with the first-order interaction energy, the inclusion of exchange was important. What emerged was that while the kinetic energy was given reasonably satisfactorily by the first-order treatment, the summation of the slowly varying potential series to infinite order in V led to a rather different potential energy, but the inclusion of exchange brought the result back to approximately the first-order value. Also, as pointed out by Alfred and March (1957), inclusion of exchange in first order completely changes the results, and appears to lead to unreasonable conclusions†. We infer then that, at least for the impurity–vacancy problem, the full calculation of Alfred and March is most probably much better than might have been supposed from the apparently severe approximation of slowly varying potentials.

---

† Nevertheless, for completeness it seemed worthwhile to include in Appendix 2 a brief derivation of the expression for the exchange energy using the density matrix formulation employed here.

§ 7. Conclusion

Within a Hartree approximation and assuming the validity of low-order perturbation theory, we have shown how a rather general treatment of interaction energies between point charges in an electron gas may be developed. In particular, the so-called 'electrostatic' model of interactions between defects in metals follows as a direct consequence of our perturbation approach. However, in view of the long-range oscillations in the electrostatic potential around a defect, it follows that the interaction energy also oscillates with distance.

It turns out that in the theory of impurity diffusion, proposed by Lazarus and recently modified by Le Claire, these oscillatory effects should not be very important, and in particular the major term, the energy of movement, should not be greatly affected. Thus, even though detailed numerical revision will eventually be called for, our work seems to substantiate further the current theory. On the other hand, we feel that stability of the di-vacancy cannot be explained in terms of the point charge model employed here. The work of Seeger and Bross (1956) has been shown to be open to criticism on the grounds that changes in sums of eigenvalues are not a proper measure of the interaction energy. Indeed, in our calculations, even the sign is changed by the terms Seeger and Bross omit.

Undoubtedly, in the applications referred to above, reservations must be made concerning the limitations of the model. No doubt relaxation effects around vacancies and impurities will eventually have to be included. Within the uniform gas approximation, a crude account could perhaps be taken of nearest-neighbour displacements using a model like that of Lee and March (1960).

Finally we might briefly refer to some recent measurements of Rayne (1961) on optical absorption in Cu–Zn and Cu–Ge alloys. These experiments may be thought of as measuring the change in the Fermi level with impurity concentration, and are in serious conflict with Friedel's earlier theory (Friedel 1954). However, since the change in the Fermi level is dependent on the interaction between the impurities, that is on the overlap of the screening distributions, it seems very likely that the present treatment, with long-range oscillatory terms, will lead to results markedly different from those based on essentially exponential screening. It is hoped to report on a quantitative treatment of this problem at a later stage.

Acknowledgments

It is a pleasure to thank Dr. A. M. Murray for valuable discussions and material help with some aspects of the work, and Dr. W. H. Young for reading a preliminary manuscript and, by means of numerous suggestions, considerably influencing the final presentation of the theory.

The work reported here was performed under contract with the United Kingdom Atomic Energy Authority, A.E.R.E., Harwell. One of us (N. H. M.) would particularly like to thank Mr. A. D. Le Claire and the other members of his group for the stimulus and encouragement which he derived from a brief visit as a Vacation Consultant in the summer of 1959, during which period the need for the present investigation became clear.

APPENDIX 1

Interaction Energy in Multi-centre Problem

We outline here the generalization of the result of § 3 for two centres to M-centres. We now write

$$V_0(\mathbf{r}) = -\frac{Z_1}{|\mathbf{r}-\mathbf{a}_1|} - \frac{Z_2}{|\mathbf{r}-\mathbf{a}_2|} - \dots = V_{0Z1}+V_{0Z2}+\dots . \qquad \text{(A 1.1)}$$

Obvious generalization of the method of § 3 then gives for the potential energy

$$PE=\tfrac{1}{2}\int d\mathbf{r}[\rho_0+\rho_1+\dots][V_{Z1}(\mathbf{r}-\mathbf{a}_1)+V_{Z2}(\mathbf{r}-\mathbf{a}_2)+\dots$$
$$+V_{0Z1}(\mathbf{r}-\mathbf{a}_1)+V_{0Z2}(\mathbf{r}-\mathbf{a}_2)+\dots]+\sum_{i>j}\frac{Z_iZ_j}{|\mathbf{a}_i-\mathbf{a}_j|}$$

and again omitting one-centre and unperturbed terms we have for the potential energy contribution to the interaction energy

$$\Delta U = -\tfrac12\sum_{i\neq j} Z_i\int d\mathbf{r}\,\frac{\rho_{1Zj}(\mathbf{r}-\mathbf{a}_j)}{|\mathbf{r}-\mathbf{a}_i|}+\tfrac12\sum_{i\neq j}\frac{Z_iZ_j}{|\mathbf{a}_i-\mathbf{a}_j|}+\tfrac12\sum_{i\neq j}\int d\mathbf{r}\,\rho_{1Zj}V_{Zi}(\mathbf{r}-\mathbf{a}_i)$$
$$= -\tfrac12\sum_{i\neq j} Z_iV_{Zj}(\mathbf{a}_i-\mathbf{a}_j)+\tfrac12\sum_{i\neq j}\int d\mathbf{r}\,\rho_{1Zj}V_{Zi}(\mathbf{r}-\mathbf{a}_i). \quad . \quad . \quad . \qquad \text{(A 1.2)}$$

Similarly, we have for the kinetic energy contribution to the interaction energy

$$\frac{k^4}{\pi^3}\sum_{i\neq j}\int\int d\mathbf{r}_1\,d\mathbf{r}_2\,\frac{V_{Zi}(\mathbf{r}_1-\mathbf{a}_i)V_{Zj}(\mathbf{r}_2-\mathbf{a}_j)j_1(2k|\mathbf{r}_1-\mathbf{r}_2|)}{(2k|\mathbf{r}_1-\mathbf{r}_2|)^2}$$

and using the result that

$$\rho_{1Zj} = -\frac{k^2}{2\pi^3}\int d\mathbf{r}_1\,\frac{V_{Zj}(\mathbf{r}_1-\mathbf{a}_j)j_1(2k|\mathbf{r}_1-\mathbf{r}_2|)}{|\mathbf{r}_1-\mathbf{r}_2|^2}$$

we find

$$\Delta T = -\tfrac12\sum_{i\neq j}\int d\mathbf{r}\,\rho_{1Zj}V_{Zi}(\mathbf{r}-\mathbf{a}_i). \quad . \quad . \qquad \text{(A 1.3)}$$

Thus from (A 1.2) and (A 1.3) we have

$$\Delta E = \Delta T+\Delta U = -\tfrac12\sum_{i\neq j} Z_iV_{Zj}(\mathbf{a}_i-\mathbf{a}_j), \quad . \quad . \qquad \text{(A 1.4)}$$

which is the desired generalization of (3.13).

APPENDIX 2

EXCHANGE ENERGY IN PERTURBATION APPROACH BASED ON THE DENSITY MATRIX

In terms of the Dirac density matrix $\rho(\mathbf{r}, \mathbf{r}_0, k)$ we may write for the exchange energy

$$A = -\tfrac{1}{4} \int\!\!\int d\mathbf{r}\, d\mathbf{r}_0 \frac{[\rho(\mathbf{r}, \mathbf{r}_0, k)]^2}{|\mathbf{r}-\mathbf{r}_0|}. \quad . \quad . \quad . \qquad (\text{A } 2.1)$$

We now insert the perturbation expansion (2.1) for ρ in (A 2.1) and we find

$$A = -\tfrac{1}{4} \int\!\!\int d\mathbf{r}\, d\mathbf{r}_0 \frac{[\rho_0{}^2 + 2\rho_0\rho_1 + \rho_1{}^2 + 2\rho_0\rho_2]}{|\mathbf{r}-\mathbf{r}_0|} \qquad (\text{A } 2.2)$$

where we retain only second-order terms in V. We may then show that

$$-\tfrac{1}{4} \int\!\!\int d\mathbf{r}\, d\mathbf{r}_0 \frac{\rho_0{}^2}{|\mathbf{r}-\mathbf{r}_0|} = -\frac{3}{4}\left(\frac{3}{\pi}\right)^{1/3} \int d\mathbf{r} [\rho_0(\mathbf{r}, \mathbf{r})]^{4/3}, \qquad (\text{A } 2.3)$$

which is the usual result for free electrons. For the next term in (A 2.2) we may write almost immediately

$$-\tfrac{1}{2} \int\!\!\int d\mathbf{r}\, d\mathbf{r}_0 \frac{\rho_0\rho_1}{|\mathbf{r}-\mathbf{r}_0|} = -\frac{k}{\pi} \int d\mathbf{r} [\rho(\mathbf{r}, \mathbf{r}) - \rho_0(\mathbf{r}, \mathbf{r})] + 0(V^2). \quad (\text{A } 2.4)$$

There are three contributions to the term of $0(V^2)$, as listed below:

(i) $$\frac{k^2}{2\pi^4} \int\!\!\int d\mathbf{r}_1\, d\mathbf{r}_2 \frac{V(\mathbf{r}_1)V(\mathbf{r}_2)}{|\mathbf{r}_1-\mathbf{r}_2|} j_0(2k|\mathbf{r}_2-\mathbf{r}_1|),$$

(ii) $$-\frac{k^4}{16\pi^6} \int\!\!\int \frac{d\mathbf{r}\, d\mathbf{r}_0}{|\mathbf{r}-\mathbf{r}_0|} \left[\int d\mathbf{r}_1 \frac{V(\mathbf{r}_1) j_1(k|\mathbf{r}_1-\mathbf{r}_0| + k|\mathbf{r}-\mathbf{r}_1|)}{|\mathbf{r}_1-\mathbf{r}_0||\mathbf{r}-\mathbf{r}_1|} \right]^2,$$

(iii) $$-\frac{k^4}{8\pi^6} \int\!\!\int d\mathbf{r}\, d\mathbf{r}_0 \frac{j_1(k|\mathbf{r}-\mathbf{r}_0|)}{|\mathbf{r}-\mathbf{r}_0|^2} \int\!\!\int d\mathbf{r}_1\, d\mathbf{r}_2 V(\mathbf{r}_1)V(\mathbf{r}_2) \times \frac{j_1(k|\mathbf{r}_1-\mathbf{r}_0| + k|\mathbf{r}_2-\mathbf{r}_1| + k|\mathbf{r}-\mathbf{r}_2|)}{|\mathbf{r}_1-\mathbf{r}_0||\mathbf{r}_2-\mathbf{r}_1||\mathbf{r}-\mathbf{r}_2|}.$$

In the case when V is constant, it is of interest to note that the sum of the above second-order terms reduces to

$$-\frac{V^2}{2\pi^3} \int d\mathbf{r}$$

or in terms of the density difference

$$-\frac{1}{6}\left(\frac{3}{\pi\rho_0{}^2}\right)^{1/3} \int d\mathbf{r} (\rho-\rho_0)^2,$$

a result which is easily shown to follow from the Dirac expression (A 2.3) for the exchange energy. This, in fact, is also true for the contribution (A 2.4).

REFERENCES

ALFRED, L. C. R., and MARCH, N. H., 1956, *Phys. Rev.*, **103,** 877; 1957, *Phil. Mag.*, **2,** 985.

BARDEEN, J., and HERRING, C., 1952, *Imperfections in Nearly Perfect Crystals* (New York: Wiley), p. 261.

BIONDI, M. A., and RAYNE, J. A., 1959, *Phys. Rev.*, **115,** 1522.

FRIEDEL, J., 1954, *Advanc. Phys.*, **3,** 44.

FUMI, F. G., 1955, *Phil. Mag.*, **46,** 1007.

HUNTINGTON, H. B., 1942, *Phys. Rev.*, **61,** 325.

LAZARUS, D., 1954, *Phys. Rev.*, **93,** 973; 1960, *Advances in Solid State Physics*, Vol. 10 (New York: Academic Press Inc.).

LE CLAIRE, A. D., 1961, *Phil. Mag.* (to be published).

LEE, P. M., and MARCH, N. H., 1960, *Phys. Rev.*; **118,** 138.

LOMER, W. M., 1959, *Progress in Metal Physics*, Vol. 8 (Pergamon Press), p. 255.

MANNING, J. R., 1958, *Phys. Rev. Letters*, **1,** 365.

MARCH, N. H., and MURRAY, A. M., 1960, *Phys. Rev.*, **120,** 830; 1961, *Proc. roy. Soc.* A, **261,** 119.

RAYNE, J. A., 1961, *Phys. Rev.*, **121,** 456.

SEEGER, A., and BROSS, H., 1956, *Z. Phys.*, **145,** 161.

WEIZER, V. G., and GIRIFALCO, L. A., 1960, *Phys. Rev.*, **120,** 837.

CORRESPONDENCE

Quench Softening of Cu Whiskers

By F. W. Schapink and H. B. M. Wolters
Koninklijke/Shell-Laboratorium, Amsterdam,
(Shell Internationale Research Maatschappij N.V.)

[Received August 9, 1961]

It has been shown recently by electron transmission microscopy that prismatic dislocation loops may be formed in f.c.c. metals by vacancy condensation after quenching (Hirsch and Silcox 1958). On subsequent ageing of the specimens the loops anneal out with an activation energy which for Al is approximately equal to the energy of self-diffusion (Silcox and Whelan 1960).

We have examined the influence of quenching upon the elastic strength of Cu whiskers, as it may be expected that prismatic dislocation loops so produced act as dislocation sources resulting in a lowering of the high elastic strength of near dislocation-free Cu whiskers.

Whiskers were prepared by hydrogen reduction of cuprous bromide, a method described by Brenner (1956). The main impurity in the specimens was silver in a concentration of about 30 p.p.m. A special search was made for the presence of residual bromine in the lattice by means of radioactivation analysis. It was established that the bromine concentration of the whiskers was certainly less than 0·5 p.p.m. Crystals were selected for perfection under the microscope. Only those with apparently perfect side faces and a diameter not exceeding 8 μ were used in the mechanical experiments. In general whiskers of larger diameter do not possess a high elastic strength (Brenner 1958).

The specimens were annealed in a miniature furnace in high vacuum (10^{-6} mm of mercury) at 950°c and subsequently rapidly cooled by turning off the current. In this way a cooling rate of about 10^3 °c/s was achieved. In later experiments the quenching rate was further increased by causing the crystals to jump out of the furnace by means of electrostatic charging. This resulted in a quenching rate estimated to be 10^4 °c/s. Afterwards the specimens were mounted in a micro-tensile tester developed for straining whiskers at a rate of 1 mm/h (Wolters and Schapink 1961). About 30 whiskers of different orientations were tested in this way. It was found that the yield strength invariably dropped to 10–20% of its original value, the lowest values corresponding to the highest cooling rates. The decrease in strength is not due to a stress concentration at surface steps produced by evaporation during vacuum annealing, as slowly-cooled specimens did not show the effect.

The diameter of the crystals ranged from 4 to 8 μ. As it was very difficult to handle still thinner whiskers of, say, less than 1 μ, a possible dependence of this effect on diameter has not been checked. Such a dependence might be expected as during quenching vacancies may travel an appreciable distance and escape through the surface. For example, according to Kimura *et al.* (1959), the number of jumps of a vacancy in Au during quenching from 900°C is about 10^9 for a cooling rate of $2{\cdot}5\times10^4$ °C/s. If the same is true for Cu, the vacancies move over a few microns and consequently the effect should decrease with decreasing whisker diameter.

If the condensation of vacancies during quenching causes the observed decrease in strength, the crystals should recover on ageing. This was verified on specimens which were cut from the same whisker, each of which received a different ageing treatment in order to keep the inevitable scatter at a minimum. It was established in this way that recovery does occur, and that it is almost complete after 30 min annealing at 150°C. Preliminary experiments to determine the activation energy for the process gave a value of about 0·8 ev. Although this is not an accurate determination, it is beyond doubt that it is much lower than the activation energy for self-diffusion in Cu, reported to be 2·05 ev (Kuper *et al.* 1954). It may be significant that the observed value is close to the energy of vacancy migration in Cu, which is about 0·7 ev (Kimura *et al.* 1959).

It should be noted that the effect of quenching on the yield strength of whiskers is just the opposite of that observed in bulk crystals, where quench-hardening is known to occur (Cottrell 1957) and which is attributed to the blocking of existing dislocations by either single vacancies or vacancy clusters.

A possible explanation of these results is furnished by the formation of Frank sessile dislocation rings originating from the collapse of vacancy discs. It was suggested by Read and Kuhlmann-Wilsdorf that such rings of Frank partial dislocation may be transformed into rings of total dislocation (Read 1953, Kuhlmann-Wilsdorf 1958). Such dislocation rings were in fact observed in quenched foils of Cu (Hirsch and Silcox 1958), although their origin was somewhat uncertain. They may act as dislocation sources under influence of a shear stress which is of the order $\tau\sim\mu\mathbf{b}/r$ where $\mathbf{b}$ is the Burgers vector of the dislocation, μ the shear modulus and r the diameter of the loop. Inserting the values for Cu : $\mu=4\times10^{11}$ dyne/cm², $\mathbf{b}=2{\cdot}5$ Å and $r=250$ Å, we obtain $\tau\sim40$ kg/mm². This crude estimate is to be compared with the experimental values of 6–12 kg/mm² for quenched specimens.

The recovery of elastic strength should be governed by the rate of shrinking of the prismatic loops during ageing. The rate of shrinking of loops in Al has been observed to be determined by the activation energy for self-diffusion (Silcox and Whelan 1960). Our value for the temperature dependence of the recovery process of yield strength in Cu whiskers is, however, much smaller than the activation energy for self-diffusion, which constitutes an obstacle to application of the ' vacancy–cluster collapse ' mechanism to the present results.

It should be noted that an alternative explanation is possible, because it is not known for certain whether the excess vacancies condense on single close-packed planes. If, for instance, condensation should occur on several adjacent $\{111\}$ planes, stable voids might be formed. The stress-concentration factor near the edge of such a void is given by: $1+2\sqrt{(t/s)}$, where s is the semi-axis in the direction of the applied stress and t the semi-major-axis of the hole (Neuber 1946). The creation of such voids would also explain the observed decrease in strength of the whiskers, if t/s reaches a value of about 10. The significance of such a model is that it makes the low activation energy for recovery plausible, because on annealing the voids probably become spherical, thus reducing their surface energy. The change in shape causes a decrease in stress-concentration factor and consequently hardening is observed on ageing. This process requires an energy not much larger than the energy for vacancy migration, in accordance with the ageing experiments.

However, the final step in the recovery will perhaps be the disappearance of the spherical voids which is controlled by self-diffusion. The present experiments are not sufficiently accurate to determine whether a larger activation energy is associated with the later stages of recovery.

REFERENCES

BRENNER, S. S., 1956, *Acta Met.*, **4,** 62 ; 1958, *Growth and Perfection of Crystals* (New York : John Wiley).

COTTRELL, A. H., 1957, *Mongr. Ser. Inst. Metals*, **23,** 1.

HIRSCH, P. B., and SILCOX, J., 1958, *Growth and Perfection of Crystals* (New York : John Wiley).

KIMURA, H., MADDIN, R., and KUHLMANN-WILSDORF, D., 1959, *Acta Met.*, **7,** 145, 154.

KUHLMANN-WILSDORF, D., 1958, *Phil. Mag.*, **3,** 125.

KUPER, A., LETAW, H., SLIFKIN, L., SONDER, E., and TOMIZUKA, C. T., 1954, *Phys. Rev.*, **96,** 1224.

NEUBER, H., 1946, *Theory of Notch Stresses* (Ann Arbor, Michigan : J. Edwards).

READ, W. T., 1953, *Dislocations in Crystals* (New York : McGraw-Hill), p. 106.

SILCOX, J., and WHELAN, M. J., 1960, *Phil. Mag.*, **5,** 1.

WOLTERS, H. B. M., and SCHAPINK, F. W., 1961, *J. sci. Instrum.*, **38,** 250.

On the Creep of Metals at very Low Temperatures

By P. Feltham
Department of Metallurgy, The University, Leeds

[Received June 28, 1961]

In 1956 Glen described a rapidly decaying type of creep occurring in cadmium crystals at 1–5°K. His analysis of the process, based on Mott's (1953) theory of low-temperature logarithmic creep, indicates that the energy barrier to the flow is of the order of 0·1 ev. Mott (1956) advanced the hypothesis that the barrier may be surmountable at such low temperatures because of the quantum mechanical tunnel effect ; Täubert (1959) believes however that the temperatures are still too high for quantum effects to assume significance in creep. The object of the present note is to show that a plausible explanation of the observations is possible also on the basis of classical dislocation theory.

The figure shows part of a ' jogged ' dislocation loop, with jogs indicated only in the predominantly ' screw ' segment. Under a small shear stress the loop would expand locally, as indicated by shading ; a component of the line tension of the dislocation would then force the jogs aside. Their movement, being conservative, will be comparatively easy until they reach the part of the dislocation which is of the mixed edge/screw type, at points such as M. Here they are stopped, for further movement could not take place without the generation of point defects, for which the effective stress is assumed too small. The displacements of the jogs are accompanied by slip arising from the increase of the area of the dislocation loop. Creep would thus occur at a rate determined by the migration velocity of the jogs ; the extent of the creep would be controlled by the mean free path of the jogs between barriers (e.g. at M), and would not be expected to be significantly temperature dependent, in agreement with experiment.

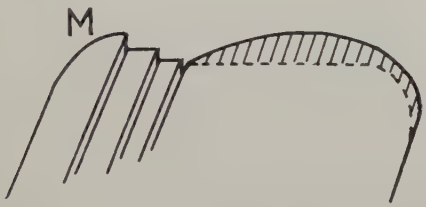

An analogous creep mechanism, involving the conservative movement of jogs in edge dislocations, and leading to logarithmic creep, has been described by Feltham (1961 a, b). The energy barrier in the latter process appears to be about $2{\cdot}5kT_{\mathrm{m}}$, where T_{m} is the melting point of the metal. In cadmium this would yield approximately 0·13 ev.

The corresponding energy barrier for the conservative migration of jogs in screw dislocations would be expected to be rather less, as the local lattice distortion is smaller than near jogs in edge dislocations (Maddin and Cottrell 1955) ; but as the jogs are inflexible they would at least have to overcome the Peierls force. In the absence of other estimates we shall take the energy barrier in the case of screw dislocations equal to $H = kT_{\mathrm{m}}$, which for cadmium yields a value close to the latent heat of melting, i.e. approximately 0·065 ev.

Now, if we write for the mean velocity of conservatively moving jogs

$$v = \nu \mathbf{b} \exp\{(-H/kT)[1-(\sigma/\sigma_0)]\},$$

where ν is an atomic frequency equal to about 10^{11} per second, $\mathbf{b}$ the Burgers vector and σ_0 the stress at which the jogs would move without the aid of thermal activation, we obtain for the stress

$$\sigma = \sigma_0[1-(kT/H)\ln(\nu\mathbf{b}/v)].$$

Assuming that if creep is readily observable the jogs will migrate with a velocity of about $0{\cdot}1\,\mu$/sec. then with $\mathbf{b} = 3\times10^{-8}$ cm and $H \equiv kT_{\mathrm{m}} = 0{\cdot}06$ ev, the term in square brackets is zero at a temperature of 35°K. Hence, irrespective of the magnitude of σ_0, this process could no longer be rate controlling at higher temperatures ; above 35°K jogs in edge dislocations might control the creep rate.

The results of Glen (1956) show that the energy barrier to transient creep in cadmium is in fact considerably higher at 77 and 90°K than at 1–5°K, indicating a transition to a new energy barrier somewhere in the range 5–77°K, in agreement with the above inference. The preceding reasoning could, of course, be applied to creep at higher temperatures as well, and therefore leads to the conclusion that similar increases in the energy barriers should occur on raising the temperature further. Thus, apart from creep at very low temperatures, one might expect to observe energy barriers associated with

(*a*) the conservative movement of jogs in edge dislocations,

(*b*) vacancy formation by jogs in rapidly gliding dislocations, as discussed by Seeger (1955),

(*c*) vacancy migration, giving rise to climb by jog displacement in dislocations of the edge or mixed types carrying a high concentration of vacancies absorbed by elastic interaction (Friedel 1956),

(*d*) vacancy formation followed by migration, in a cooperative glide/climb process of mixed dislocations, in which the vacancies generated in the non-conservative displacement of the jog subsequently lead to its migration resulting in climb, and

(*e*) vacancy formation followed by vacancy migration, in the movement of jogged screw dislocations (Mott 1956).

Expressed as fractions of the activation energy of self-diffusion the barriers in close-packed metals would then be expected to be equal to about 0·13, 0·4, 0·6, 1·0 and 1·0 respectively. In high purity aluminium Sherby *et al.* (1957) established the existence of a series of activation energies in creep in the range 77–880°K ; again, in terms of the activation energy of self-diffusion these appeared to be equal to about 0·14, 0·5, 0·75 and 1·0. The intermediate values may need correcting, as was pointed out by Basinski (1957) ; nevertheless agreement with the assumed values of the corresponding fractions may be regarded as being satisfactory. The strong elastic interaction between point defects and dislocations, particularly vacancies, may also give rise to creep barriers. Friedel (1956) estimates the interaction energy between vacancies and edge dislocations in copper to be equal to 0·35 ev ; the corresponding energy for interstitial atoms would be expected to be lower by an order of magnitude. Jogs, as well as interstitials formed in the early stages of creep, may thus control the creep rate at very low temperatures.

Finally, it is of interest to note that (*a*) the to-and-fro movement of jogs on screw dislocations and (*b*) the pinning and un-pinning of edge dislocations at interstitial sites, may be responsible for the two ‘ Bordoni ’ peaks observed for example in the damping capacity versus temperature curves of copper subjected to oscillating stresses at very low temperatures. Both effects could account qualitatively for the observation that in slightly strained metals, in which jogs and interstitials could be assumed to be abundant, the damping is much more intense than in well-annealed ones (Niblett and Wilks 1960).

References

Basinski, Z. S., 1957, *Acta Met.*, **5,** 684.
Feltham, P., 1961 a, *J. Inst. Met.*, **89,** 210 ; 1961 b, *Phil. Mag.*, **6,** 259.
Friedel, J., 1956, *Les Dislocations* (Paris : Gauthier-Villars), p. 237.
Glen, J. W., 1956, *Phil. Mag.*, **1,** 400.
Maddin, R., and Cottrell, A. H., 1955, *Phil. Mag.*, **46,** 735.
Mott, N. F., 1953, *Phil. Mag.*, **44,** 742 ; 1956, *Ibid.*, **1,** 568.
Niblett, D. H., and Wilks, J., 1960, *Advanc. Phys.*, **9,** 1.
Seeger, A., 1955, *Phil. Mag.*, **46,** 1194.
Sherby, O. D., Lytton, J. L., and Dorn, J. E., 1957, *Acta Met.*, **5,** 219.
Täubert, P., 1959, *Abh. dtsch. Akad. Wiss. Berl.*, No. 7.

The Stacking-fault Energy of Graphite

By C. BAKER, Y. T. CHOU and A. KELLY
Department of Metallurgy, University of Cambridge

[Received August 21, 1961]

STACKING-FAULT energies can be obtained from electron transmission micrographs by two methods. The first, due to Whelan (1958), involves measurement of the radius of curvature of a partial dislocation at an extended node. The interaction of the various partial dislocations at the measuring point is neglected and the value to be taken for the line tension of the partial dislocation is uncertain, in cases where the radius of curvature of the partial dislocations is comparable with the thickness of the foil. The second method is to measure the equilibrium separation of the partial dislocations in a long straight extended dislocation. This has the advantage that the solution of the elasticity equations is exact provided the thickness of the foil is much larger than the equilibrium separation of the partial dislocations. We have applied the second method to graphite using anisotropic elasticity.

In the hexagonal lattice the elastic constants are invariant for a rotation about the hexagonal axis, so that for a few special problems the use of anisotropic elasticity becomes much simpler than for a cubic crystal. Using anisotropic elasticity and the Fourier synthesis method (Chou and Eshelby 1961) the width of a long straight extended dislocation with its line and Burgers vector both lying in the basal plane is given by:

$$W=\frac{\mathbf{b}^2}{8\pi\gamma}\{K_s(1+2\cos 2\alpha)+K_e(1-2\cos 2\alpha)\}.$$

Here $\mathbf{b}$ is the Burgers vector of the partial dislocations, α is the angle between the dislocation line and the total Burgers vector and γ is the stacking-fault energy;

$$K_s=\{\tfrac{1}{2}C_{44}(C_{11}-C_{12})\}^{1/2},$$

$$K_e=(\bar{C}_{13}+C_{13})\left\{\frac{C_{44}(\bar{C}_{13}-C_{13})}{C_{33}(\bar{C}_{13}+C_{13}+2C_{44})}\right\}^{1/2},$$

where $\bar{C}_{13}=(C_{11}C_{33})^{1/2}$.

Thus for a total dislocation in the edge orientation we have

$$W_e=\frac{\mathbf{b}^2}{8\pi\gamma}(3K_e-K_s)$$

and for a screw

$$W_s=\frac{\mathbf{b}^2}{8\pi\gamma}(3K_s-K_e).$$

The best values of the elastic constants for graphite are those derived by Bowman and Krumhansl (1958) from spectra, compressibility and specific heat measurements. The values obtained are:

$$C_{11}=1{\cdot}13\times10^{13}\text{ dynes cm}^{-2};\qquad C_{12}=0{\cdot}28\times10^{13}\text{ dynes cm}^{-2};$$

$$C_{33}\geqslant1{\cdot}8\;\;\times10^{11}\text{ dynes cm}^{-2};\qquad C_{44}=2{\cdot}3\;\;\times10^{10}\text{ dynes cm}^{-2}.$$

The accuracy claimed for these figures is 20–50%. A value of C_{13} is not obtained. In determining the stacking-fault energy of graphite we have, therefore, two unknowns: the stacking-fault energy and one of the elastic constants, i.e. K_e is unknown. Figure 1† shows a loop of extended dislocation lying in the basal plane of a graphite crystal. The partial dislocations are clearly resolved and their Burgers vectors lie along $\langle 10\bar{1}0\rangle$ directions. These loops of extended dislocation are found in material irradiated in BEPO to a dose of $\sim5\times10^{18}$ n.v.t. The radiation induced defects have pinned dislocation sources operating in the crystal during cleavage. Figure 2 shows graphically how the separation of the partial dislocations varies around the loop. The maximum separation of 1500 Å occurs when the total dislocation is in edge orientation and the minimum of 800 Å in the screw orientation. We have then,

$$\frac{W_e}{W_s}=1{\cdot}88=\frac{3K_e-K_s}{3K_s-K_e}.$$

From this, and $K_s=3{\cdot}12\times10^{11}$ dynes cm^{-2}, we find $K_e=4{\cdot}24\times10^{11}$ dynes cm^{-2}, whence $C_{13}=7{\cdot}7\times10^{11}$ dynes cm^{-2}.

Since K_e and K_s are now known γ is obtained from either W_e or W_s, giving in both cases $\gamma=0{\cdot}51$ ergs cm^{-2}. In the above calculations $C_{33}=1{\cdot}8\times10^{11}$ dynes cm^{-2} has been used. The value of γ is subject to the error in the elastic constants and there may also be a systematic error in the measurements of W_e and W_s due to the fact that the image of a dislocation does not coincide with the position of the dislocation. There may also be an error due to the fact that in graphite the thickness of the foil is not many times greater than the separation of the partial dislocations.

Preliminary estimates of the stacking-fault energy of graphite have been given, Williamson (1960), Amelinckx and Delavignette (1960) using either an assumed value of the shear modulus or treating C_{44} as the relevant shear modulus and assuming isotropic elasticity. Siems *et al.* (1961) have recently submitted for publication a comprehensive treatment of stacking-fault energies in layer structures also using anisotropic elasticity. Their treatment for graphite is slightly different from that used here in that C_{13} is not obtained explicitly, an effective value of Poisson's ratio being derived instead. The value obtained for γ is $0{\cdot}58$ erg cm^{-2} in excellent agreement with that obtained here.

The values obtained using anisotropic elasticity differ by more than an order of magnitude from those obtained using isotropic elasticity. For instance the radius of curvature of partial dislocations at a node in graphite is 0·95 μ. Using Whelan's formula

---

† Figure 1 is shown as a plate.

$$\gamma = G\mathbf{b}^2/2R$$

with $G = 2{\cdot}3 \times 10^{10}$ dynes cm^{-2} gives $\gamma = 0{\cdot}025$ ergs cm^{-2}. If the equilibrium separation of partial dislocations in a long straight extended dislocation is used to find γ employing the formula

$$\gamma = \frac{G\mathbf{b}^2}{8\pi W}\left(\frac{2-\nu}{1-\nu}\right)\left[1 - \frac{2\nu}{2-\nu}\cos 2\alpha\right],$$

Fig. 2

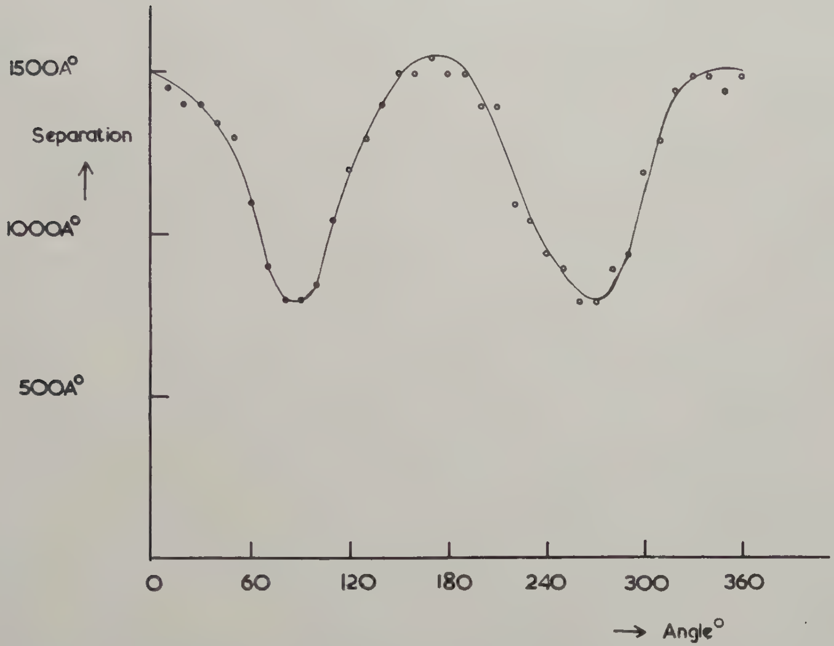

Variation of the equilibrium partial dislocation separation with the angle to the total Burgers vector (angle not equal to α) for a dislocation loop. Maximum separation 1500 Å in edge orientation and minimum 800 Å in screw orientation.

where ν = Poisson's ratio, then one finds from the value of W_e and W_s given above that $\nu = 0{\cdot}265$. If G is assumed to be $2{\cdot}3 \times 10^{10}$ dynes cm^{-2}, then $\gamma = 0{\cdot}038$ ergs cm^{-2}. It is quite clear that in graphite and possibly in many other materials which are elastically anisotropic that the anisotropy must be considered in deriving values of the stacking-fault energy. All the stacking-fault energies reported here have been determined on irradiated crystals. Irradiation to these doses produces no measurable change in the radius of curvature observed at an extended node and hence no measurable change in stacking-fault energy.

REFERENCES

AMELINCKX, S., and DELAVIGNETTE, P., 1960, *J. appl. Phys.*, **31,** 2126.
BOWMAN, J. C., and KRUMHANSL, J. A., 1958, *J. Phys. Chem. Solids*, **6,** 367.
CHOU, Y. T., and ESHELBY, J. D., 1961, *J. Mech. Phys. Solids* (in the press).
SIEMS, R., AMELINCKX, S., and DELAVIGNETTE, P., 1961 (to be published).
WHELAN, M. J., 1958, *Proc. roy. Soc.* A, **249,** 114.
WILLIAMSON, G. K., 1960, *Proc. roy. Soc.* A, **257,** 457.

REVIEWS OF BOOKS

Progress in Low Temperature Physics. Vol. III. Edited by C. J. GORTER. (Amsterdam: North-Holland Publishing Co., 1961.) [Pp. xiii+495.] Price £4 16*s*. 0*d*.

IN his preface Professor Gorter tells of the doubts that have assailed him, whether there was a continuing need for reviews of the progress in low temperature physics. I have shared and given expression to these doubts, but am for the moment silenced by his latest production. If he can continue to give us such magnificent value for our money, may he long continue to edit this series. What is characteristic of the present volume is that the topics discussed, though having their origin in the realm of low temperatures, involve problems that are the very stuff of physics. Vinen on vortex lines in Helium II, Grilly and Hammel on ^{3}He, Bardeen and Schrieffer on superconductivity, all these illuminate the central theme of the quantum mechanical many-body problem; Azbel' and Lifshitz, on electron resonances in metals, are concerned with metals and not just with metals at low temperatures; and one could extend the list to cover almost every one of the eleven articles. Here indeed we see low temperature physics in its proper perspective as part of a much more important whole, and Professor Gorter is to be warmly thanked for revealing the truth so clearly, while providing a series of reviews that will have an enduring worth. A. B. P.

Mechanical Radiation. By ROBERT BRUCE LINDSAY. (McGraw-Hill Book Co., 1960.) International Series in Pure and Applied Physics. [Pp. ix+415.] Price £3 17*s*. 6*d*.

THIS is a substantial textbook on the theory of waves and radiation, of a mechanical nature, in solids, fluids and gases, designed for advanced undergraduate work or first-year post-graduate work at American universities. It is well written and, although comprehensive in scope, deals with a great variety of topics in detail. There are copious references, many of them to recent work, both theoretical and experimental. The treatment is theoretical, but the point of view is a thoroughly physical one. There are three introductory chapters on the general theory of waves and vibrations. The general theory is then applied to a variety of subjects, in chapters dealing with waves in strings, membranes, elastic media, rods and plates, incompressible fluids, sound waves in fluids, elastic waves in the atmosphere, the sea, and the earth, and acoustic radiation in closed spaces. As may perhaps be expected in view of the author's own work, the chapter on sound waves in fluids is the most substantial of these. The book concludes with a useful account of the relation of mechanical radiation and the properties of matter. F. G. F.

Proceedings of the Fourth Conference on Carbon held at the University of Buffalo, New York. (Pergamon Press, 1960.) [Pp. 778.] Price £7 10*s*. 0*d*.

THE Biennial Conferences on Carbon have since their inception in 1953 provided a meeting place for industrial and academic scientists interested in carbon in all its aspects. The Proceedings of the Fourth Conference, held in 1959, contain over 70 papers from laboratories in many countries. These cover a wide variety of topics ranging from theoretical papers on electronic structure, energy levels and Fermi surfaces to the technology of carbon brushes and fillers. The book probably provides the most comprehensive available survey of current researches on carbon and as such is invaluable to anyone concerned with the detailed properties of carbon.

The book is superbly produced by Pergamon Press, and is unusual in including colour reproductions of photomicrographs taken in polarized light.

Crystal Structure Analysis. By MARTIN J. BUERGER. (New York and London: John Wiley & Sons, Inc., 1960.) [Pp. xvii+668.] Price £7 8*s.* 0*d.*

THE author, who is Director of the School for Advanced Study at M.I.T. and Professor of Mineralogy and Crystallography there, is well known for his earlier textbooks on structural crystallography and for the fact that he is co-editor of the *Zeitschrift für Kristallographie.* He has always had the direction and supervision of the work of many research students and others engaged in learning the methods of crystal-structure analysis and the present book has grown out of the notes that he prepared to help them.

As would be expected, the style is excellent. One can only regret that the price may prevent purchase of this book by the students who would most benefit from having a personal copy. This is all the more reason why it should be available in all scientific and technical libraries. Some of the material given here is to be found equally well treated in other textbooks but attention may be drawn especially to the discussion of twinning in relation to the collection of data for crystal structure analysis, and to the detailed description of intensity measurement. Throughout the book there is a precise and detailed account of recommended techniques, together with many useful tables and informative diagrams.

Subjects not treated in detail are the Patterson synthesis and vector space (which are the subject of a companion volume published in 1959), reflection statistics, optical analogue methods of analysis and the determination and study of anisotropic thermal motion, bonding anisotropy and disorder. K. L.

X-Ray Microscopy. By V. E. COSSLETT and W. C. NIXON. (Cambridge: University Press, 1960.) Cambridge Monographs on Physics. [Pp. 406.] Price £4 0*s.* 0*d.*

FOR years Cosslett, with his collaborators, has excited considerable interest in the development of X-ray microscopes and we welcome indeed this first comprehensive account by Cosslett and Nixon of the use of X-rays for microscopical investigations with both low and high magnification. Both have contributed much in this field. This is a technique, which 20 years ago appeared to offer very real possibilities, but it has taken many years to overcome the formidable difficulties encountered in connection with focusing X-rays. Resolutions obtained are perhaps only twice that of the optical microscope, but of course with X-rays internal X-ray photographs are obtained with all the fascinating additional information these offer, especially for opaque materials. Then there are X-ray emission analysis, micro-diffraction and stereo-microscopy and quantitative analysis as additional attractive features. The book is very comprehensive indeed. First, contact microradiography is examined in detail and its ultimate resolution discussed carefully. Then X-ray microscopy by point projection (to which the authors have contributed much), is examined. This is followed by a chapter on reflexion methods and mirror systems, a section which is very well illustrated. Reflexion from curved crystals follows. Chapters follow on the biologically important methods of X-ray absorption and emission micro-analysis, and here we have chapters packed with practical 'know-how' of immense value to the experimenter. Chapters 8, 9, 10, 11 are all also mines of know-how. Eight gives an account of methods of exciting X-rays and X-ray sources and their characteristics, 9 describes specimen preparation techniques, 10 is devoted to techniques of contact microradiography and 11 to techniques of projection microscopy. Applications to biology and to metallurgy receive their full treatments and a final chapter on very recent techniques is included. Some valuable tables on absorption and emission data are added in appendices. A close packed bibliography fills no less than

23 pages. The index is rather brief. Although the book is naturally expensive it is generally admirably produced and certainly not over-priced. There is one weakness in production, for although there are 32 pages of delightful plates, these are all fastened together in one group in the centre of the book. How much better it would have been to have distributed these plates to be near the pages of their corresponding text.

We are convinced this will remain an authoritative text on the subject for quite a long time.

S. T.

Thermodynamics. By P. T. Landsberg. (Interscience Publishers, 1961.) [Pp. viii + 499.] Price £5 9*s*. 0*d*.

The author of this textbook has for some time made notable contributions to the more abstract aspects of thermodynamics; as befits a professor of applied mathematics he is here mainly concerned with these aspects and with their mathematical formulation. To quote from the author's preface: " The abstract nature of the subject is always allowed to become fully evident in this book ", " General principles rather than detailed applications or physical mechanisms are emphasized ", and " Questions of historical detail and of experimental results are omitted ".

Although the author claims that " this text should be suitable for anyone who is not deterred by abstract thought ", this reviewer feels that only the exceptionally brave physicist will venture to use this volume. If he does, he will be rewarded as the reasons for the rather general fear of physicists for thermodynamics will become clearer to him, and his understanding of this extremely difficult subject should greatly improve.

Apart from the basic laws of thermodynamics this text also gives a few basic applications and a thorough discussion of the relation between thermodynamics and statistical mechanics. The text is generously interlaced with problems of a great variety.

D. ter Haar.

Close Binary Systems. By Zdenek Kopal. (London: Chapman & Hall, 1959.) [Pp. xiv + 558.] Price £5 5*s*. 0*d*.

In this comprehensive book on a very fascinating astrophysical domain the author provides a well-written, informative and in most respects exhaustive treatment. There could hardly have been anyone better qualified to write it than Professor Kopal, who could draw on his wide personal and pioneering experience in a field to which he has contributed since the 1930's. Six main sections illuminate the subject from many angles: we start with a development of a celestial mechanics of two closely associated stars, and follow the effects of various dynamical properties of bodies distorted by axial rotation and mutual tidal action on the observable orbit about their common centre of gravity. The evaluation of the potential and kinetic energy terms leading to the Lagrangian equations of motion, internal structure, precession and nutation of fluid components, etc., are some of the items dealt with. Observational features are introduced in the subsequent two sections on the theory of the light-curves and of the radial-velocity changes. The treatment is aimed to be as complete as possible to first-order terms, but we find frequent suggestions about the fruitful possibilities of an extension to higher orders. More than 170 pages are devoted to the determination of the geometrical orbits, derived from the preceding analysis. Here, the progress made within the last two decades is impressive: the previous semi-empirical approach is now replaced by the introduction of exact-mathematical functions. However, in spite of the complexity of this new apparatus, problems like those of extremely close distorted systems are still beyond our full grasp. The author asks the question

" where do we go from here? " and indicates that the future might perhaps see the replacement of the present brightness-time analysis of the light-changes by that of their Fourier transforms, i.e. by the study of their frequency-spectrum. In conclusion, we should mention that the importance of these stars for our general ideas on stellar evolution is emphasized by numerous interesting interpretations. A. B.

Techniques of High Energy Physics. By D. M. RITSON. (Interscience Publishers, 1961.) [Pp. 540.] Price £6 6*s*. 0*d*.

HERE's how to do it: distillate of practical physicist, a careful comprehensive, and for the most part accurate survey of the present techniques for detecting and measuring elementary particles. Bubble chambers, cloud chambers, emulsions, ionization counters, scintillation and Cerenkov counters are all exhaustively discussed. If you want to design a beam, write a computer programme, or use a transistor, you can dip into this collection and find the snags, the tricks, and the design factors all carefully laid out. Once or twice the pale ghost of a particle appears.

This collection of essays is clearly intended as a compact reference work for research workers, and as such may well leave the ordinary reader rather breathless. However, worthy of special mention are a delightfully written chapter on Scintillation and Cerenkov counters by Ritson and Weinstein, and a thoughtful and critical little monograph on Emulsions by Widgoff. The first chapter is a valuable summary of formulae concerning the general properties and kinematics of particles and γ-rays, although a number of printing errors and occasional textual errors are confusing. Reading about autocode in the chapter on digital computers only strengthens my belief that it is easier to programme in the basic machine code. However, it is a pleasure to read that the design of magnets, like that of other experimental apparatus, leaves room for personal preference. D. V. B.

BOOK NOTICES

Noise in Electronic Devices. Papers based on material presented at a conference held by the Electronics Group of The Institute of Physics at the Services Electronics Research Laboratory, Baldock, Hertfordshire on October 2–3, 1959. (London: Chapman & Hall, 1961.) [Pp. 100.] Price £1 15*s*. 0*d*.

Classical Mechanics. Second edition. By H. C. CORBEN and PHILIP STEHLE. (New York and London: John Wiley & Sons, 1961.) [Pp. 389.] Price £4 16*s*. 0*d*.

Physical Chemistry. Second revised edition. By E. A. MOELWYN-HUGHES. (Oxford: Pergamon Press, 1961.) [Pp. 1333.] Price £4 4*s*. 0*d*.

Fast Reactors. By R. G. PALMER and A. PLATT. *Nuclear Engineering* Monographs No. 12. (London: Temple Press, 1961.) [Pp. 93.] Price 12*s*. 6*d*.

Turbulence: Classic Papers on Statistical Theory. Edited by S. K. FRIEDLANDER and L. TOPPER. (New York and London: Interscience Publishers, 1961.) [Pp. 187.] Price £2 5*s*. 0*d*.

[*The Editors do not hold themselves responsible for the views expressed by their correspondents.*]

Fig. 5

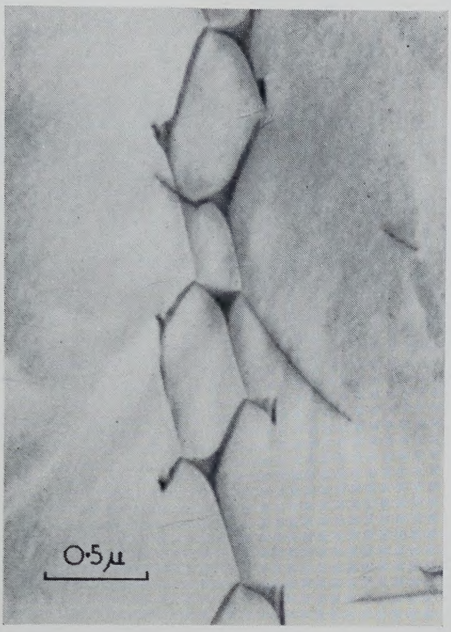

Extended and contracted nodes in a Cu + 8% Al alloy ($R \approx 3000$ Å). One of the nodes lies on a different plane from the others.

Fig. 6

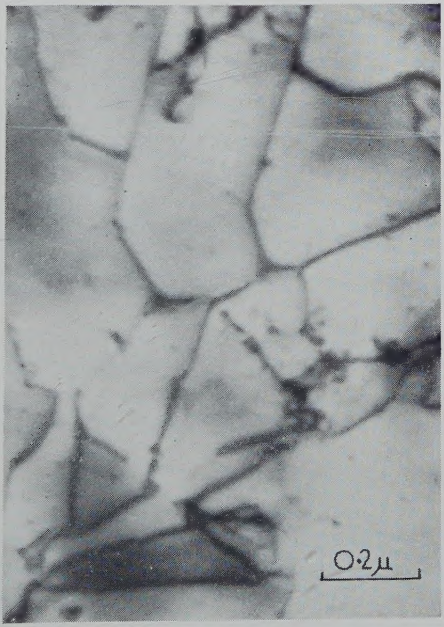

Nodes in Ag + 2% Zn alloy ($R \approx 300$ Å).

Fig. 8

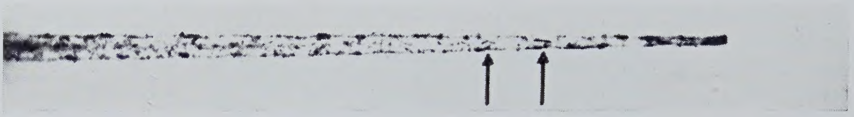

X-ray micrograph of zone-refined Al crystal. Axial orientation parallel to $\langle 110 \rangle$ direction. Growth rate: 1·3 mm/min. Reflecting plate: (111). Magnification: 24×. In the thin region (right of photograph), note arrows pointing to scattered, rather long dislocations in interior of crystal. The thick region (left of photograph) contains many short dislocations. Note great number of dislocations lying near surface of crystal.

Fig. 9

X-ray micrograph of zone-refined Al crystal. Axial orientation parallel to $\langle 111 \rangle$ direction. Growth rate: 2 mm/min. Reflecting plane: (220). Magnification: 47×.

Fig. 10

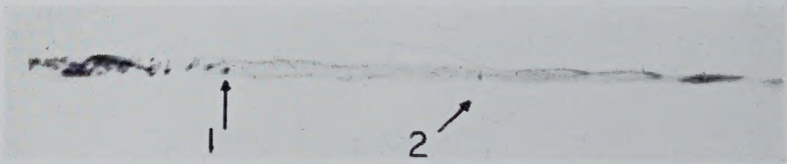

X-ray micrograph of crystal shown in fig. 9 after electropolishing. Arrow 1 indicates isolated dislocations. Arrow 2 indicates scratch in emulsion. Note that region to right of arrow 1 is free of visible dislocations. Magnification: 28×.

Fig. 11

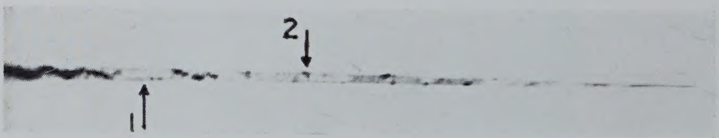

X-ray micrograph of 99·999% pure Al crystal. Axial orientation parallel to $\langle 110 \rangle$ direction. Growth rate: 4 mm/min. Reflecting plane: (111). Magnification: 22×.

Fig. 12

X-ray micrograph of crystal in fig. 11 after electropolishing. Arrow 1 indicates the same dislocation-free area in both pictures. Arrow 2 in fig. 11 indicates dislocation near surface that disappeared after electropolishing. Magnification: 22×.

Fig. 1

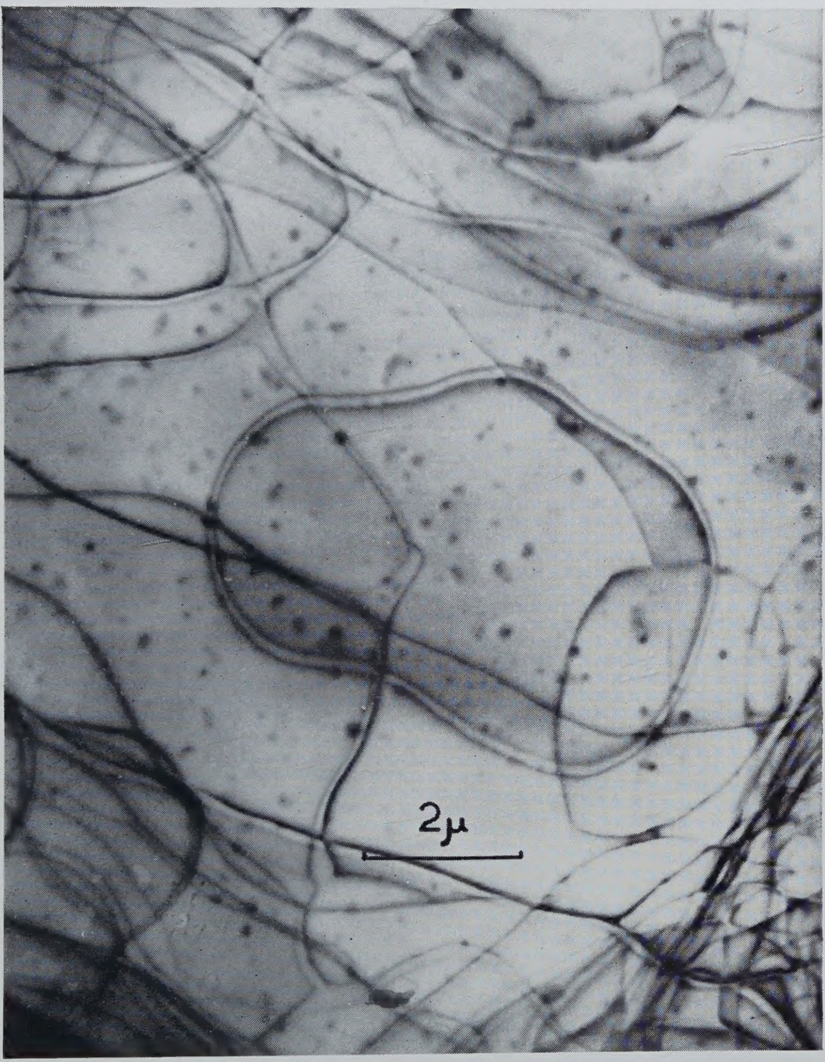

Transmission micrograph of graphite, irradiated to a dose of $\sim 5\times 10^{18}$ n.v.t., showing a dislocation loop with its Burgers vector in the basal plane. The partial dislocation separation in edge orientation of the total dislocation is nearly double that in screw orientation.